Alma Mater Studiorum · Università di Bologna

Dipartimento di Fisica e Astronomia "Augusto Righi"
Corso di Laurea in Fisica

Architecture of coexistence: structural constraints of biodiversity in competitive GLV ecosystems

Relatore:
Prof. Armando Bazzani

Presentata da:
Giulia Montagnani

Anno Accademico 2025/2026

Alle cose che cambiano e alle persone che restano.

Abstract

Understanding transitions between dynamical regimes is crucial for predicting the persistence and fragility of complex ecosystems.

In this work, we investigate how network structure shapes local stability and dynamical evolution in competitive Generalized Lotka–Volterra (GLV) systems, focusing on two structural parameters: connectance (C) and modularity (Q).

Building on Robert May's complexity–stability framework, we characterize how C and Q affect equilibrium spectra using random matrix theory, and use these results to interpret their consequences for equilibrium stability and feasibility. We then perform a statistical classification of the attractor space: numerical simulations are compared with established analytical results for the onset of multistability and unbounded growth in fully connected networks ($C = 1, Q = 0$), and we study how network structure modifies these transitions and the resulting equilibrium states using observables such as the fraction of surviving species, the final community structure, and the resulting species abundance distributions (SADs).

We find that feasibility, rather than linear stability, is the primary constraint limiting the existence of interior equilibria, while reduced connectance consistently promotes feasibility, stability and species persistence. Network structure has an asymmetric effect: anti-modularity (i.e., stronger inter-module than intra-module interactions) destabilizes equilibria through a spectral outlier, leading dynamically to module-selective bistability in which one module goes extinct depending on initial conditions across a broad range of connectance values. Positive modularity (i.e., stronger intra-module than inter-module interactions) instead tends to dynamically decouple modules. Finally, SADs become increasingly heavy-tailed as connectance increases, revealing a trade-off between species richness and the persistence of rare, near-extinction species.

Sommario

Comprendere le transizioni tra diversi regimi dinamici è fondamentale per prevedere la persistenza e la fragilità degli ecosistemi complessi.

In questo lavoro studiamo come la struttura della rete di interazione influenzi la stabilità locale e l'evoluzione dinamica dei sistemi GLV (*Generalized Lotka–Volterra*) competitivi, concentrandoci su due parametri strutturali: la connettività (C) e la modularità (Q).

Basandoci sul framework complessità–stabilità introdotto da Robert May, caratterizziamo l'impatto di C e Q sugli spettri degli equilibri mediante strumenti di *Random Matrix Theory*, utilizzando poi questi risultati per interpretarne gli effetti sulla stabilità e sulla fattibilità (ossia, la condizione in cui tutte le specie presentano abbondanze positive) degli equilibri. Successivamente, svolgiamo un'analisi statistica dello spazio degli attrattori: confrontiamo le simulazioni numeriche con risultati analitici consolidati sull'insorgenza di multistabilità e di crescita illimitata nelle reti *fully–connected* ($C = 1$, $Q = 0$), e studiamo come la struttura della rete modifichi queste transizioni e i corrispondenti stati di equilibrio, utilizzando osservabili quali la frazione di specie sopravvissute, la struttura finale della comunità e le risultanti distribuzioni delle abbondanze delle specie (SADs).

I risultati mostrano che la fattibilità, più della stabilità lineare, rappresenta il principale fattore limitante per l'esistenza di equilibri interni, mentre una minore connettività favorisce sistematicamente la fattibilità degli equilibri, la loro stabilità e la sopravvivenza delle specie nell'evoluzione dinamica. La struttura di rete esercita un effetto asimmetrico: la modularità negativa, corrispondente a reti dominate da interazioni tra moduli, destabilizza gli equilibri attraverso un outlier spettrale, dando luogo dinamicamente a una bistabilità selettiva tra moduli, in cui uno dei moduli viene portato all'estinzione a seconda delle condizioni iniziali, su un ampio intervallo di valori di connettività. Al contrario, la modularità positiva, corrispondente a reti con interazioni concentrate all'interno dei moduli, tende a disaccoppiare dinamicamente i moduli. Infine, le SAD assumono code sempre più pesanti (*heavy-tailed*) all'aumentare della connettività, evidenziando un trade-off tra la ricchezza delle singole specie e la persistenza di specie rare, prossime all'estinzione.

Contents

1

Introduction

1.1 A discursive outline

Modeling complex dynamical systems inevitably requires a trade-off between descriptive detail and generality. While increasingly detailed models may provide a more faithful representation of a specific system, they often become less suitable for identifying general mechanisms that extend beyond the particular case under study.

Ecology, understood as the study of the interactions among organisms and between organisms and their environment, is a paradigmatic example of this modeling philosophy.

Over the past decades, the development of quantitative ecology has enabled mathematicians, and more recently physicists and computer and data scientists, to contribute to the field through the formulation and analysis of increasingly sophisticated mathematical models.

Among these, the Lotka–Volterra framework has become one of the standard approaches for describing the dynamics of multispecies communities. Despite its simple mathematical structure, it can be naturally extended in several directions, allowing an increasing level of complexity to be reached.

An ecological community is characterized both by the nature of the interactions among species and by the topology of the interaction network. It is therefore natural to represent it as a weighted network, whose links encode the strength and sign of pairwise interactions.

When studying real ecosystems, reconstructing both the interaction strengths and the underlying network structure from empirical observations remains a challenging task [1]. Conversely, when working with theoretical models, it is essential to state explicitly the assumptions made about both the interaction dynamics and the network structure, since the resulting predictions may depend critically on these choices.

The objective of this thesis is to investigate how the structure of the interaction network influences the stability properties and dynamical evolution of ecosystems described by the Generalized Lotka–Volterra (GLV) model in the competitive interaction regime.

1.2 Structure and objectives of the thesis

This thesis investigates how two of the most widely studied structural descriptors of ecological networks—connectance (C) and modularity (Q)—affect both the properties of ecological equilibria and the dynamical evolution of ecosystems under different interaction regimes.

Chapter 2 introduces the ecological model adopted throughout this work, namely the Generalized Lotka–Volterra (GLV) framework. The chapter also presents the assumptions underlying the model and the parametrization used to generate interaction networks with prescribed structural properties.

Chapter 3 investigates the effects of C and Q on the properties of static equilibria through a combination of analytical methods—drawing on probability theory and Random Matrix Theory (RMT)—and Monte Carlo simulations over ensembles of ecological communities. In particular, the analysis addresses the following questions:

- What is the relationship between the local stability of an equilibrium and its feasibility, i.e., the requirement that all equilibrium abundances are strictly positive? Under which conditions does such a relationship hold?
- How do connectance and modularity influence the stability and feasibility of equilibria in the GLV model, and how can these effects be interpreted mathematically?

Chapter 4 presents the main original contribution of this thesis, which concerns the study of the dynamical evolution of ecological communities. Analytical results are used to complement numerical simulations and to provide benchmark predictions under the assumptions required by the theory. This comparison allows us to assess the robustness of the numerical results when these assumptions are relaxed.

The chapter focuses on the following questions:

- Does the dynamics converge to a limited set of characteristic equilibria (attractors)? How do different interaction regimes determine the transition between the corresponding dynamical behaviors, and are the available analytical predictions robust for finite-size systems?
- How do connectance and modularity influence the organization of the attractor space and the properties of the resulting ecological communities?

Finally, Chapter 5 summarizes the main findings of this work, discusses the limitations of the adopted framework, and outlines possible directions for future extensions. Additional analytical derivations and details of the numerical methods are provided in the Appendices.

2

Model

This chapter introduces the ecological model employed throughout the thesis, details its parametrization, and discusses the assumptions underlying the analysis, highlighting their potential impact on the generality of the results.

2.1 The Generalized Lotka–Volterra equations

The most widely used mathematical framework for describing the dynamics of complex ecological communities is the ***Generalized Lotka–Volterra model (GLV)***, a multidimensional extension of the classical two–species model introduced independently by Alfred Lotka [2] and Vito Volterra [3] at the beginning of the twentieth century, that models the binary interactions among individuals of different populations.

Throughout this thesis we will consider the formulation

$$\frac{dN_i}{dt}(t) = N_i(t)\left(r_i + \sum_{j=1}^{n} a_{ij}N_j(t)\right), \qquad i = 1, \dots, n, \tag{2.1}$$

where

- $N_i(t)$ denotes the abundance of species i;
- r_i is its intrinsic growth rate (i.e. the fitness of a species in a given environment);
- a_{ij} for $i \neq j$ quantifies the effect of species j on reproduction of species i due to individual interactions; $a_{ii} < 0$ represents the intraspecific competition (self-limitation) term, accounting for the finite availability of environmental resources;
- n is the number of species in the community.

In vector form, the GLV equations can be written as

$$\frac{d\mathbf{N}}{dt} = \mathrm{diag}(\mathbf{N})\,(\boldsymbol{r} + \mathbf{A}\mathbf{N})\,. \tag{2.2}$$

where $\mathbf{N}(t) \in \mathbb{R}^n$ is the abundance vector at time t, $\boldsymbol{r} \in \mathbb{R}^n$ is the vector of intrinsic growth rates. The matrix $\mathbf{A} = (a_{ij})$ is often referred to as the ***interaction matrix*** [1, 4].

For biological reasons, we restrict our analysis to the positive orthant,

$$\mathbf{N}(t) \in \mathbb{R}^n_{>0},$$

since negative abundances have no ecological interpretation. Accordingly, only trajectories entirely contained in the positive orthant are regarded as biologically meaningful. In Subsection 2.1.1 we demonstrate that the positive orthant is invariant under the model dynamics.

2.1.1 Density dependence and positive invariance

Equation (2.1) belongs to the broader class of systems

$$\frac{dN_i}{dt} = N_i\, g_i(N_1, \ldots, N_n), \qquad i = 1, \ldots, n, \tag{2.3}$$

where the functions g_i encode the ecological interactions among species.

Systems of the form (2.3) are called ***density–dependent (DD)*** because the per–capita growth rate of each species,

$$\frac{1}{N_i}\frac{dN_i}{dt},$$

depends on the current state of the community.

An important consequence of this structure is the invariance of the positive orthant.

Proposition 1 (Positive invariance)**.** *Let* $\mathbf{N}(t)$ *be a solution of* (2.3) *with initial condition*

$$\mathbf{N}(0) = \mathbf{N}_0 \in \mathbb{R}^n_{>0}.$$

such that

$$\lim_{N_i \to 0^+} N_i\, g_i(\mathbf{N}) = 0, \qquad i = 1, \ldots, n \tag{2.4}$$

and the vector field $N_i g_i(\mathbf{N})$ *is smooth. Then*

$$\mathbf{N}(t) \in \mathbb{R}^n_{>0} \qquad \forall t$$

for which the solution exists.

Proof. Consider the hyperplane

$$H_i = \{\mathbf{N} \in \mathbb{R}^n : N_i = 0\}.$$

If $N_i = 0$, then from (2.3)

$$\frac{dN_i}{dt} = 0,$$

independently of the values of the remaining components. Therefore each hyperplane H_i is invariant under the dynamics. This is a direct consequence of the DD structure (2.3) under the assumption of Eq. (2.4).

Suppose by contradiction that a trajectory starting from

$$\mathbf{N}_0 \in \mathbb{R}^n_{>0}$$

reaches the boundary of the positive orthant at some time t^*. Then there exists an index i such that

$$N_i(t^*) = 0.$$

Hence the state $\mathbf{N}(t^*)$ belongs to the invariant hyperplane H_i. The solution entirely contained in H_i and passing through $\mathbf{N}(t^*)$ is therefore a valid solution of the DD system.

Since the vector field is smooth, the *Cauchy–Lipschitz theorem* guarantees existence and uniqueness of solutions. Consequently, two distinct trajectories cannot pass through the same point in phase space. The trajectory originating from $\mathbf{N}_0$ would therefore have to coincide with the one lying entirely in H_i, contradicting the fact that $N_i(0) > 0$.

Therefore no component can vanish or become negative in finite time, and the positive orthant $\mathbb{R}^n_{>0}$ is positively invariant. □

The GLV model of Eq. (2.1) satisfies the assumptions of Lemma 1. Indeed,

$$F_i(\mathbf{N}) = N_i \left(r_i + \sum_{j=1}^{n} a_{ij} N_j \right)$$

is a polynomial vector field, hence F_i is smooth on $\mathbb{R}^n$ and $N_i = 0 \implies F_i(\mathbf{N}) = 0$. Therefore the positive orthant is invariant for the GLV dynamics.

While Proposition 1 ensures that population densities remain non-negative, it does not prevent the mathematical possibility of unbounded growth ($N_i \to +\infty$). In natural systems, finite environmental resources dictate that populations must remain bounded; therefore, diverging dynamics represent an unphysical regime of the model [5].

In the Generalized Lotka-Volterra framework, boundedness is tied to the properties of the interaction matrix $\mathbf{A}$. In Section 2.2 we will discuss the assumptions on interactions used in this thesis and in particular in Subsection 2.2.4 we will discuss under which conditions the diverging dynamics is prevented.

2.1.2 Equilibria of the GLV model

The equilibrium points of the system are obtained by imposing

$$\frac{dN_i}{dt} = 0, \qquad i = 1, \dots, n.$$

Not all equilibrium points are biologically meaningful. An equilibrium is said to be ***feasible*** if

$$\mathbf{N}^* \in \mathbb{R}^n_{\geq 0}.$$

Feasible equilibria lying in the interior of the positive orthant satisfy

$$\mathbf{N}^* \in \mathbb{R}^n_{>0},$$

and are called *interior equilibria*, whereas feasible *boundary equilibria* possess one or more zero components

$$N_i^* = 0$$

and are thus located on the boundary of the positive orthant.

By the positive invariance property established in Proposition 1, trajectories starting from strictly positive initial conditions can only converge to feasible equilibria. Moreover, under the interaction assumptions introduced in Subsection 2.2.4, divergent trajectories are excluded, so feasible equilibria are the only asymptotic states accessible from the positive orthant.

Lemma 2 (Interior equilibrium of the GLV model)**.** *Let* $\mathbf{A}$ *be invertible. Then the GLV system* (2.1) *admits at most one interior equilibrium. Such an equilibrium necessarily satisfies*

$$\mathbf{A}\mathbf{N}^* = -\boldsymbol{r}, \tag{2.5}$$

or equivalently

$$\mathbf{N}^* = -\mathbf{A}^{-1}\boldsymbol{r}.$$

Proof. At equilibrium one has

$$0 = N_i^* \left(r_i + \sum_{j=1}^{n} a_{ij} N_j^* \right), \qquad i = 1, \dots, n.$$

For an interior equilibrium, by definition

$$N_i^* > 0, \qquad i = 1, \dots, n,$$

and therefore

$$r_i + \sum_{j=1}^{n} a_{ij} N_j^* = 0, \qquad i = 1, \dots, n.$$

Collecting the equations in vector form yields

$$\mathbf{A}\mathbf{N}^* = -\boldsymbol{r}.$$

Since $\mathbf{A}$ is invertible, the solution is unique and is given by

$$\mathbf{N}^* = -\mathbf{A}^{-1}\boldsymbol{r}.$$

□

The invertibility of the interaction matrix $\mathbf{A}$ is not guaranteed in general. When $\mathbf{A}$ is singular, the equilibrium equation (2.5) may admit either no solution or infinitely many solutions. In such cases, generalized inverses, most notably the *Moore–Penrose pseudoinverse*, can be employed to characterize the set of admissible equilibria.

It is worth noting that, even when $\mathbf{A}$ is invertible, the equilibrium satisfying (2.5) is not necessarily feasible. In such cases, the equilibrium has no biological interpretation, despite being mathematically well-defined.

Besides the possible interior equilibrium, the GLV model generally admits boundary equilibria. Indeed, for any subset of species one may impose

$$N_i = 0$$

for all species belonging to that subset. Since the hyperplanes

$$H_i = \{\mathbf{N} \in \mathbb{R}^n : N_i = 0\}$$

are invariant under the dynamics (Lemma 1), the remaining species evolve according to a reduced GLV system,

$$\frac{dN_i}{dt} = N_i \left(r_i + \sum_{j=1}^{m} a_{ij}^{\text{red}} N_j \right), \qquad i = 1, \dots, m,$$

where $\mathbf{A}_{\text{red}}$ denotes the interaction matrix obtained by removing the rows and columns corresponding to extinct species.

Whenever $\mathbf{A}_{\text{red}}$ is invertible, the corresponding equilibrium satisfies

$$\mathbf{A}_{\text{red}} \mathbf{N}_{\text{red}}^* = -\boldsymbol{r}_{\text{red}},$$

namely

$$\mathbf{N}_{\text{red}}^* = -\mathbf{A}_{\text{red}}^{-1} \boldsymbol{r}_{\text{red}}.$$

Since each species can be either present or extinct, there exist at most 2^n distinct equilibrium supports, including the trivial equilibrium $\mathbf{N}^* = \mathbf{0}$.

The existence of feasible boundary equilibria has an important biological implication. By Lemma 1, trajectories starting in the positive orthant cannot reach the boundary in finite time. Nevertheless, a species abundance may satisfy

$$N_i(t) > 0 \qquad \forall t < \infty,$$

while

$$\lim_{t \to \infty} N_i(t) = 0.$$

Consequently, within the deterministic GLV framework, extinction corresponds to the limit

$$N_i(t) \to 0 \qquad \text{as} \qquad t \to \infty.$$

In practice, however, once the abundance becomes sufficiently small, the assumptions underlying the GLV model cease to be valid, and finite-population effects should be taken into account. In the numerical simulations presented in Chapter 4 we introduce an extinction treshold: whenever the abundance of a species falls below a prescribed cutoff, it is set to zero and removed from the dynamics.

2.1.3 Logistic model for isolated species

If from Eq. (2.1) we reduce to the case of an isolated species ($N_j = 0$ for $j \neq i$), the dynamics reduce to a *logistic form*

$$\frac{dN_i}{dt} = N_i(r_i - d_i N_i), \tag{2.6}$$

where $a_{ii} = -d_i < 0$. The isolated species has equilibrium corresponding to its *carrying capacity*

$$N_i^* = \frac{r_i}{d_i}.$$

The logistic dynamics exhibit a simple monotonic behavior determined by the sign of the growth term. Indeed, Eq. (2.6) implies that

$$\frac{dN_i}{dt} \begin{cases} > 0, & \text{if } 0 < N_i < r/d, \\ = 0, & \text{if } N_i = r/d, \\ < 0, & \text{if } N_i > r/d. \end{cases}$$

Therefore, solutions with initial condition $N_i(0) < r/d$ increase monotonically toward the carrying capacity, while solutions with $N_i(0) > r/d$ decrease monotonically toward it. In particular, for the Cauchy-Lipschitz theorem (see proof of Proposition 1) the carrying capacity cannot be crossed by any trajectory, and every solution satisfies the bound

$$N_i(t) \leq \max\left\{N_i(0), \frac{r}{d}\right\}, \qquad \forall\, t \geq 0. \tag{2.7}$$

2.2 Interactions

This section presents the parametrization of the interaction matrix and the assumptions adopted to model the competitive interaction regime. The implications, advantages, and limitations of these assumptions are also discussed.

2.2.1 Interaction matrix as a Hadamard product

In order to characterize the interaction matrix $\mathbf{A}$, it is useful to separate the biological properties of species interactions from the structural organization of the ecological network.

This can be achieved by expressing $\mathbf{A}$ as the *Hadamard* (entrywise) *product* of two matrices:

$$\mathbf{A} = \mathbf{W} \circ \mathbf{K}, \tag{2.8}$$

where $\mathbf{W}$ is the ***weight matrix*** and $\mathbf{K}$ is the ***adjacency matrix***.

The matrix $\mathbf{W}$ encodes the biological properties of the interactions, namely their strength and sign. The matrix $\mathbf{K}$ has binary entries,

$$K_{ij} \in \{0, 1\},$$

and its entries specifies whether species j directly interacts with species i, thereby determining the structure of the ecological network.

This decomposition allows us to study separately the effects of interaction strengths and network structure on community equilibria and dynamics.

Here, uppercase letters denote random variables, while lowercase letters denote their specific realizations. Therefore, for interspecific interactions ($i \neq j$), a realization of the matrix satisfies

$$a_{ij} = w_{ij}k_{ij}$$

In contrast, self-interactions are not treated as random variables. Since self-regulation must always be present and have a negative effect (see comment on Eq. (2.1)), we impose the diagonal entries separately by setting

$$W_{ii} = -d_i < 0, \qquad K_{ii} = 1 \implies A_{ii} = -d_i.$$

In this section, we discuss the assumptions adopted for the weight matrix **W** and for the remaining parameters governing species growth and interactions. The ecological structures considered for **K** are presented in Section 2.3.

2.2.2 The random interaction hypothesis

In principle, a complete characterization of a GLV model requires the specification of all interaction coefficients A_{ij}. For large ecological communities this task is generally impossible, as empirical information on every pairwise interaction is rarely available [1].

To overcome this difficulty, Robert May [6] proposed in 1972 a statistical approach in which interaction coefficients are treated as random variables. This idea was inspired by earlier developments in nuclear physics, where random matrices had been successfully employed by Wigner [7, 8] to describe the statistical properties of energy levels in heavy atomic nuclei. His complete argument is reported in Subsection 3.1.

Following May's approach, we assume that the entries of the weight matrix are independently sampled from a probability distribution

$$W_{ij} \sim \rho(\mu, \sigma^2)$$

with finite mean μ and finite variance σ^2.

Under this assumption, the interaction matrix becomes a random matrix, allowing the application of methods from random matrix theory and statistical physics [9, 10]. This setting is widely used because it keeps large-N analysis tractable while obatining general analytical results.

However, empirical-network studies caution that random matrices can misrepresent real ecosystems: for instance, James et al. [11] noted that, across 21 empirically derived community matrices, observed systems were more stable by orders of magnitude than comparable random constructions, and the discrepancy reflected biologically structured interaction strengths (encoded in matrix **W** in our framework) more than simple topology alone (described by matrix **K** in our framework) .

In our work, we choose the **Gaussian distribution** to sample the coefficients of the weight matrix:

$$W_{ij} \sim \mathcal{N}(\mu, \sigma^2) \tag{2.9}$$

However, in the large-n limit, the characterization of the interaction matrix spectrum that we will perform is expected to be independent of this particular choice. This follows from universality results in random matrix theory due to Tao, Vu et al. [12, 13], which show that the asymptotic spectral properties of random matrices are largely determined by the first two moments of the entries, under mild regularity conditions (in particular, sufficiently fast decay of higher-order moments) [14]. Hence, after proper centering and rescaling, ensembles with non-Gaussian entries share the same asymptotic spectral behavior as the Gaussian case.

2.2.3 Parameter normalization: assumptions and caveats

In the following analysis of the GLV model (2.1), we assume that all species share the **same intrinsic growth rate** and the **same intraspecific interaction strength**:

$$r_i = r, \qquad W_{ii} = -d, \qquad i = 1, \dots, n.$$

Considering Eq. (2.6), the assumption $r_i = r$ corresponds to a homogeneous community in which all species have the same fitness if isolated in the environment. This simplification is commonly adopted in theoretical studies for analytical tractability ([15], e.g. [16–19]). This choice is analitically convenient and it is useful for some of the analytical results derived in the following chapters (e.g. the feasibility treshold for fully connected networks, Proposition 16), but it suppresses biologically meaningful variation among species and therefore should be understood as a modeling idealization rather than an empirical claim [11].

The condition $W_{ii} = -d$ imposes identical self-regulation across species. The negative sign ensures bounded growth in the absence of interspecific interactions (Eq. (2.6)). Given (2.8), in combination with $K_{ii} = 1$ it implies

$$A_{ii} = -d.$$

This assumption corresponds to May's hypothesis of homogeneous intraspecific interactions [6] and is widely used in random GLV models (e.g. [17–20]). It yields a diagonal contribution proportional to the identity matrix for the interaction matrix $\mathbf{A}$, which substantially simplifies the analysis of feasibility and stability properties we will carry on in Section 3.

Evidence on diagonal heterogeneity suggests that the equal-diagonal assumption is often acceptable only in a restricted sense. A recent review [9] summarizes Tang et al. results [21] as showing that moderate variance in diagonal terms has limited effects on stability, but large variance can matter depending on how self-regulation covaries with network interspecific interactions. Furthermore, when diagonal variability is introduced in empirically inferred community matrices, stability can be significantly reduced [11].

Further empirical evidence demonstrates that, for instance, introduced and invasive plant populations frequently exhibit significantly reduced intraspecific competition

compared to native populations of the same species, suggesting that self-limitation can shift rapidly depending on biogeographical and ecological contexts [22].

The parameters r and d set the scales of time and abundance, respectively. By **rescaling time and abundance variables**, one can set

$$r = 1, \qquad d = 1.$$

This is a standard nondimensionalization and, unless otherwise stated, it will be used throughout the thesis.

The ODE associated with the model (Eq. 2.1) considered in this thesis is therefore

$$\frac{dN_i}{dt}(t) = N_i(t)\left(1 + \sum_{j=1}^{n} a_{ij}N_j\right) \tag{2.10}$$

while the equation for the internal equilibrium given by Eq. (2.5) considered is

$$\mathbf{A}\mathbf{N}^* = -\mathbf{1}_n \tag{2.11}$$

where $\mathbf{1}_n$ is the all-ones $n \times 1$ column vector.

2.2.4 Strength and sign of interactions

In this work, we focus exclusively on **competitive communities**, implying that all interspecific interaction coefficients are non-positive ($A_{ij} \leq 0$ for $i \neq j$), implying that we extract the interaction coefficients W_{ij} of Eq. (2.9) from a normal distribution with negative mean

$$\mu = -c, \qquad 0 < c < 1.$$

Given the normalization framework established in Section 2.2.3, where intraspecific regulation is fixed to $A_{ii} = -1$, this parameterization enforces the condition that, on average, **intraspecific competition is stronger than interspecific competition** ($|W_{ii}| > |W_{ij}|$).

This structural choice is grounded in empirical literature showing that stronger self-limitation relative to interspecific effects is a primary stabilizing mechanism that permits species coexistence. However, this assumption constitutes a statistical idealization of natural systems, which exhibit profound variance in diagonal and off-diagonal terms [23].

While acknowledging this empirical heterogeneity, maintaining $A_{ii} = -1$ while constraining the mean interspecific intensity to $c < 1$ provides a necessary analytical baseline to investigate the feasibility and stability thresholds of the system under globally dominant self-limitation.

We now comment on how the assumptions introduced in this section for the interaction matrix $\mathbf{A}$ can prevent the unrealistic unbounded-growth behavior discussed in Subsection 2.1.1.

Specifically, the assumption of strict intraspecific self-regulation ($A_{ii} = -d = -1$), if paired with purely competitive interspecific interactions ($a_{ij} \leq 0$ for $i \neq j$), ensures

that the per-capita growth rate is always bounded above by the isolated logistic growth rate of Eq. (2.6). For any species i in the positive orthant,

$$\frac{dN_i}{dt} = N_i\left(r - dN_i + \sum_{j\neq i} a_{ij}N_j\right) \leq N_i(r - dN_i).$$

By the standard comparison theorem for differential equations (see Basic Comparison Theorem in [24], with $u(t) = N_i(t)$, $v(t)$ the solution of $v' = v(r - dv)$ satisfying $v(0) = N_i(0)$ and $f(x) = x(r - dx)$), it follows that $N_i(t) \leq v_i(t)$ for alla $t \geq 0$. Since the logistic solution satisfies Eq. (2.7), we conclude that

$$N_i(t) \leq \max(N_i(0), r/d) = \max(N_i(0), 1)$$

under our normalization hypothesis (Subsection 2.2.3).

However, if the variance of the interspecific interactions is sufficiently large, positive interaction coefficients may still arise with non-negligible probability. The resulting positive feedback loops can overcome the stabilizing effect of intraspecific self-regulation, leading to trajectories that diverge. Consequently, avoiding unbounded growth requires constraints not only on the mean interaction strength but also on the variance of the interaction matrix $\mathbf{A}$.

In the following, we restrict our numerical analysis to representative values of the interaction parameters (c, σ) lying well within the bounded region of the phase diagram. As shown in Figure 4.1, the two parameter sets considered throughout this thesis are both far from the analytically predicted unbounded-growth region derived by Bunin [25], ensuring that all reported numerical results correspond to bounded dynamical regimes.

2.3 Structure

In this section, we characterize the adjacency matrix $\mathbf{K}$ introduced in Subsection 2.2.1, which determines the topology of the ecological network through (2.8).

In particular, we focus on two structural properties of the network: ***connectance*** C and ***modularity*** Q. Connectance quantifies the fraction of possible pairwise interactions that are present in the network, while modularity measures the extent to which species are organized into groups with dense internal interactions and comparatively sparse interactions between groups.

These quantities allow us to construct interaction networks that depart systematically from an unstructured random topology. In the following sections, we introduce the network ensembles considered in this thesis and describe how their structural properties are controlled through C and Q.

The main objective of this work will be to investigate how variations in network structure affect the equilibria properties and dynamical behaviour of the GLV model.

2.3.1 Random network: Erdős–Rényi ensemble

The topological baseline used to generate the interaction matrices is a *directed Erdős–Rényi random graph* $D(n, C)$. It consists of n nodes, where each ordered pair (i, j)

with $i \neq j$ is connected independently with probability C.

In this framework, C is the ***connectance*** of the interaction network. The adjacency matrix $\mathbf{K}$, with entries $K_{ij} \in \{0, 1\}$, is defined by

$$\mathbb{P}(K_{ij} = 1) = C, \qquad \mathbb{P}(K_{ij} = 0) = 1 - C, \qquad i \neq j.$$

Thus, for $i \neq j$, the entries K_{ij} are independent *Bernoulli random variables*. In particular, K_{ij} and K_{ji} are generated independently, so that in general $K_{ij} \neq K_{ji}$. The resulting interaction network is therefore directed.

We additionally impose

$$K_{ii} = 1,$$

to ensure that intraspecific interactions are always present, coherently to what discussed in Subsection 2.2.1. These diagonal entries are treated separately from interspecific links.

Because we adopt the convention that K_{ij} denotes an interaction exerted by species j on species i, the number of interspecific interactions received by species i is its *in-degree*,

$$K_i^{\text{in}} = \sum_{j \neq i} K_{ij}.$$

Since K_i^{in} is the sum of $n-1$ independent Bernoulli variables with success probability C, it follows a binomial distribution:

$$K_i^{\text{in}} \sim \text{Bin}(n - 1, C).$$

Therefore,

$$\mathbb{P}\left(K_i^{\text{in}} = k\right) = \binom{n-1}{k} C^k (1 - C)^{n-1-k}, \qquad k = 0, \ldots, n - 1.$$

Its mean and variance are

$$\mathbb{E}\left[K_i^{\text{in}}\right] = (n - 1)C, \qquad \text{Var}\left(K_i^{\text{in}}\right) = (n - 1)C(1 - C).$$

If C is kept fixed while n increases, then

$$\mathbb{E}\left[K_i^{\text{in}}\right] \simeq nC \to \infty.$$

Hence, the average number of interactions per node increases with system size, and the network becomes progressively denser.

Because all ordered pairs of species interact with the same probability, the directed Erdős–Rényi ensemble does not impose any community structure. It is therefore used as a null model without prescribed modular organization ($Q = 0$).

2.3.2 Bipartite structure: modular parametrization

To introduce internal structure in the interaction network, we consider an ecosystem composed of at most two subsystems, hereafter referred to as modules, which represents communities. The resulting network is described by a ***stochastic two-block model*** [15].

Let $\alpha \in (0, 1/2]$ denote the fraction of species assigned to the first module. The module sizes are

$$n_1 = \lfloor \alpha n \rfloor, \qquad n_2 = n - n_1. \tag{2.12}$$

The adjacency matrix $\mathbf{K}$ is then partitioned into two diagonal blocks $\mathbf{K}_{rr}$, representing within-module interactions, and two off-diagonal blocks $\mathbf{K}_{rs}$, representing between-module interactions, with block indexes $r, s \in \{1, 2\}$. Explicitly:

$$\mathbf{K} = \begin{bmatrix} \mathbf{K}_{11} & \mathbf{K}_{12} \\ \mathbf{K}_{21} & \mathbf{K}_{22} \end{bmatrix}.$$

Let $\mathcal{M}_r$ denote the set of species belonging to module r, with $r \in \{1, 2\}$. We indicate with E_{rs} the number of links connecting any node in module r to any node in module s

$$E_{rs} = \sum_{i \in \mathcal{M}_r} \sum_{j \in \mathcal{M}_s} K_{ij},$$

while $E = \sum_{r,s=1}^{2} E_{rs}$ is the total number of links in the network. We can define the expected fraction of links from module r to module s

$$e_{rs} := \frac{\mathbb{E}[E_{rs}]}{\mathbb{E}[E]}, \tag{2.13}$$

while the expected fraction of link ends attached to module r is defined as

$$a_r := \sum_{s=1}^{2} e_{rs}. \tag{2.14}$$

Modularity quantifies the excess of within-module links relative to the expectation under a random null model, such as the Erdős–Rényi model discussed in Subsection 2.3.1. Following Newman [26],

$$Q = \sum_{r} \left(e_{rr} - a_r^2 \right), \tag{2.15}$$

The interpretation for parameter Q is clarified by the following result.

Lemma 3. *For the Erdős–Rényi model, $e_{rr} = a_r^2$ in expectation, and consequently $\mathbb{E}[Q] = 0$.*

Proof. In the Erdős–Rényi model the connection probability is the same, C, for every ordered pair of species. Using the definition in Eq. (2.13), we therefore have

$$e_{rs} = \frac{C\, n_r n_s}{C\, n^2} = \frac{n_r n_s}{n^2},$$

where n_r, n_s are the module sizes (Eq. (2.12)) for $r, s, \in \{1, 2\}$. Explicitly

$$e_{11} = \frac{n_1^2}{n^2} = \alpha^2 \qquad e_{12} = \frac{n_1 n_2}{n^2} = \alpha(1-\alpha)$$

and thus, using the definition in Eq. (2.14),

$$a_1 = e_{11} + e_{12} = \alpha.$$

Proceeding analogously

$$a_2 = 1 - \alpha.$$

Hence $e_{11} = a_1^2$, $e_{22} = a_2^2$, and $Q = 0$. □

Following [27], we introduce two connection probabilities: C_{in} for pairs of species belonging to the same module, and C_{out} for pairs belonging to different modules. Their definitions are analogous to the global connectance one for the Erdős–Rényi graph (Subsection 2.3.1), namely the probability of non-zero within-module and between-module interactions. Given the two-block structure for the adjacency matrix of Eq. (2.3.2)

$$\mathbb{P}(K_{ij} = 1) = \begin{cases} C_{\text{in}} & \text{if } i, j \in \mathcal{M}_r \\ C_{\text{out}} & \text{if } i \in \mathcal{M}_r, j \in \mathcal{M}_s \text{ and } r \neq s \end{cases} \qquad 0 < C_{\text{in}}, C_{\text{out}} \leq 1, \tag{2.16}$$

where $r, s \in \{1, 2\}$ are the block indexes and $\mathcal{M}_r$ denotes the set of species belonging to module r.

Therefore, the expected block edge counts are

$$\mathbb{E}[E_{11}] = C_{\text{in}} n_1^2, \qquad \mathbb{E}[E_{22}] = C_{\text{in}} n_2^2, \qquad \mathbb{E}[E_{12}] = \mathbb{E}[E_{21}] = C_{\text{out}} n_1 n_2, \tag{2.17}$$

Proposition 4. *Let*

$$\beta := \alpha^2 + (1-\alpha)^2. \tag{2.18}$$

For the global connectance C to be preserved, it must be

$$\beta C_{\text{in}} + (1-\beta) C_{\text{out}} = C. \tag{2.19}$$

Proof. Starting from (2.17) the global expected counts are

$$\mathbb{E}[E] = C_{\text{in}}(n_1^2 + n_2^2) + 2C_{\text{out}} n_1 n_2.$$

Dividing for n^2 and using $n_1 = \alpha n$, $n_2 = (1-\alpha)n$:

$$\frac{\mathbb{E}[E]}{n^2} = C_{\text{in}} \left(\alpha^2 + (1-\alpha)^2\right) + 2C_{\text{out}} \alpha(1-\alpha).$$

Defining

$$\beta := \alpha^2 + (1-\alpha)^2$$

completes the proof, because $1 - \beta = 2\alpha(1-\alpha)$ and by definition $\frac{\mathbb{E}[E]}{n^2} = C$. □

Internal and external connectance are parametrized respectively as

$$C_{\text{in}} = C\left(1 + \frac{Q}{\beta}\right), \qquad C_{\text{out}} = C\left(1 - \frac{Q}{1-\beta}\right),$$

where β is given by Eq. (2.18). It is easy to demonstrate that this choice respects (2.19).

The admissible values of Q are constrained by the requirements

$$0 \leq C_{\text{in}} \leq 1, \qquad 0 \leq C_{\text{out}} \leq 1.$$

Substituting in (2.3.2), one obtain the conditions

$$Q_{\min} = \max\left\{-\beta, -(1-\beta)\left(\frac{1}{C} - 1\right)\right\} \qquad Q_{\max} = \min\left\{1-\beta, \beta\left(\frac{1}{C} - 1\right)\right\}. \tag{2.20}$$

These bounds depend on both the module-size asymmetry α and the global connectance C.

Throughout this work we restrict to **balanced modules**,

$$\alpha = \frac{1}{2}, \qquad n_1 = n_2 = \frac{n}{2}.$$

For balanced modules, internal and external connectance are parametrized respectively as

$$C_{\text{in}} = C(1 + 2Q), \qquad C_{\text{out}} = C(1 - 2Q).$$

Under this assumption, complete separation between the two modules, $C_{\text{out}} = 0$, corresponds to $Q = 1/2$. Thus, this convention is not normalized to have maximum modularity equal to one.

Three topological regimes can be distinguished:

- **Modular regime ($Q > 0$).** Here $C_{\text{in}} > C_{\text{out}}$, so interactions are more likely within modules than between them.
- **Neutral regime ($Q = 0$).** Here $C_{\text{in}} = C_{\text{out}} = C$, recovering the directed Erdős–Rényi ensemble.
- **Anti-modular regime ($Q < 0$).** Here $C_{\text{in}} < C_{\text{out}}$, so interactions are more likely between modules than within them.

Note that, even for modules of the same size, the parametrization is not symmetrical. A system described by Q is not topologically equivalent to one described by $-Q$. This asymmetry arises because the main diagonal of the adjacency matrix $\mathbf{K}$, which represents species self-regulation (K_{ii}), is always contained within the diagonal blocks and is therefore structurally constrained to depend on C_{in}.

For the directed version of the model used in this work, each entry K_{ij} with $i \neq j$, is sampled independently according to Eq. (2.16). The diagonal condition $K_{ii} = 1$ is imposed separately.

To sum up the hypothesis for the interaction matrix (2.8) used in this work, as discussed in this Section and in Section 2.2:

$$W_{ii} = -1, \qquad W_{ij} \sim \mathcal{N}(-c, \sigma^2), \tag{2.21}$$

$$K_{ii} = 1, \qquad \mathbb{P}(K_{ij} = 1) = \begin{cases} C_{\text{in}}, & \text{if species } i \text{ and } j \text{ belong to the same module,} \\ C_{\text{out}}, & \text{otherwise,} \end{cases} \tag{2.22}$$

and $A_{ij} = W_{ij} k_{ij}$ are the entries of the interaction matrix.

3

Equilibrium points analysis

In this chapter, we investigate the effects of the structural parameters C and Q on the local stability of equilibrium points in the generalized Lotka–Volterra model with competitive interactions. We begin by reviewing the classical results obtained through random matrix theory, thereby motivating the relevance of this approach and discussing its limits. We then employ these tools to characterize the spectral properties of the interaction matrix $\mathbf{A}$, and interpret the results of Monte Carlo simulations in light of the corresponding theoretical predictions.

3.1 Classic result: complexity inhibits stability

In his seminal work [6, 28], Robert May used random matrix theory to study the local stability of equilibria in ecological systems under general assumptions. In this section, we review the hypotheses and results of this classical argument, which motivated a large body of literature in theoretical ecology. Later, we will extend this spectral approach to our specific setting.

3.1.1 May's model hypothesis

May's analysis is *model-independent*: its conclusions apply to a broad class of systems governed by ordinary differential equations of the form

$$\frac{dN_i}{dt} = f_i(N_1, \dots, N_n), \qquad i = 1, \dots, n, \tag{3.1}$$

or, in vector form,

$$\frac{d\mathbf{N}}{dt} = \mathbf{f}(\mathbf{N}),$$

where the vector field $\mathbf{f} : \mathbb{R}^n_{\geq 0} \to \mathbb{R}^n_{\geq 0}$ generally describes nonlinear interactions among species.

May's argument relies on three strong assumptions, which became standard in classical theoretical ecology. Its argument can be described as following [15]:

Hypothesis 1: existence of an equilibrium. *Species abundances are assumed to be close to a dynamical equilibrium*

$$\mathbf{N}^* = (N_1^*, \dots, N_n^*) \tag{3.2}$$

such that

$$\mathbf{f}(\mathbf{N}^*) = 0.$$

Consider a small perturbation $\mathbf{x}(t) = (x_1(t), \dots, x_n(t))$, such that

$$N_i(t) = N_i^* + x_i(t), \qquad |x_i| \ll 1.$$

Assuming that $\mathbf{f}$ is continuously differentiable in a neighborhood of $\mathbf{N}^*$, we can expand f_i to first order around $\mathbf{N}^*$:

$$f_i(\mathbf{N}^* + \mathbf{x}) = f_i(\mathbf{N}^*) + \sum_{j=1}^{n} \left.\frac{\partial f_i}{\partial N_j}\right|_{\mathbf{N}^*} x_j + O(\|\mathbf{x}\|^2).$$

Since $\frac{dN_i}{dt} = \frac{dx_i}{dt}$ and $f_i(\mathbf{N}^*) = 0$, the linearized dynamics are

$$\frac{d\mathbf{x}}{dt} = \mathbf{S}\mathbf{x}. \tag{3.3}$$

Here $\mathbf{S} = (S_{ij})$ is the Jacobian matrix evaluated at $\mathbf{N}^*$, whose entries are

$$S_{ij} = \left.\frac{\partial f_i}{\partial N_j}\right|_{\mathbf{N}^*}.$$

In ecology, $\mathbf{S}$ is called the ***community matrix*** [29].

Hypothesis 2: random sparse interspecific interactions. *Interspecific interactions are assumed to be sufficiently complex to be modelled as random Bernoulli variables.*

This is coherent with assumption discussed in Subsection 2.2.2 for the GLV model and will also be central to our analysis. The relation between $\mathbf{S}$ and the interaction matrix $\mathbf{A}$ defined for the GLV model will be discussed in Subsection 3.2.1.

Since S_{ij} represents, in sign and magnitude, the effect of a perturbation of species j on the growth rate of species i about the equilibrium point $\mathbf{N}^*$, May assumes that its off-diagonal entries are independently drawn from a fixed distribution:

$$W_{ij} \sim \rho(0, \sigma^2), \qquad K_{ij} = \begin{cases} 1, & \text{with probability } C, \\ 0, & \text{with probability } 1 - C, \end{cases} \qquad S_{ij} = W_{ij}K_{ij}.$$

where C is the connectance introduced in Subsection 2.3.1. This parametrization does not account for internal structure, therefore it represents a Erdős-Rényi graph with $Q = 0$.

May also works in the **neutral interactions regime**, imposing $\mu = 0$. In Section 3.2 we discuss the expansion of this framework to the competitive interaction regime for the GLV model.

Hypothesis 3: identical intraspecific interactions. *Intraspecific interactions are assumed to be identical for all species.*

Since S_{ii} represents the self-regulation of species i, May sets

$$W_{ii} = -1, \qquad K_{ii} = 1 \implies S_{ii} = -1, \qquad i = 1, \dots, n.$$

This is the same assumption discussed in Subsection 2.2.3 for the interaction matrix $\mathbf{A}$ of the GLV model.

3.1.2 Preliminary notions: local stability and Lyapunov method

We are interested in the response of the system to small perturbations around $\mathbf{N}^*$ of Eq. (3.2), and in particular in characterizing whether such perturbations decay in time: we refer to this property as *local stability* of $\mathbf{N}^*$.

Let $\|\cdot\|$ denote a norm in $\mathbb{R}^n$. We can enunciate more precise definitions relating to local stability.

Definition 5 (Lyapunov stability)**.** *The equilibrium* $\mathbf{N}^*$ *is said to be* Lyapunov stable *if for every* $\varepsilon > 0$ *there exists* $\delta = \delta(\varepsilon) > 0$ *such that*

$$\|\mathbf{N}(t_0) - \mathbf{N}^*\| < \delta \quad \Rightarrow \quad \|\mathbf{N}(t) - \mathbf{N}^*\| < \varepsilon \quad \forall t \geq t_0.$$

This notion ensures that trajectories starting sufficiently close to the equilibrium remain close for all future times, but it does not imply convergence.

Definition 6 (Asymptotic stability)**.** *The equilibrium* $\mathbf{N}^*$ *is* asymptotically stable *if it is Lyapunov stable and there exists* $\delta > 0$ *such that*

$$\|\mathbf{N}(t_0) - \mathbf{N}^*\| < \delta \quad \Rightarrow \quad \lim_{t\to\infty} \mathbf{N}(t) = \mathbf{N}^*.$$

Asymptotic stability corresponds to the case where perturbations decay to zero as time goes to infinity. The definition does not specify the rate of convergence.

We now consider the linearized dynamics obtained in Eq. (3.3). The *Lyapunov indirect method* relates local stability of the nonlinear system to the spectral properties of the Jacobian matrix.

Proposition 7 (Lyapunov indirect method for local stability)**.** *Let* $\mathbf{S}$ *be the Jacobian matrix evaluated at* $\mathbf{N}^*$*. The equilibrium* $\mathbf{N}^*$ *is locally asymptotically stable if and only if for the eigenvalues of* $\mathbf{S}$ *the* spectral abscissa

$$\Lambda(\mathbf{S}) := \max_i \Re(\lambda_i(\mathbf{S})) \tag{3.4}$$

satisfies

$$\Lambda < 0.$$

In this case, perturbations of the linearized system decay exponentially in time. The eigenvalues of $\mathbf{S}$ determine the local behavior of the dynamics and will be referred to as the *spectrum* of the community matrix.

This result shows that **local stability is fully characterized by the spectrum of the Jacobian** (community matrix), which will be analyzed in the following section using random matrix theory. We emphasize that this approach characterizes uniquely the behavior of trajectories that originate sufficiently close to the equilibrium point $\mathbf{N}^*$ (i.e., under sufficiently small perturbations).

3.1.3 Circular Law and spectral characterization

Under the assumptions enunciated in Subsection 3.1.1, the community matrix $\mathbf{S}$ has form

$$\mathbf{S} = -\mathbf{I} + \mathbf{B}, \tag{3.5}$$

where $\mathbf{I}$ is the identity matrix while $\mathbf{B}$ is a random interaction matrix with vanishing diagonal. More precisely:

$$B_{ii} = 0,$$

and for $i \neq j$,

$$W_{ij} \sim \rho(0, \sigma^2), \qquad K_{ij} = \begin{cases} 1, & \text{with probability } C, \\ 0, & \text{with probability } 1 - C, \end{cases} \qquad B_{ij} = W_{ij} K_{ij}. \tag{3.6}$$

Proposition 8. *For $i \neq j$, the entries B_{ij} defined in* (3.6) *are random variables with moments*

$$\mathbb{E}[B_{ij}] = 0, \qquad \mathrm{Var}(B_{ij}) = C\sigma^2. \tag{3.7}$$

Proof. By the definition of variance,

$$\mathrm{Var}(B_{ij}) = \mathbb{E}[B_{ij}^2] - \big(\mathbb{E}[B_{ij}]\big)^2.$$

Since $\mathbb{E}[B_{ij}] = 0$, it follows that

$$\mathrm{Var}(B_{ij}) = \mathbb{E}[B_{ij}^2].$$

Moreover, by the definition of B_{ij},

$$\mathbb{E}[B_{ij}^2] = C\mathbb{E}[b_{ij}^2] + (1 - C) \cdot 0 = C\sigma^2.$$

Indeed, since $\mathbb{E}[b_{ij}] = 0$, we have

$$\sigma^2 = \mathrm{Var}(b_{ij}) = \mathbb{E}[b_{ij}^2] - \big(\mathbb{E}[b_{ij}]\big)^2 = \mathbb{E}[b_{ij}^2].$$

□

The spectrum of $\mathbf{B}$ can be characterized starting from a central result in random matrix theory, commonly referred to as the *Circular Law* (see Theorem 2.8.1 in [30]).

Theorem 9 (Circular Law)**.** *Let $\widetilde{\mathbf{B}}$ be an $n \times n$ matrix with independent and identically distributed entries having zero mean and unit variance.*

Then, the empirical spectral measure *of $\hat{\mathbf{B}} = \frac{1}{\sqrt{n}}\widetilde{\mathbf{B}}$, i.e. the probability measure*

$$\mu_{\hat{\mathbf{B}}} := \frac{1}{n} \sum_{j=1}^{n} \delta_{\lambda_j(\hat{\mathbf{B}})},$$

where δ_x denotes the Dirac measure *at x and $\lambda_j(\hat{\mathbf{B}}) \in \mathbb{C}$ is an eigenvalue of $\hat{\mathbf{B}}$, converges almost surely[1] to the uniform probability measure on the unit disk in the complex plane:*

$$\mu_{\mathrm{circ}}(dz) = \frac{1}{\pi} \mathbf{1}_{\{|z| \leq 1\}} \, d^2 z,$$

[1] Convergence *almost surely* refers to convergence with probability one with respect to the underlying probability space.

where d^2z denotes the Lebesgue measure on $\mathbb{C} \simeq \mathbb{R}^2$. Intuitively, the eigenvalues of the normalized matrix $\hat{\mathbf{B}}$ become asymptotically distributed over the unit disk in the complex plane:

$$\{z \in \mathbb{C} : |z| \leq 1\},$$

with eigenvalues spread approximately uniformly over its interior.

Applying this result to $\mathbf{B}$ yields the following asymptotic characterization.

Corollary 10. *In the limit $n \to \infty$, the empirical spectral distribution of $\mathbf{B}$ defined in* (3.6) *converges to the uniform distribution on the disk*

$$\left\{z \in \mathbb{C} : |z| \leq \sigma\sqrt{nC}\right\}.$$

Proof. By Proposition 8, the off-diagonal entries of $\mathbf{B}$ have variance $C\sigma^2$. Define

$$\widetilde{\mathbf{B}} := \frac{1}{\sigma\sqrt{C}}\mathbf{B}.$$

Then the off-diagonal entries of $\widetilde{\mathbf{B}}$ have zero mean and unit variance. Hence, by Theorem 9, the empirical spectral distribution of

$$\hat{\mathbf{B}} := \frac{1}{\sqrt{n}}\widetilde{\mathbf{B}} = \frac{1}{\sigma\sqrt{nC}}\mathbf{B}$$

converges almost surely to the uniform probability measure on the unit disk.

Since the eigenvalues scale linearly under scalar multiplication, the eigenvalues of $\mathbf{B}$ are obtained by multiplying those of

$$\frac{1}{\sigma\sqrt{nC}}\mathbf{B}$$

by $\sigma\sqrt{nC}$. Therefore, the limiting spectral distribution of $\mathbf{B}$ is uniform on the disk

$$\left\{z \in \mathbb{C} : |z| \leq \sigma\sqrt{nC}\right\}.$$

□

Remark. Strictly speaking, Theorem 9 applies to random matrices with i.i.d. entries, whereas the diagonal entries of $\mathbf{B}$ are deterministic, namely $B_{ii} = -1$ for all i. This difference is asymptotically negligible. Although the eigenvalues of non-Hermitian matrices may be highly sensitive to perturbations, the limiting empirical spectral distribution is unchanged under deterministic diagonal perturbations D_n whose operator norm remains uniformly bounded. Since in our case $D_n = -I$, we have $|D_n| = 1$ for every n, and therefore the Circular Law continues to hold in the limit $n \to \infty$ (see, e.g., Remark 1.5 in [31]).

To analyze the spectrum of the community matrix $\mathbf{S}$, we first of all state a general result of interest.

Lemma 11. *Let $\mathbf{B} \in \mathbb{C}^{n\times n}$ and let $d \in \mathbb{C}$. Define*

$$\mathbf{S} = d\mathbf{I} + \mathbf{B}.$$

Then the eigenvalues of $\mathbf{S}$ are obtained by translating those of $\mathbf{B}$:

$$\lambda_i(\mathbf{S}) = d + \lambda_i(\mathbf{B}),$$

while the eigenvectors remain unchanged.

Proof. Let $x \neq 0$ be an eigenvector of $\mathbf{B}$ associated with the eigenvalue λ. Then

$$\mathbf{B}x = \lambda x.$$

Hence,

$$\mathbf{S}x = (d\mathbf{I} + \mathbf{B})x = dx + \lambda x = (d + \lambda)x.$$

Therefore, x is also an eigenvector of $\mathbf{S}$, now associated with the eigenvalue $d + \lambda$. Since every eigenpair of $\mathbf{B}$ gives rise to an eigenpair of $\mathbf{S}$, the spectrum of $\mathbf{S}$ is obtained by shifting the spectrum of $\mathbf{B}$ by d. □

Then the following result follows from Theorem 9:

Corollary 12. *Under the assumptions of Corollary 10, as $n \to \infty$, the empirical spectral distribution of the matrix $\mathbf{S}$ defined in* (3.5) *converges to the uniform distribution over the disk*

$$\left\{z \in \mathbb{C} : |z + 1| \leq \sigma\sqrt{nC}\right\}.$$

Proof. Since

$$\mathbf{S} = -\mathbf{I} + \mathbf{B},$$

Lemma 11 implies that every eigenvalue of $\mathbf{S}$ is obtained from an eigenvalue of $\mathbf{B}$ by translation:

$$\lambda_i(\mathbf{S}) = -1 + \lambda_i(\mathbf{B}).$$

By Corollary 10, as $n \to \infty$ the empirical spectral distribution of $\mathbf{B}$ converges to the uniform distribution over the disk

$$\{z \in \mathbb{C} : |z| \leq \sigma\sqrt{nC}\}.$$

Since adding $-\mathbf{I}$ translates every eigenvalue by -1, the empirical spectral distribution of $\mathbf{S}$ converges to the uniform distribution over the translated disk

$$\{z \in \mathbb{C} : |z + 1| \leq \sigma\sqrt{nC}\}.$$

This proves the claim. □

Figure 3.1 shows that, for sufficiently large systems (here $n = 1000$), the asymptotic predictions for the spectra of both $\mathbf{B}$ and $\mathbf{S}$ are in agreement with the numerical results. As will be shown in the following sections, these analytical predictions remain accurate even for considerably smaller values of n, providing a reliable benchmark for ecosystem sizes of practical interest.

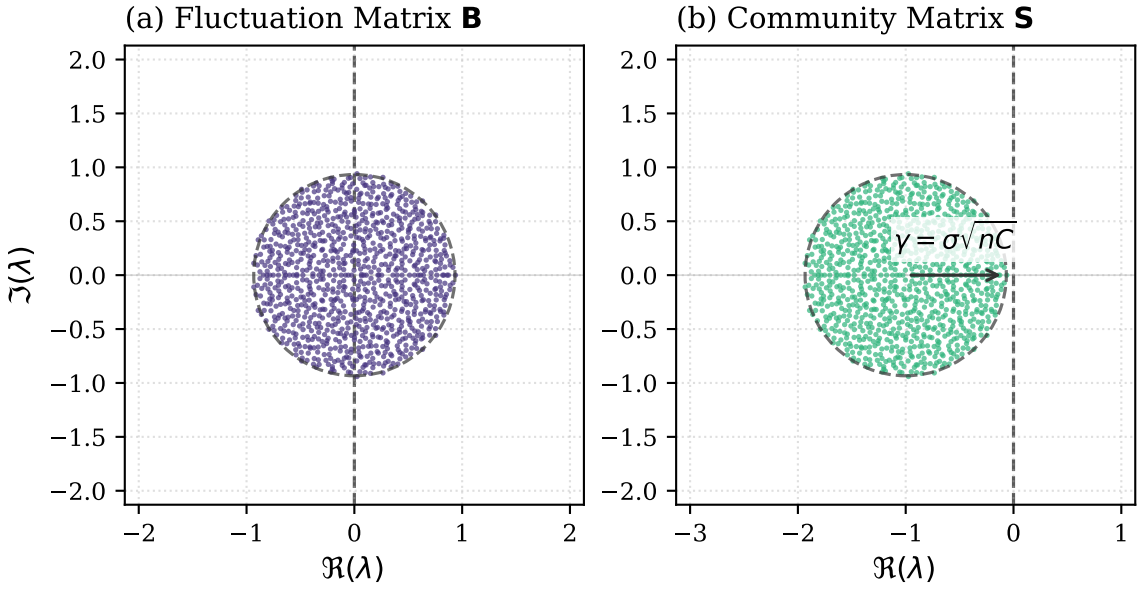

Figure 3.1.. Eigenvalue distribution in the complex plane for (a) the fluctuation matrix **B** (purple) and (b) the community matrix $\mathbf{S} = -\mathbf{I} + \mathbf{B}$ (green) for a system of $n = 1000$ species. We use a normal distribution to extract the weights (W_{ij} in Eq. (3.6)) Parameters are set to $C = 1.0$ and $\sigma = 0.03$, yielding a complexity $\gamma = \sigma\sqrt{nC} \approx 0.95$ (indicated by the arrow in panel b). Dashed circles represent the theoretical boundaries predicted by the Circular Law (Corollary 10 and Corollary 12) with radius γ. The system is locally stable as the entire spectrum of **S** lies in the left half-plane, bounded away from the imaginary axis (vertical dashed line at $\Re(\lambda) = 0$).

3.1.4 Implications and critical discussion

Combining the Lyapunov stability criterion of Proposition 7 with the spectral characterization of the community matrix obtained in Corollary 12, one obtains a condition for local stability in terms of the spectral radius of **S**.

Because the eigenvalues of **S** are asymptotically distributed in a disk centered at -1 with radius $\sigma\sqrt{nC}$, stability requires that this disk lies entirely in the left half of the complex plane, i.e. that its rightmost boundary is negative.

This yields the classical May stability condition:

$$\boxed{\gamma = \sigma\sqrt{nC} < 1} \tag{3.8}$$

We will refer to the parameter γ as ***complexity***, as it simultaneously quantifies system size (n), connectance (C), and interaction variability (σ). In this sense, higher complexity generically reduces the probability of stability in the neutral random interaction model.

We remark that May's result is asymptotic, i.e. it holds for $n \gg 1$. We are therefore interested in studying the reliability of this condition for finite size systems. In Figure 3.2, we perform a Monte Carlo analysis for different system sizes n: for each value of the discretized interval of the complexity parameter γ, an ensemble of 50

randomly generated matrices is considered. The fraction of realizations leading to locally stable equilibria is then computed using the Lyapunov criterion for the community matrices **S** of the form given in Eq. (3.5).

We observe that the stability threshold at $\gamma = 1$ becomes increasingly sharp as n increases, as expected. However, even for relatively small systems ($n = 20$), the threshold remains a good qualitative indicator of the onset of instability.

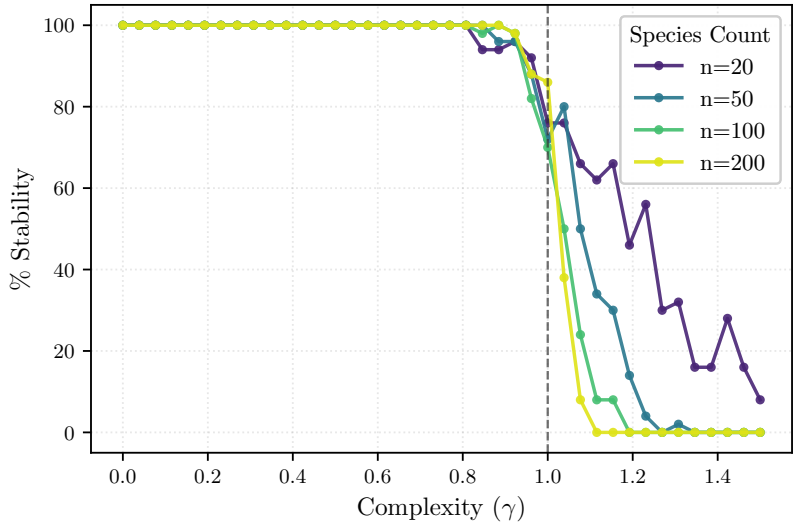

Figure 3.2.. Fraction of locally stable matrices in an ensemble of 50 realizations as a function of the complexity parameter γ, for different system sizes n. For each value of γ, stability is assessed using the Lyapunov criterion applied to the community matrix **S** defined in Eq. (3.5). In this simulation, the scan over γ is obtained by fixing C and n (here $C = 0.8$, with different curves corresponding to different values of n) and varying σ according to the definition in Eq. (3.8); an equivalent parametrization would be obtained by fixing σ and varying C.

Equation (3.8) implies that large, highly connected systems with strong interactions are generically unstable under the assumptions of the neutral random model of Subsection 3.1.1. Stability can only be recovered by reducing connectance or interaction strength, i.e. by approaching a weak-interaction regime.

This result was historically in tension with earlier ecological intuition and observations [1]. The so-called *stability–complexity paradox* remains a central topic in theoretical ecology even if empirical evidence remains mixed, with laboratory microcosms and microbial systems showing different trends depending on the experimental design and underlying constraints [32–34]. A large body of subsequent work has explored how relaxing May's assumptions modifies his conclusions. In particular:

- **Type of interactions.** The original May framework assumes large random interaction matrices with neutral interactions. Subsequent work has shown that different sign structures of interactions play a central role in determining

stability. In particular, predator–prey interactions are generally more stabilizing than purely mutualistic or competitive ones, at fixed system size and connectance [1, 35].

Predator–prey structures can sustain locally stable equilibria even in large and highly connected systems [21, 35], whereas mutualistic and competitive interactions typically reduce the probability of stability under comparable statistical assumptions [1].

Systems with mixed interaction types have also been proposed to stabilize ecological communities, potentially reversing May's complexity–stability relationship under specific modelling assumptions [36]. However, this conclusion has been challenged, with subsequent work showing that the reported stabilization depends critically on the underlying assumptions rather than on interaction diversity itself [37].

- **Violations of randomness: correlations and self-regulation.** A second line of extensions relaxes the Hypothesis 2 of independence and identical distribution of interaction coefficients. In fact, even when population abundances are explicitly included, the asymptotic stability of large communities remains primarily determined by the structure of the interaction matrix [38].

  In this context, correlations between reciprocal interaction strengths have been shown to play a key role in determining stability properties of ecological networks [21], and May's treshold (3.8) has been expanded to include correlation between S_{ij} and J_{ji} . In particular, this correlation structure can be as relevant as the network topology itself in setting stability properties.

  Furthermore, relaxing Hypothesis 3 by modifying the distribution of self-regulation terms – for instance by drawing them from a prescribed distribution [11, 21] or by assuming sublinear self-regulation [39] – can significantly change May's conclusions. In many cases, these extensions restore stability at higher levels of complexity or even reverse the stability–complexity relationship [39].

- **Imposed ecological structure.** A third and broader direction considers deviations from purely random models through the introduction of empirically motivated ecological structure [1, 15].

  Importantly, imposing realistic trophic or ecological structure does not guarantee increased stability: structured networks may even be less stable than random ones if interaction strengths are not appropriately constrained [35].

  In particular, spatial structure and environmental heterogeneity have been explicitly incorporated into ecological networks, showing that they can strongly affect stability and coexistence properties [40–43].

In summary, **no universal complexity–stability relationship exists**, as outcomes depend jointly on interaction type, correlation structure and ecological organization.

3.2 Extension to the competitive GLV model

We now extend the previous analysis to the competitive GLV model. Since the GLV dynamics are density-dependent (i.e. it has functional form given by Eq. (2.3), see Subsection 2.1.1), May's original argument does not apply directly. Nevertheless, under the assumptions introduced in this work, we show that under some additional assumptions the local stability analysis can still be reduced to the spectral analysis of the interaction matrix $\mathbf{A}$. This provides a justification for extending May's random-matrix approach to the competitive GLV setting.

3.2.1 May's result VS density dependent models

The results obtained by May and the associated analytical framework introduced in Section 3.1 apply to models of the form given by Eq. (3.1), in which the absolute growth rate of each species is entirely determined by interspecific interactions.

By contrast, as discussed in Subsection 2.1.1, the GLV model is density dependent and has the general form

$$\frac{dN_i}{dt} = N_i\, g_i(N_1, N_2, \dots, N_n), \qquad i = 1, 2, \dots, n,$$

where the per-capita growth rate is multiplied by the species abundance, introducing a density-dependent term.

For density-dependent systems, the random matrix theory results used by May are not directly applicable [19]. To characterize local stability, we linearize Eq. (2.3) around a feasible equilibrium $\mathbf{N}^*$ by introducing a small perturbation $\mathbf{x}(t)$ such that

$$N_i(t) = N_i^* + x_i(t), \qquad |x_i| \ll 1.$$

Expanding g_i to first order around $\mathbf{N}^*$ gives

$$g_i(\mathbf{N}^* + \mathbf{x}) = g_i(\mathbf{N}^*) + \sum_{j=1}^{n} \left.\frac{\partial g_i}{\partial N_j}\right|_{\mathbf{N}^*} x_j + O(\|\mathbf{x}\|^2).$$

Since $\frac{dN_i}{dt} = \frac{dx_i}{dt}$ and $g_i(\mathbf{N}^*) = 0$, the linearized dynamics become

$$\frac{d\mathbf{x}}{dt} = \mathbf{S}\mathbf{x},$$

as in Eq. (3.3). In this case, however, the community matrix $\mathbf{S} = (S_{ij})$ is given by

$$S_{ij} = N_i^* \left.\frac{\partial g_i}{\partial N_j}\right|_{\mathbf{N}^*}.$$

In particular, the community matrix of the GLV model takes a particularly simple form.

Proposition 13. *For the GLV model in Eq.* (2.1)*, the linearized dynamics around a feasible equilibrium* $\mathbf{N}^*$ *are*

$$\frac{d\mathbf{x}}{dt} = \mathbf{DAx}, \tag{3.9}$$

where $\mathbf{A} = (a_{ij})$ *is a realization of the interaction matrix defined as in Section 2.1, and*

$$\mathbf{D} = \mathrm{diag}(N_1^*, \dots, N_n^*)$$

is the diagonal matrix of equilibrium abundances.

Proof. The GLV model is

$$\frac{dN_i}{dt} = N_i \left(r_i + \sum_{j=1}^{n} a_{ij} N_j \right).$$

Let

$$N_i(t) = N_i^* + x_i(t), \qquad |x_i| \ll 1,$$

where $\mathbf{N}^*$ is a feasible equilibrium. Substituting into the equations gives

$$\frac{dx_i}{dt} = (N_i^* + x_i) \left[r_i + \sum_{j=1}^{n} a_{ij} (N_j^* + x_j) \right].$$

Expanding the right-hand side,

$$\frac{dx_i}{dt} = (N_i^* + x_i) \left[r_i + \sum_{j=1}^{n} a_{ij} N_j^* + \sum_{j=1}^{n} a_{ij} x_j \right].$$

Since $\mathbf{N}^*$ is an equilibrium,

$$r_i + \sum_{j=1}^{n} a_{ij} N_j^* = 0,$$

and therefore

$$\frac{dx_i}{dt} = (N_i^* + x_i) \sum_{j=1}^{n} a_{ij} x_j.$$

Neglecting second-order terms $x_i x_j$ yields

$$\frac{dx_i}{dt} = N_i^* \sum_{j=1}^{n} a_{ij} x_j.$$

Writing the system in matrix form gives

$$\frac{d\mathbf{x}}{dt} = \mathbf{DAx},$$

which proves the claim. □

Therefore, by the indirect method of Lyapunov (Proposition 7), **local stability of equilibria for the GLV model is determined by the eigenvalues of the community matrix**

$$\mathbf{S} = \mathbf{DA} = \mathrm{diag}(\mathbf{N}^*)\mathbf{A} \tag{3.10}$$

rather than by those of the interaction matrix $\mathbf{A}$ alone.

This distinction arises because the presence of the diagonal matrix $\mathbf{D}$ distorts the standard identity matrix within the characteristic equation. Indeed, assuming a feasible equilibrium ($\mathbf{N}^* > \mathbf{0}$), the eigenvalues $\lambda(\mathbf{S})$ of the community matrix $\mathbf{S}$ are the roots of $\det(\mathbf{DA} - \lambda(\mathbf{S})\mathbf{I}_n) = 0$. Since $\mathbf{D}$ has non-zero determinat $\det(\mathbf{D}) = \prod_{i=1}^{n} N_i^*$, it is invertible and this condition can be rewritten by factoring out $\mathbf{D}$, yielding

$$\det\left(\mathbf{A} - \lambda(\mathbf{S})\mathbf{D}^{-1}\right) = 0. \tag{3.11}$$

While the spectrum of $\mathbf{A}$ is determined by the standard uniform shift $\det(\mathbf{A} - \lambda(\mathbf{A})\mathbf{I}_n) = 0$, Eq. (3.11) shows that the presence of the equilibrium abundances replaces the identity matrix $\mathbf{I}_n$ with the heterogeneous diagonal matrix $\mathbf{D}^{-1} = \mathrm{diag}(1/N_1^*, \ldots, 1/N_n^*)$. This non-uniform weighting deforms the geometry of the spectrum, lifting the direct applicability of the Circular Law and breaking any immediate equivalence between the stability of $\mathbf{A}$ and that of $\mathbf{S}$.

Figure 3.3 compares the spectrum of an interaction matrix $\mathbf{A}$ with that of the corresponding community matrix $\mathbf{S} = \mathbf{DA}$. Here, $\mathbf{A}$ is a May matrix,

$$\mathbf{A} = -\mathbf{I} + \mathbf{B},$$

where $\mathbf{B}$ is defined by Eq. (3.6), and the equilibrium abundances are sampled according to $\mathbf{N}^* \sim \mathcal{U}(0, 1]$. Although the Circular Law (Theorem 9) characterizes the spectrum of $\mathbf{A}$, the figure illustrates that the stability of $\mathbf{A}$ does not, in general, imply the stability of the corresponding community matrix $\mathbf{S}$. In the next section, however, we show that under physically motivated assumptions the stability of $\mathbf{A}$ becomes a sufficient condition for the stability of $\mathbf{S}$.

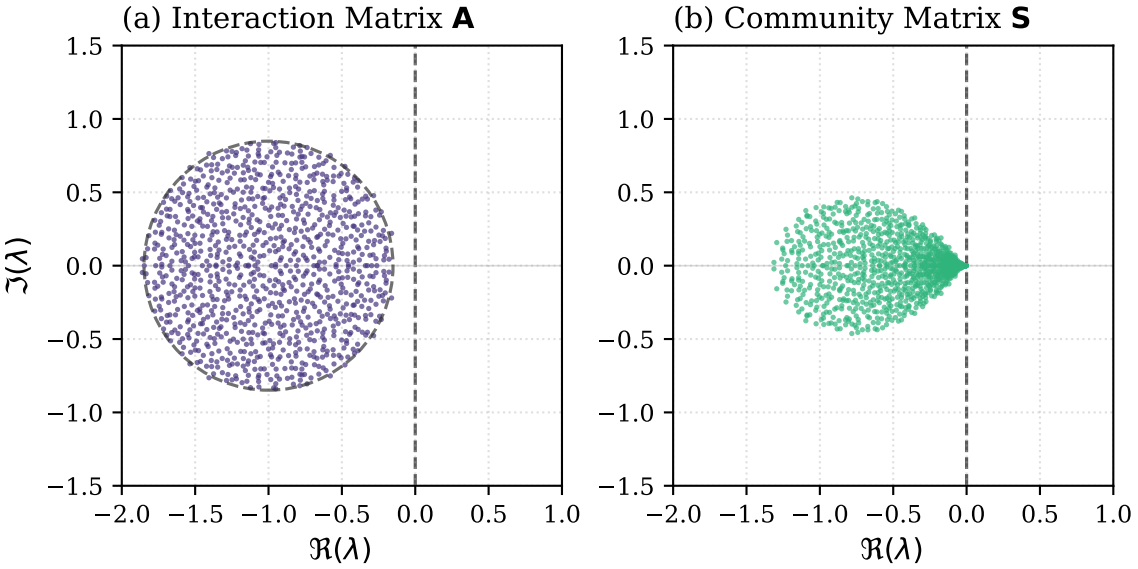

Figure 3.3.. Comparison between the spectra of the interaction matrix $\mathbf{A}$ and the corresponding community matrix $\mathbf{S} = \mathbf{DA}$ for the same realization of $\mathbf{A}$. The parameters are $n = 1000$, $\sigma = 0.03$, and $C = 0.8$. The equilibrium abundances are sampled independently from the uniform distribution $\mathcal{U}(0, 1]$.

3.2.2 Relation between the stability of A and S

In Subsection 3.2.1, we explained why the matrix governing the local stability of equilibria in the GLV model is the community matrix

$$\mathbf{S} = \mathbf{DA},$$

rather than the interaction matrix $\mathbf{A}$. However, the analysis of $\mathbf{S}$ is generally more involved, since its construction requires the equilibrium abundances $\mathbf{N}^*$, which must be obtained from Eq. (2.11). In general, this entails inverting the interaction matrix or approximating the solution numerically.

It is therefore natural to ask whether there exist parameter regimes in which the spectral properties of $\mathbf{A}$ alone are sufficient to determine the local stability of GLV equilibria, without explicitly computing $\mathbf{S}$.

To address this question, we introduce the following notion [44].

Definition 14 (D-stability)**.** *A matrix* $\mathbf{A}$ *is called* D-stable *if, for every positive diagonal matrix*

$$\mathbf{D} = \mathrm{diag}(d_1, \ldots, d_n), \qquad d_i > 0,$$

the matrix $\mathbf{DA}$ *is locally stable.*

In the GLV model, whenever an equilibrium is feasible, the community matrix satisfies

$$\mathbf{S} = \mathbf{D}(\mathbf{N}^*)\mathbf{A},$$

where $\mathbf{D}(\mathbf{N}^*)$ is a positive diagonal matrix. Consequently, if $\mathbf{A}$ is D-stable, then every feasible equilibrium is necessarily locally stable.

Although D-stability is a strong property and no complete characterization is known for matrices of dimension greater than three, the following sufficient condition is available [44].

Proposition 15. *If there exists a positive diagonal matrix* $\mathbf{D}$ *such that*

$$\mathbf{DA} + \mathbf{A}^T\mathbf{D}$$

is negative definite (equivalently the equilibrium is Volterra–Lyapunov stable*), then* $\mathbf{A}$ *is* D*-stable.*

An immediate consequence is the following. If $\mathbf{A}$ is symmetric and stable, then choosing $\mathbf{D} = \mathbf{I}_n$ gives

$$\mathbf{A} + \mathbf{A}^T = 2\mathbf{A},$$

which is negative definite. Hence, every symmetric stable matrix is D-stable.

More generally, if a stable (not generally simmetric) matrix $\mathbf{A}$ satisfies

$$\mathbf{A} + \mathbf{A}^T < 0,$$

(i.e. it has all negative eigenvalues) then it is D-stable. Therefore, every feasible equilibrium of the corresponding GLV system is locally stable.

3.2.3 Feasibility condition for fully-connected competitive communities ($C = 1$, $Q = 0$)

We are interested uniquely in feasible equilibria.

In this subsection, we recall a result originally derived by Stone [19] for fully connected ($C = 1$, $Q = 0$) competitive GLV models, in which the interaction matrix takes the form

$$W_{ii} = -1, \qquad K_{ii} = 1 \;\Rightarrow\; A_{ii} = -1, \tag{3.12}$$

and, for $i \neq j$,

$$W_{ij} \sim \mathcal{N}(-c, \sigma^2), \qquad K_{ij} = 1, \qquad A_{ij} = W_{ij}K_{ij}. \tag{3.13}$$

Equivalently, $\mathbf{K} = \mathbf{J}_n$, where $\mathbf{J}_n$ denotes the $n \times n$ all-ones matrix.

Proposition 16 (Feasibility of fully-connected competitive GLV)**.** *Consider the GLV model with interaction matrix* $\mathbf{A}$ *defined by Eq.* (3.12) *and Eq.* (3.13)*. Then, in the limit* $n \to \infty$*, the probability that the internal equilibrium of Eq.* (2.11) *is feasible tends to one only if*

$$\gamma = \sqrt{n}\,\sigma \ll 1.$$

where γ *is the complexity defined in Eq.* (3.8)*.*

We report the heuristic derivation of this result in Appendix A.1. Since the argument relies on several simplifying assumptions—including a first-order expansion and the approximate independence of equilibrium abundances—it should be regarded as an approximation rather than an exact characterization.

Figure 3.4 compares the analytical prediction for feasibility probability

$$\mathbb{P}(\mathbf{N}^* > 0) = \left[\Phi\left(\frac{1-c}{\gamma}\right)\right]^n,$$

where Φ denotes the cumulative distribution function of the standard normal distribution, with Monte Carlo simulations.

For each system size n, the markers represent the fraction of feasible realizations (Eq. (2.5)) obtained from an ensemble of 50 randomly generated interaction matrices following Eq. (3.12) and Eq. (3.13), for each value of γ, while the solid line of the corresponding color shows the theoretical prediction. The latter is constructed by approximating the equilibrium abundance of each species as a Gaussian random variable, computing the probability that a single species has positive equilibrium abundance, and assuming that the abundances of different species are independent, so that the feasibility probability of the whole community is the product of the single-species probabilities.

Despite its simplicity, the approximation reproduces both the location and the sharpness of the transition between the feasible and non-feasible regimes already for moderately sized systems.

A systematic leftward shift of the numerical curves relative to the analytical prediction is nevertheless observed, indicating that the heuristic slightly overestimates the probability of feasibility. This discrepancy is mainly due to the neglected correlations between equilibrium abundances, which are coupled through the inverse interaction matrix $\mathbf{A}^{-1}$ and therefore cannot be treated as independent. Additional deviations arise from the first-order linearization of the equilibrium equations and from finite-size effects (stronger for smaller n), for which the Gaussian approximation provided by the central limit theorem is not exact.

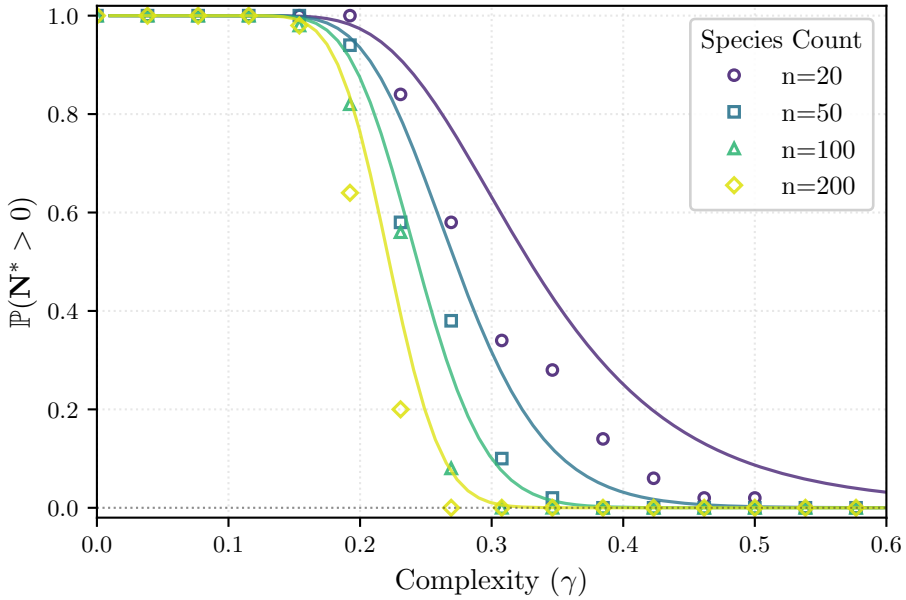

Figure 3.4.. Probability of feasibility as a function of the complexity $\gamma = \sigma\sqrt{n}$ for a fully-connected ($C = 1$) competitive GLV model with mean interaction $c = 0.4$. Solid lines represent the analytical prediction of Proposition 16 derived under the mean-field approximation and the assumption of independent species abundances (see derivation in Appendix A.1). Distinct empty markers correspond to empirical values obtained from Monte Carlo simulations across different system sizes: $n = 20$ (circles), $n = 50$ (squares), $n = 100$ (triangles), and $n = 200$ (diamonds). Each empirical data point is computed over an ensemble of 50 independent matrix realizations.

Therefore, feasibility constitutes a strong constraint in this regime, restricting the set of parameter values for which realistic equilibria exist, and consequently for which it is meaningful to analyze their properties. In the following, we extend this observation through numerical simulations, showing that the feasibility condition remains more restrictive than the stability of $\mathbf{A}$ across all structural regimes considered (see Subsection 3.3.4 and Subsection 3.4.3).

3.3 Effect of C in competitive GLV

In this section, we analyze the spectral properties of the interaction matrix $\mathbf{A}$ in the absence of modularity (Erdős-Rényi structure; see Subsection 2.3.1) and investigate whether, for competitive GLV systems (2.10), a connectance $C < 1$ leads to different effects on stability and feasibility compared to the fully-connected case of the same model.

3.3.1 Distribution associated with $\mathbf{A}$

Given assumptions 2.22, we reduce to the case $Q = 0$, so that

$$W_{ii} = -1, \qquad K_{ii} = 1 \implies A_{ii} = -1 \tag{3.14}$$

and, for $i \neq j$,

$$W_{ij} \sim \mathcal{N}(-c, \sigma^2), \qquad K_{ij} = \begin{cases} 1 & \text{with probability } C, \\ 0 & \text{with probability } 1 - C, \end{cases} \qquad A_{ij} = W_{ij} K_{ij}. \tag{3.15}$$

We now quantify the effect of a non-zero mean interaction strength $-c$ on the variance of the interspecific interactions.

Proposition 17. *Given an interaction matrix* $\mathbf{A}$ *whose off-diagonal entries are defined by Eq.* (3.15)*, the random variable* A_{ij} *satisfies*

$$\mathbb{E}[A_{ij}] = -cC, \qquad \mathrm{Var}(A_{ij}) = C\sigma^2 + c^2 C(1 - C). \tag{3.16}$$

Proof. By definition,

$$\mathbb{E}[A_{ij}] = C\,\mathbb{E}[W_{ij}] + (1 - C) \cdot 0 = -cC.$$

Moreover,

$$\mathbb{E}[W_{ij}^2] = \mathrm{Var}(W_{ij}) + \big(\mathbb{E}[W_{ij}]\big)^2 = \sigma^2 + c^2.$$

Therefore,

$$\mathbb{E}[A_{ij}^2] = C\,\mathbb{E}[W_{ij}^2] + (1 - C) \cdot 0 = C(\sigma^2 + c^2).$$

Hence,

$$\mathrm{Var}(A_{ij}) = \mathbb{E}[A_{ij}^2] - \big(\mathbb{E}[A_{ij}]\big)^2 = C(\sigma^2 + c^2) - c^2 C^2 = C\sigma^2 + c^2 C(1 - C),$$

which proves the claim. □

The first contribution to the variance grows linearly with the connectance C, consistently with May's classical result in Eq. (3.7). The second contribution arises from the random network topology and is proportional to $C(1 - C)$. This term vanishes for both $C \to 0$ and $C = 1$, attaining its maximum at $C = 1/2$.

3.3.2 Spectral analysis and instability threshold

We now determine analytically how the spectrum of $\mathbf{A}$ differs from May's classical case when a non-zero competitive mean interaction strength c is introduced.

To this end, we move from the Hadamard formalism adopted so far to the analysis of the full matrix. We decompose $\mathbf{A}$, whose entries are defined by Eqs. (3.14) and (3.15), as

$$\mathbf{A} = \mathbf{M} + \mathbf{B}, \tag{3.17}$$

where $\mathbf{M}$ is the ***mean interaction matrix***, given by

$$\mathbf{M} = -\mathbf{I}_n(1 - cC) - cC\,\mathbf{J}_n, \tag{3.18}$$

using Eq. (3.16), where $\mathbf{J}_n$ is the $n \times n$ all-ones matrix; $\mathbf{B}$ is the ***fluctuation matrix***, satisfying the following properties.

Proposition 18. *Let* $\mathbf{B}$ *be the matrix defined by Eq.* (3.17)*, where the off-diagonal entries of* $\mathbf{A}$ *are given by Eq.* (3.15)*. Then the off-diagonal entries of* $\mathbf{B}$ *have zero mean and the same variance as those of* $\mathbf{A}$*:*

$$\mathbb{E}[B_{ij}] = 0, \qquad \mathrm{Var}(B_{ij}) = C\sigma^2 + c^2C(1-C). \tag{3.19}$$

Proof. By definition,

$$\mathbf{B} = \mathbf{A} - \mathbf{M}.$$

Since, for $i \neq j$,

$$M_{ij} = -cC,$$

it follows that

$$B_{ij} = A_{ij} + cC.$$

Therefore,

$$\mathbb{E}[B_{ij}] = \mathbb{E}[A_{ij}] + cC = -cC + cC = 0.$$

Moreover, the variance is invariant under translations, so that

$$\mathrm{Var}(B_{ij}) = \mathrm{Var}(A_{ij}) = C\sigma^2 + c^2C(1-C),$$

where the last equality follows from Proposition 18. This proves the claim. □

Therefore, we can use the Circular Law (Theorem 9) to determine the spectrum of $\mathbf{B}$ as done in Corollay 10. For large n, its eigenvalues are asymptotically uniformly distributed over the disk

$$\left\{z \in \mathbb{C} : \ |z| \leq \sigma_{\text{eff}}\sqrt{n}\right\},$$

where we will denote σ_{eff} as the *effective variance*, given by

$$\sigma_{\text{eff}}^2 = C\sigma^2 + c^2C(1-C). \tag{3.20}$$

As for $\mathbf{M}$, we first state a preliminary result.

Lemma 19. *The* $n \times n$ *all-ones matrix,* $\mathbf{J}_n$*, has* $n-1$ *zero eigenvalues and a single eigenvalue equal to* n*.*

Proof. Since all the rows of $\mathbf{J}_n$ are identical, the matrix has rank equal to 1. By the *rank–nullity theorem* it must be $\dim(\ker(\mathbf{J}_n)) + \mathrm{rk}(\mathbf{J}_n) = n$, therefore

$$\dim(\ker(\mathbf{J}_n)) = n - 1,$$

so that 0 is an eigenvalue with geometric multiplicity $n-1$.

On the other hand, the vector

$$\mathbf{e}_n = (1, \ldots, 1)^T$$

satisfies

$$\mathbf{J}_n\mathbf{e}_n = n\mathbf{e}_n,$$

showing that n is an eigenvalue of $\mathbf{J}_n$.

Finally, the sum of the eigenvalues, counted with algebraic multiplicity, equals the trace of the matrix:

$$\mathrm{tr}(\mathbf{J}_n) = n.$$

Since n is already one eigenvalue and the remaining ones are zero, the spectrum of $\mathbf{J}$ is

$$n, \underbrace{0, \ldots, 0}_{n-1 \text{ times}}.$$

□

We thus obtain the following result for the spectrum of $\mathbf{M}$.

Proposition 20. *The eigenvalues of* $\mathbf{M}$ *are*

- *a single eigenvalue*

$$\lambda_{\text{out}} = -1 - cC(n-1);$$

- $n-1$ *degenerate eigenvalues*

$$\lambda_{\text{bulk}} = -1 + cC.$$

Proof. By Lemma 19, the eigenvalues of $-cC\mathbf{J}_n$ are

- one eigenvalue with multiplicity one:

$$\lambda_1(-cC\mathbf{J}_n) = -cCn;$$

- one zero eigenvalue with multiplicity $n-1$:

$$\lambda_2(-cC\mathbf{J}_n) = 0.$$

Moreover, by Lemma 11, adding the multiple of the identity matrix $-(1-cC)\mathbf{I}_n$ shifts all eigenvalues by the constant $-(1-cC)$ without changing the corresponding eigenvectors. Therefore,

$$\lambda_{\text{out}} = -cCn - (1-cC) = -1 - cC(n-1),$$

and

$$\lambda_{\text{bulk}} = 0 - (1-cC) = -1 + cC,$$

which proves the claim. □

Therefore, $\mathbf{M}$ has a single isolated eigenvalue, referred to as the *outlier*, which becomes increasingly negative as n grows. The remaining $n-1$ eigenvalues form a degenerate *bulk*, whose location depends on the parameters c and C.

To characterize the spectrum of $\mathbf{A}$ from these results, we rely on the following theorem formulated by Tao (Theorem 1.7 in [45]):

Theorem 21 (Outliers for low-rank perturbations)**.** *Let $\mathbf{X}_n$ be a random $n \times n$ matrix whose entries are i.i.d. with zero mean, unit variance, and finite fourth moment. Let $\mathbf{C}_n$ be a deterministic $n \times n$ matrix of rank $j = O(1)$.*

If $\mathbf{C}_n$ possesses exactly j non-zero eigenvalues $\lambda_1(\mathbf{C}_n), \ldots, \lambda_j(\mathbf{C}_n)$ such that $|\lambda_i(\mathbf{C}_n)| > 1 + \delta$ for some $\delta > 0$ and all n sufficiently large, then, almost surely:

- *The spectrum of $\frac{1}{\sqrt{n}}\mathbf{X}_n + \mathbf{C}_n$ consists of a bulk contained in the unit disk $\{z \in \mathbb{C} : |z| \leq 1 + o(1)\}$;*
- *Exactly j isolated eigenvalues (outliers) lie outside the bulk and satisfy*

$$\lambda_i\left(\frac{1}{\sqrt{n}}\mathbf{X}_n + \mathbf{C}_n\right) = \lambda_i(\mathbf{C}_n) + o(1) \quad \text{as } n \to \infty$$

  for each $1 \leq i \leq j$.

It follows that we can prove the following proposition.

Proposition 22. *Let $\mathbf{A}$ be a matrix whose diagonal entries are given by Eq.* (3.14) *and whose off-diagonal entries are given by Eq.* (3.15)*. Then, for large n, its spectrum is given by*

- *the bulk spectrum, which is contained in a disk centered at $(-1 + cC, 0)$ with radius $\sigma_{\text{eff}}\sqrt{n}$, where σ_{eff} is given by Eq.* (3.20)*;*
- *an isolated eigenvalue (outlier), which asymptotically converges to:*

$$\lambda_{\text{out}}(\mathbf{A}) = -1 - cC(n-1) + o(\sqrt{n}) \xrightarrow[n\to\infty]{} \lambda_{\text{out}}, \tag{3.21}$$

  where λ_{out} is the outlier eigenvalue of $\mathbf{M}$ (Proposition 20).

Proof. To apply Theorem 21 to our model, we perform an algebraic transformation of the matrix $\mathbf{A}$. Recall the decomposition of Eq. (3.17), where the mean interaction matrix is given by Eq. (3.18).

Introducing the unit vector $\hat{\boldsymbol{e}}_n$ of Eq. (**??**), we can rewrite the all-ones matrix as $\mathbf{J}_n = n\hat{\boldsymbol{e}}_n\hat{\boldsymbol{e}}_n^*$. We thus obtain:

$$\mathbf{A} = \mathbf{B} - (1 - cC)\mathbf{I}_n - cCn\hat{\boldsymbol{e}}_n\hat{\boldsymbol{e}}_n^*. \tag{3.22}$$

We now define the normalized random matrix $\hat{\mathbf{B}} = \frac{1}{\sigma_{\text{eff}}}\mathbf{B}$. By construction, the entries of $\hat{\mathbf{B}}$ have zero mean and unit variance, matching the assumptions of Theorem 21.

We rescale the entire matrix $\mathbf{A}$ by dividing by the asymptotic bulk radius $\sigma_{\text{eff}}\sqrt{n}$:

$$\frac{\mathbf{A}}{\sigma_{\text{eff}}\sqrt{n}} = \frac{1}{\sqrt{n}}\hat{\mathbf{B}} - \frac{1 - cC}{\sigma_{\text{eff}}\sqrt{n}}\mathbf{I}_n + \mathbf{C}_n, \tag{3.23}$$

where the deterministic perturbation is defined as:

$$\mathbf{C}_n = -\frac{cC}{\sigma_{\text{eff}}}\sqrt{n}\hat{\boldsymbol{e}}_n\hat{\boldsymbol{e}}_n^*. \tag{3.24}$$

The matrix $\mathbf{C}_n$ has rank $1 = O(1)$, and its sole non-zero eigenvalue is:

$$\lambda_1(\mathbf{C}_n) = -\frac{cC}{\sigma_{\text{eff}}}\sqrt{n}. \tag{3.25}$$

Since $\lambda_1(\mathbf{C}_n)$ scales as $O(\sqrt{n})$, its magnitude satisfies $|\lambda_1(\mathbf{C}_n)| > 1 + \delta$ for any fixed $\delta > 0$ and all sufficiently large n.

Applying Theorem 21 to the matrix $\frac{1}{\sqrt{n}}\hat{\mathbf{B}} + \mathbf{C}_n$, its spectrum consists of a bulk contained in the unit disk and a single outlier located at:

$$\lambda_1\left(\frac{1}{\sqrt{n}}\hat{\mathbf{B}} + \mathbf{C}_n\right) = -\frac{cC}{\sigma_{\text{eff}}}\sqrt{n} + o(1). \tag{3.26}$$

The additive term $-\frac{1-cC}{\sigma_{\text{eff}}\sqrt{n}}\mathbf{I}_n$ is a multiple of the identity, whose only effect is to rigidly shift the entire spectrum (Lemma 11). Therefore, the spectrum of the rescaled matrix $\frac{\mathbf{A}}{\sigma_{\text{eff}}\sqrt{n}}$ possesses an outlier at:

$$\lambda_{\text{out}}\left(\frac{\mathbf{A}}{\sigma_{\text{eff}}\sqrt{n}}\right) = -\frac{cC}{\sigma_{\text{eff}}}\sqrt{n} - \frac{1-cC}{\sigma_{\text{eff}}\sqrt{n}} + o(1). \tag{3.27}$$

Finally, multiplying by the scaling factor $\sigma_{\text{eff}}\sqrt{n}$ to return to the spectrum of the original matrix $\mathbf{A}$, we obtain:

$$\lambda_{\text{out}}(\mathbf{A}) = -cCn - (1 - cC) + o(\sqrt{n}) = -1 - cC(n-1) + o(\sqrt{n}), \tag{3.28}$$

which completes the proof. □

From these considerations, the isolated eigenvalue λ_{out} is asymptotically separated from the bulk spectrum and remains strongly negative for all admissible parameter values. It therefore does not contribute to the stability boundary of the system, and the matrix $\mathbf{A}$ is said to be a *Google matrix* [46].

Figure 3.5 displays the numerically computed eigenvalue spectrum of a single realization of the interaction matrix $\mathbf{A}$ under the current model assumptions. The numerical results are compared against the theoretical predictions formulated in Proposition 22, specifically regarding the radius of the bulk spectrum disk and the exact coordinate of the isolated outlier. A precise agreement is observed between the empirical data and the analytical boundaries.

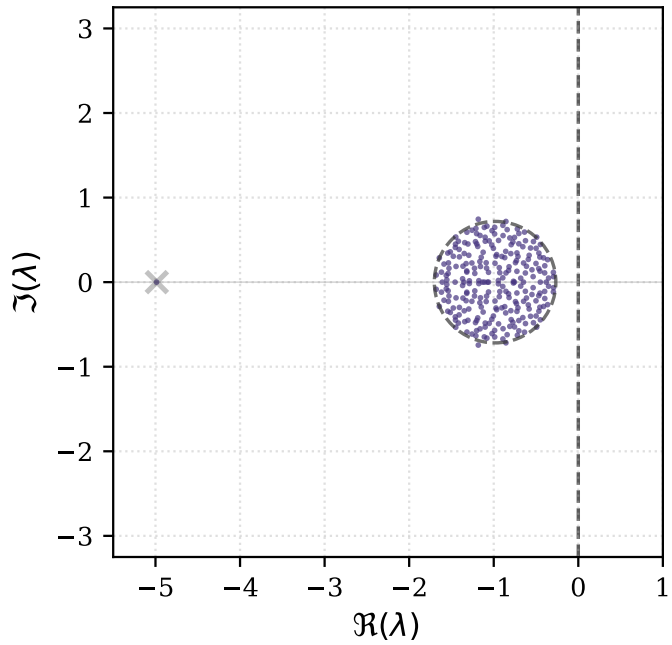

Figure 3.5.. Eigenvalue spectrum in the complex plane for a single realization of the interaction matrix $\mathbf{A}$ with $n = 250$ species, connectance $C = 0.8$, standard deviation of interactions $\sigma = 0.05$, and a weak competitive mean interaction strength $c = 0.02$. The dashed circle represents the theoretical boundary of the bulk spectrum, centered at $(-1 + cC, 0) = (-0.984, 0)$ with an effective radius of $\sigma_{\text{eff}}\sqrt{n} \approx 0.045$, computed via the effective variance $\sigma^2_{\text{eff}} = C\sigma^2 + c^2C(1 - C)$. The isolated outlier eigenvalue $\lambda_{\text{out}}(\mathbf{A})$ is highlighted by the markers, strictly adhering to the asymptotic prediction $-1 - cC(n - 1) = -5$. The perfect alignment confirms the validity of the derivation in the large-n regime under the $Q = 0$ condition.

Stability is thus governed by the rightmost edge of the bulk spectrum. Denoting by Λ the spectral abscissa of $\mathbf{A}$, for n sufficiently large we obtain

$$\Lambda \simeq -1 + cC + \sqrt{n\left[C\sigma^2 + c^2C(1 - C)\right]}. \tag{3.29}$$

By Lyapunov's criterion (Proposition 7), the system is stable if and only if $\Lambda < 0$, which yields

$$\sqrt{n\left[C\sigma^2 + c^2C(1 - C)\right]} < 1 - cC.$$

This condition shows that stability is controlled by the competition between the deterministic shift $1 - cC$ and the fluctuation-induced spectral radius of the bulk.

By setting $C = 1$, we isolate the effect of competition on the stability threshold relative to the neutral regime studied by May (Subsection 3.1.4). In this case, the stability condition shifts from the classical threshold

$$\gamma < 1$$

(Eq. (3.8)) to

$$\gamma < 1 - c. \tag{3.30}$$

Thus, in a *fully connected* competitive network, increasing the average interaction strength c has a destabilizing effect, since stability is achieved only for smaller values of the complexity parameter γ. Moreover, because the connectance is fixed at $C = 1$, reducing the complexity is equivalent to reducing the variance σ^2 of the interspecific interaction strengths.

Figure 3.6 verifies the theoretical threshold by means of a Monte Carlo analysis. For each value of γ, an ensemble of 50 interaction matrices generated according to Eq. (3.14) and Eq. (3.15) was considered, with parameters fixed to $C = 1$ and $c = 0.4$.

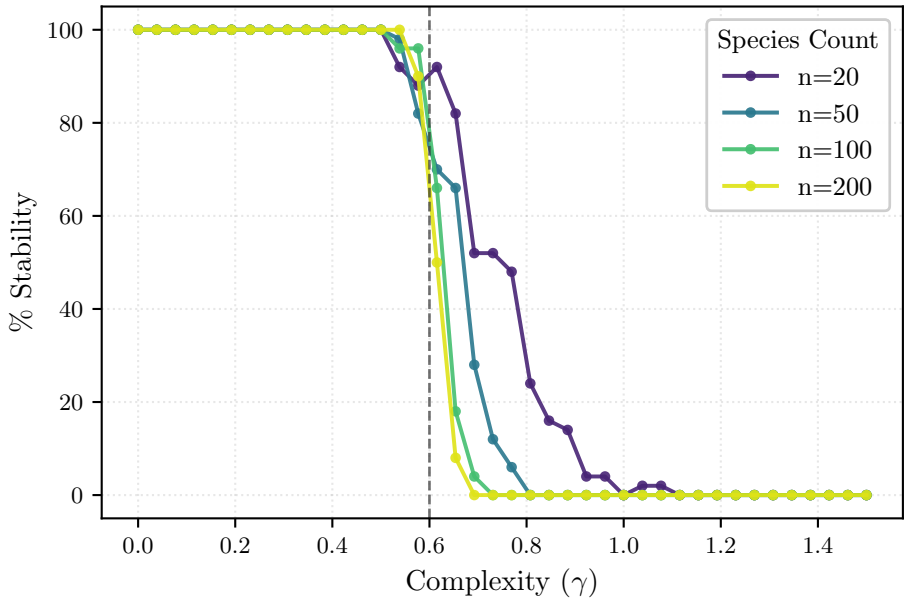

Figure 3.6.. Fraction of stable interaction matrices as a function of the complexity parameter γ for the fully connected competitive model ($C = 1$, $c = 0.4$) and different system sizes n. The vertical dashed line marks the theoretical threshold predicted by Eq. (3.30), obtained as the $C = 1$ specialization of the general stability condition in Eq. (3.3.2). The numerical results are consistent with the theoretical prediction, which provides a good qualitative estimate of the onset of instability even for relatively small system sizes. The scan over γ is performed by fixing C and n (one curve for each value of n) and varying σ.

In the following, we instead investigate the effect of the connectance C on the instability threshold while keeping the average competition strength c fixed.

3.3.3 Prediction of the *spectral shift*

To quantify the stabilizing or destabilizing effect induced by the connectance C, we introduce the *spectral shift*

$$\Delta\Lambda_C(\mathbf{A}) = \Lambda_C(\mathbf{A}) - \Lambda_{C=1}(\mathbf{F_A}), \tag{3.31}$$

where $\Lambda = \max_i \Re(\lambda_i)$ denotes the spectral abscissa of the corresponding matrix.

Here, $\mathbf{F_A}$ denotes the *fully-connected* ($C = 1$) matrix obtained from $\mathbf{A}$ by preserving the weight matrix $\mathbf{W}$ and replacing only the adjacency matrix $\mathbf{K}$ with the $n \times n$ matrix of ones $\mathbf{J}_n$ in the Hadamard representation.

Therefore the quantity $\Delta\Lambda_C(\mathbf{A})$ measures the change in spectral abscissa induced solely by reducing the connectance from $C = 1$ while keeping the same realization of the interaction strengths. In particular,

$$\begin{aligned} \Delta\Lambda_C(\mathbf{A}) < 0 &\implies \text{stabilizing effect of the connectance,} \\ \Delta\Lambda_C(\mathbf{A}) > 0 &\implies \text{destabilizing effect of the connectance.} \end{aligned}$$

Since $\mathbf{A}$ is random, $\Delta\Lambda_C(\mathbf{A})$ is itself a random variable. In the following, we derive an analytical prediction for its expectation as a function of C and compare it with numerical simulations.

Using the results of Subsection 3.3.2, where $\mathbf{A}$ was shown to be a Google matrix, comparing $\Lambda_C(\mathbf{A})$ and $\Lambda_{C=1}(\mathbf{F_A})$ reduces to comparing the rightmost eigenvalue of the *bulk* spectrum of the two matrices.

In particular, using Eq. (3.29) for the large n limit:

- for the matrix $\mathbf{A}$ with connectivity $0 < C \leq 1$,

$$\Lambda_C(\mathbf{A}) = (-1 + cC) + \sqrt{n}\,\sigma_{\text{eff}},$$

  where σ_{eff} is given by Eq. (3.20);

- for the corresponding fully connected matrix $\mathbf{F_A}$,

$$\Lambda_{C=1}(\mathbf{F_A}) = (-1 + c) + \sqrt{n}\,\sigma.$$

Therefore,

$$\Delta\Lambda_C = -c(1 - C) + \sqrt{n}\,(\sigma_{\text{eff}} - \sigma). \tag{3.32}$$

This behaviour can be understood by taking in account the effective variance σ_{eff} of the entries of $\mathbf{A}$. When $C < 1$, the presence or absence of an interaction is itself a random variable, introducing an additional source of fluctuations on top of the intrinsic variability σ of the interaction strengths.

Note that, in the limit $C \to 0$, corresponding to isolated species, the effective variance of Eq. (3.20) satisfies $\sigma_{\text{eff}} \to 0$. Consequently,

$$\Lambda_C(\mathbf{A}) \longrightarrow -1,$$

and the spectral shift converges to the finite value

$$\Delta\Lambda_C(\mathbf{A}) \longrightarrow -c - \sqrt{n}\,\sigma.$$

Thus, in the limit of vanishing connectance, the interaction matrix is always more stable than its fully connected counterpart by an amount equal to $c + \sqrt{n}\,\sigma$ in terms of the spectral abscissa. Therefore, higher variance of interactions emphasises this effect.

By setting the first derivative of Eq. (3.43) with respect to C to zero, we find that a positive deviation ($\Delta\Lambda_C > 0$)—which drives destabilization at incomplete connectance ($C < 1$)—occurs if and only if

$$\frac{\sigma^2}{c^2} < \frac{\sqrt{n+1}-1}{\sqrt{n+1}+1}. \tag{3.33}$$

This implies that incomplete connectance can be destabilizing only when interaction strengths are sufficiently homogeneous, i.e. when σ^2 is small relative to the squared mean interaction strength c^2.

The theoretical prediction of Eq. (3.32) is validated by the excellent agreement with the Monte Carlo analysis reported in Figure 3.7, even for relatively small values of n. The narrow width of the shaded region indicates that the variability across realizations is small, so the median accurately captures the typical behavior. For each sampled value of C, the average value of $\Delta\Lambda_C(\mathbf{A})$ was computed over an ensemble of 500 independently generated interaction matrices $\mathbf{A}$, with the interaction parameters (c, σ) held fixed.

The median and the 5th and 95th percentiles were used to analyze the simulation data. This non-parametric framework ensures that the empirical distributions are described without relying on a priori distribution assumptions.

Equation (3.32) provides an asymptotic prediction ($n \to \infty$) for the spectral shift, depending only on the generation parameters (C, c, σ). For finite n, however, Proposition 22 describes only the asymptotic location of the bulk. The actual spectral abscissa of a realization $\mathbf{A}$ fluctuates around its limiting value because the boundary of the bulk is not deterministic. Consequently, Monte Carlo simulations exhibit a non-zero dispersion around the average value. As n increases, the ensemble average converges to the theoretical prediction (3.32).

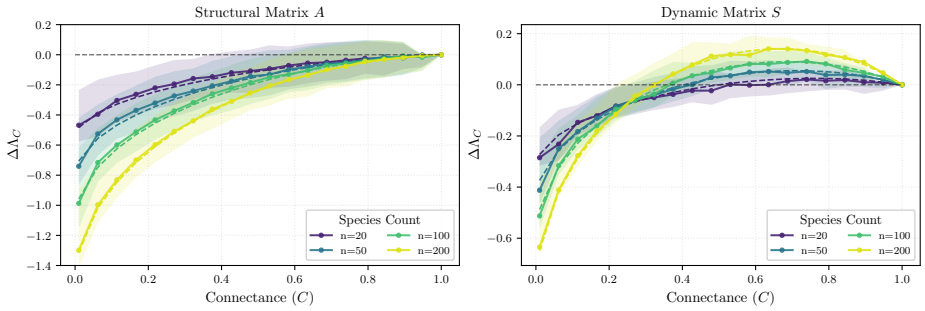

Figure 3.7.. Spectral shift $\Delta\Lambda_C$ as a function of connectance, compared with the theoretical prediction of Eq. (3.32). The solid line represents the median over an ensemble of 500 interaction matrices satisfying Eqs. (3.14) and (3.15) for each parameter set, while the shaded region denotes the 5th–95th percentile range. Panel (a) corresponds to the case $\sigma \ll c$ ($c = 0.1$, $\sigma = 0.05$), whereas panel (b) shows the regime $c \sim \sigma$ ($c = 0.1$, $\sigma = 0.1$). As predicted by Eq. (3.33), the spectral shift exhibits a maximum at intermediate connectance in the former case, whereas is monotonic in the latter.

3.3.4 Numerical results and discussion

We compare the average spectral shift as a function of connectance for both the interaction matrix **A** and the GLV community matrix **S** (Figure 3.8). We consider two parameter regimes: one corresponding to relatively homogeneous interactions, satisfying Eq. (3.33), and another characterized by interaction strengths with variance large compared to the mean level of competition. Only realizations for which both the original system and the corresponding fully connected system admit a feasible interior equilibrium (Eq. (2.11)) are included in the analysis.

Again, we report the median together with the 5th–95th percentile range, thereby avoiding any parametric assumptions about the underlying distribution of the spectral shift.

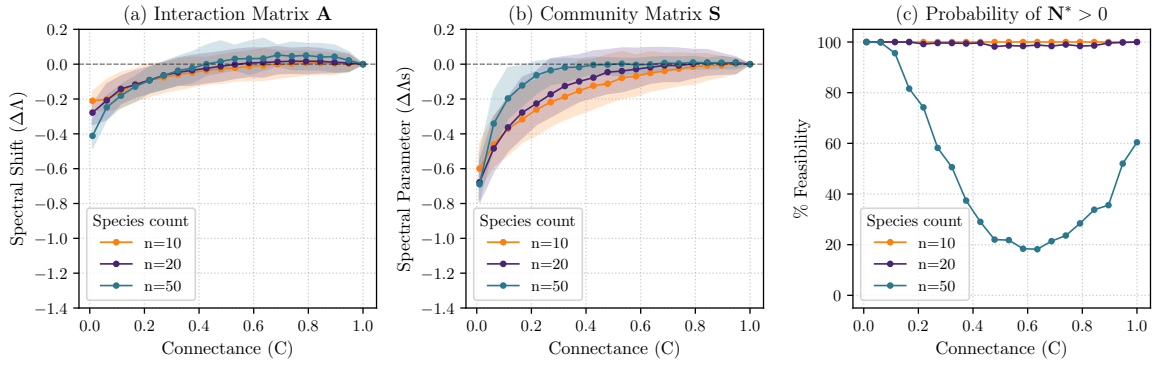

(1) Homogeneous interactions ($\sigma \ll c$)

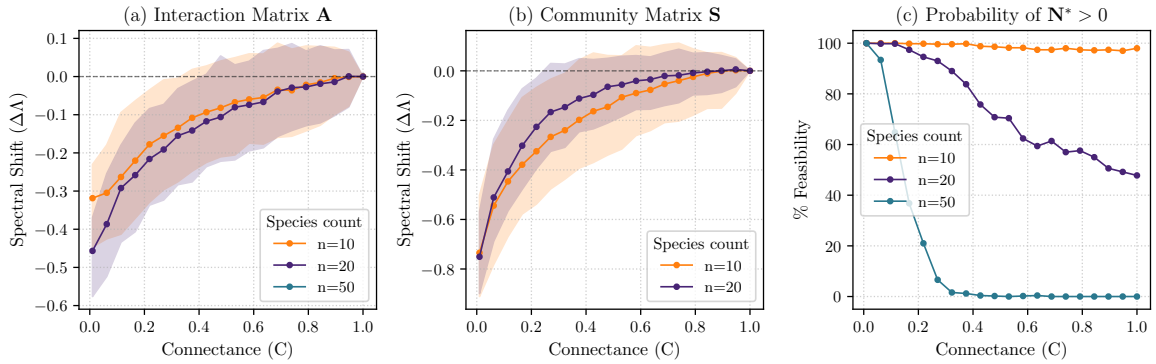

(2) Diverse interactions ($\sigma \sim c$)

Figure 3.8.. Average spectral shift $\Delta\Lambda_C$ as a function of connectance C for the interaction matrix **A** (Eq. (3.14) and Eq. (3.15)) and the GLV community matrix **S**. Panel (1) corresponds to the regime of homogeneous interactions, with $\sigma \ll c$ ($c = 0.1$, $\sigma = 0.05$), whereas panel (2) shows the case of high variance in interaction strengths ($c = 0.1$, $\sigma = 0.1$). For both **A** and **S**, only realizations admitting a feasible equilibrium were included. The solid lines represent the median over 500 independent realizations, while the shaded regions denote the 5th–95th percentile range.

The numerical results show that, although the qualitative behaviour predicted for

A is preserved for **S**, the destabilizing effect at intermediate connectance predicted for homogeneous interactions ($\sigma \ll c$) in **A** is, on average, no longer observed in **S**. This discrepancy arises from the combined effects of the feasibility constraint and the diagonal rescaling induced by the equilibrium abundances $\mathbf{N}^*$ (Eq. (3.10)).

However, imposing the additional feasibility constraint substantially increases the variability among realizations. This is already evident for the interaction matrix **A**, whose fluctuations are considerably larger than in the unconstrained case (Fig. 3.7). As a result, the spectral shift of **S** exhibits no clear dependence on connectance, making it difficult to draw firm conclusions from this comparison alone.

In contrast, for both interaction regimes, the stabilizing effect associated with sufficiently low connectance remains clearly observable and is even more pronounced for the community matrix. Indeed, connectance values below unity are still associated with greater stability than the fully connected case ($C = 1$). We therefore conclude that, within the competitive GLV model considered here, **reduced connectance has an overall stabilizing effect on feasible equilibria**. This conclusion appears to be robust with respect to the relative magnitude of c and σ, unlike the behaviour of the interaction matrix **A**, for which the ratio σ/c qualitatively affects the spectral shift. Equivalently, reducing the average number of interactions per species promotes the local stability of feasible equilibria.

As regards feasibility, we consistently find that **reduced connectance increases the probability of feasible equilibria** relative to the fully connected case.

Finally, the fraction of feasible realizations decreases as the system size n increases. This behaviour is consistent with the theoretical predictions discussed in Subsection 3.2.3 for the fully connected case, according to which feasibility requires $\gamma \ll 1$. This also explains why we restricted our simulations to smaller values of n than in the previous analysis: imposing feasibility for both the original and the corresponding fully connected system substantially reduces the number of admissible realizations, especially as n increases.

3.4 Effect of Q in competitive GLV

We now move from the analysis of interaction matrices with arbitrary connectance C but no internal structure to the study of the effect of network structure on the stability of equilibria through the introduction of a non-zero modularity parameter Q (see Subsection 2.3.2). In this section, we extend the spectral analysis of **A** and interpret the effect of modularity on local stability in light of this spectral characterization.

3.4.1 Distribution associated with $\mathbf{A}$

We consider a generic interaction matrix **A** in the presence of modularity $Q \neq 0$, with parameters defined in Eq. (2.22), namely

$$W_{ii} = -1, \qquad K_{ii} = 1 \quad \Rightarrow \quad A_{ii} = -1,$$

and for $i \neq j$,

$$W_{ij} \sim \mathcal{N}(-c, \sigma^2),$$
$$\mathbb{P}(K_{ij} = 1) = \begin{cases} C_{\text{in}}, & i, j \text{ in same module}, \\ C_{\text{out}}, & i, j \text{ in different modules}. \end{cases}$$
$$A_{ij} = W_{ij} K_{ij}.$$

As in Subsection 3.3.1, we compute the mean and variance of the interspecific entries A_{ij}.

Lemma 23. *Given an interaction matrix* $\mathbf{A}$ *whose entries are defined by Eq.* (2.22)*, the off-diagonal random variables* A_{ij}*, for* $i \neq j$*, satisfy:*

- *if* i *and* j *belong to the same module,*

$$\mathbb{E}[A_{ij}] = -cC_{\text{in}}, \qquad \text{Var}(A_{ij}) = C_{\text{in}}\sigma^2 + c^2 C_{\text{in}}(1 - C_{\text{in}}); \tag{3.34}$$

- *if* i *and* j *belong to different modules,*

$$\mathbb{E}[A_{ij}] = -cC_{\text{out}}, \qquad \text{Var}(A_{ij}) = C_{\text{out}}\sigma^2 + c^2 C_{\text{out}}(1 - C_{\text{out}}); \tag{3.35}$$

The proof is analogous to that of Proposition 17, treating separately the cases in which i and j belong to the same module or to different modules.

We now restrict our attention to the case of two balanced modules of equal size ($\alpha = \frac{1}{2}$; see Subsection 2.3.2).

Proposition 24. *For two modules of equal size* $\frac{n}{2}$*, in the large-*n *limit, the off-diagonal entries of the interaction matrix* $\mathbf{A}$ *have the same average variance along every row. We define this common value as the* effective variance *of the matrix:*

$$\sigma^2_{\text{eff}} = \frac{C_{\text{in}} + C_{\text{out}}}{2}\sigma^2 + c^2 \left[\frac{C_{\text{in}}(1 - C_{\text{in}}) + C_{\text{out}}(1 - C_{\text{out}})}{2} \right]. \tag{3.36}$$

Proof. Let i be a fixed row index corresponding to a species in one of the two modules. Since the modules have equal size, row i contains $n/2 - 1$ off-diagonal entries corresponding to species in the same module and $n/2$ entries corresponding to species in the other module. Hence, in the large-n limit, the fractions of intra- and inter-module entries both converge to $1/2$.

Therefore, the average variance of the off-diagonal entries in row i is

$$\sigma^2_{\text{eff}} = \frac{1}{2}\,\text{Var}(A_{ij} \mid i, j \text{ in the same module}) + \frac{1}{2}\,\text{Var}(A_{ij} \mid i, j \text{ in different modules}).$$

Using Lemma 23, we obtain

$$\sigma^2_{\text{eff}} = \frac{1}{2}\left[C_{\text{in}}\sigma^2 + c^2 C_{\text{in}}(1 - C_{\text{in}})\right] + \frac{1}{2}\left[C_{\text{out}}\sigma^2 + c^2 C_{\text{out}}(1 - C_{\text{out}})\right].$$

Collecting terms gives

$$\sigma^2_{\text{eff}} = \frac{C_{\text{in}} + C_{\text{out}}}{2}\sigma^2 + c^2 \left[\frac{C_{\text{in}}(1 - C_{\text{in}}) + C_{\text{out}}(1 - C_{\text{out}})}{2} \right],$$

which is Eq. (3.36). Since every row contains asymptotically the same proportions of intra- and inter-module entries, this average variance is independent of the choice of i. Thus, every row has the same effective variance, completing the proof. □

3.4.2 Spectral analysis and instability threshold

We now characterize the spectrum of $\mathbf{A}$, whose entries are defined by Eq. (2.22), assuming two balanced modules of equal size.

As in Eq. (3.17), we decompose $\mathbf{A}$ as

$$\mathbf{A} = \mathbf{M} + \mathbf{B}, \tag{3.37}$$

where $\mathbf{M}$ is the mean interaction matrix and $\mathbf{B}$ is the fluctuation matrix.

As shown for the Erdős–Rényi case ($Q = 0$) in Proposition 18, the matrix $\mathbf{B}$ is a random matrix.

Proposition 25. *Let* $\mathbf{B}$ *be the matrix defined by Eq.* (3.37)*, where the off-diagonal entries of* $\mathbf{A}$ *are given by Eq.* (2.22)*. Then the off-diagonal entries of* $\mathbf{B}$ *have zero mean and the same variances as the corresponding entries of* $\mathbf{A}$ *given in Lemma 23.*

The proof is analogous to that of Proposition 18, treating separately the cases in which i and j belong to the same module or to different modules.

For random matrices with a block-structured variance profile, the effective variance that determines the spectral radius predicted by the Corollary 10 of the Circular Law is given by the average variance of the entries along each row of the matrix. Therefore, under the assumption of two balanced modules and in the large-n limit, Proposition 24 implies that the eigenvalues of $\mathbf{B}$ are asymptotically uniformly distributed over the disk

$$\left\{ z \in \mathbb{C} : \, |z| \leq \sigma_{\text{eff}} \sqrt{n} \right\},$$

where σ_{eff} is given by Eq. (3.36).

Ordering the species indexes so that the first $n/2$ belong to module 1 and the remaining $n/2$ to module 2, $\mathbf{M}$ takes the symmetric block form

$$\mathbf{M} = \begin{pmatrix} \mathbf{M}_{\text{in}} & \mathbf{M}_{\text{out}} \\ \mathbf{M}_{\text{out}} & \mathbf{M}_{\text{in}} \end{pmatrix},$$

with

$$\mathbf{M}_{\text{in}} = -\mathbf{I}_{n/2}(1 - cC_{\text{in}}) - cC_{\text{in}}\mathbf{J}_{n/2}, \tag{3.38}$$

$$\mathbf{M}_{\text{out}} = -cC_{\text{out}}\mathbf{J}_{n/2}. \tag{3.39}$$

Here $\mathbf{S}_m$ and $\mathbf{I}_m$ denote the all-ones and identity matrices of size m, respectively. Equivalently,

$$M_{ij} = \begin{cases} -1, & i = j, \\ -cC_{\text{in}}, & i \neq j \text{ within the same module}, \\ -cC_{\text{out}}, & \text{across modules}. \end{cases}$$

This block-constant structure implies that the indexes partition (equivalently the species ordering) is *equitable* in the sense that all rows in a given module have identical total interactions both within their own module and with the other module.

We now introduce the *quotient matrix* $\mathbf{Q} \in \mathbb{R}^{2\times 2}$, that encodes the average total interaction from nodes between the two modules:

$$\mathbf{Q} = \begin{pmatrix} -1 - cC_{\text{in}}\left(\frac{n}{2} - 1\right) & -cC_{\text{out}}\frac{n}{2} \\ -cC_{\text{out}}\frac{n}{2} & -1 - cC_{\text{in}}\left(\frac{n}{2} - 1\right) \end{pmatrix}. \tag{3.40}$$

An algebraic interpretation of $\mathbf{Q}$ is provided bt the following standard result for equitable partitions (see, e.g., Lemma 2.3.1 of [47])

Lemma 26 (Spectrum induced by an equitable partition)**.** *Let* $\mathbf{M}$ *admit an equitable partition with quotient matrix* $\mathbf{Q}$*, and let* $\mathcal{U}$ *denote the subspace of vectors that are constant on each module, i.e.*

$$\mathbf{x}_{\mathcal{U}} = (\mathbf{x}_{\mathcal{U}}^{(1)}, \mathbf{x}_{\mathcal{U}}^{(2)})^T = (a\mathbf{1}_{n/2}, b\mathbf{1}_{n/2})^T, \quad a, b \in \mathbb{R}.$$

Then $\mathcal{U}$ *is invariant under* $\mathbf{M}$*, and the restriction of* $\mathbf{M}$ *to* $\mathcal{U}$ *is represented by* $\mathbf{Q}$*. Consequently, every eigenvalue of* $\mathbf{Q}$ *is an eigenvalue of* $\mathbf{M}$*.*

Therefore, $\mathbf{M}$ leaves the subspace $\mathcal{U}$ invariant. Since $\mathbf{M}$ is symmetric, the orthogonal complement $\mathcal{U}^{\perp}$ is also invariant, and these two subspaces are orthogonal and have dimensions 2 and $n - 2$, respectively. Hence, the spectrum of $\mathbf{M}$ consists of the two eigenvalues of $\mathbf{Q}$ together with the eigenvalues associated with its orthogonal invariant complement $\mathcal{U}^{\perp}$.

We find that

Proposition 27. *The quotient matrix* $\mathbf{Q}$ *of Eq.* (3.40) *has eigenvalues*

$$\lambda_1 = -1 + cC_{in} - c\frac{n}{2}(C_{in} + C_{out}), \tag{3.41}$$

$$\lambda_2 = -1 + cC_{in} - c\frac{n}{2}(C_{in} - C_{out}). \tag{3.42}$$

This two eigenvalues are also eigenvalues for $\mathbf{M}$*.*

Proof. The matrix $\mathbf{Q}$ has the symmetric structure

$$\mathbf{Q} = \begin{pmatrix} a & b \\ b & a \end{pmatrix},$$

with

$$a = -1 - cC_{\text{in}}\left(\frac{n}{2} - 1\right), \qquad b = -cC_{\text{out}}\frac{n}{2}.$$

The characteristic polynomial is

$$(\lambda - a)^2 - b^2$$

hence the eigenvalues are

$$\lambda_{1,2} = a \pm b,$$

corresponding respectively to the eigenvectors $(1, 1)^T$ and $(1, -1)^T$.

Substituting the expressions of a and b gives

$$\begin{aligned} \lambda_1 &= -1 - cC_{\text{in}}\left(\frac{n}{2} - 1\right) - cC_{\text{out}}\frac{n}{2} \\ &= -1 + cC_{\text{in}} - c\frac{n}{2}(C_{\text{in}} + C_{\text{out}}), \end{aligned}$$

and

$$\begin{aligned}\lambda_2 &= -1 - cC_{\text{in}}\left(\frac{n}{2} - 1\right) + cC_{\text{out}}\frac{n}{2} \\ &= -1 + cC_{\text{in}} - c\frac{n}{2}(C_{\text{in}} - C_{\text{out}}).\end{aligned}$$

Because of Lemma 26, this two eigenvalues are also eigenvalues for $\mathbf{M}$. This completes the proof. □

Moreover,

Proposition 28. *The remaining $n-2$ eigenvalues of $\mathbf{M}$ are all equal to*

$$\lambda_0 = -1 + cC_{\text{in}}.$$

Hence λ_0 has algebraic multiplicity $n-2$.

Proof. Let

$$\mathbf{x}_{\mathcal{U}^\perp} = \left(\mathbf{x}^{(1)}_{\mathcal{U}^\perp}, \mathbf{x}^{(2)}_{\mathcal{U}^\perp}\right)^T$$

belong to the orthogonal complement $\mathcal{U}^\perp$ of the subspace $\mathcal{U}$ of vectors that are constant on each module. Choosing the standard basis of $\mathcal{U}$ given by

$$u_1 = \begin{pmatrix}\mathbf{1}_{n/2} \\ \mathbf{0}_{n/2}\end{pmatrix}, \qquad u_2 = \begin{pmatrix}\mathbf{0}_{n/2} \\ \mathbf{1}_{n/2}\end{pmatrix},$$

by definition of orthogonality we obtain

$$\mathbf{1}^T_{n/2}\mathbf{x}^{(1)}_{\mathcal{U}^\perp} = 0, \qquad \mathbf{1}^T_{n/2}\mathbf{x}^{(2)}_{\mathcal{U}^\perp} = 0.$$

Since consequently $\mathbf{J}_{n/2}\mathbf{x}^{(i)}_{\mathcal{U}^\perp} = \mathbf{0}$, from Eq. (3.38) and Eq. (3.39) we obtain

$$\mathbf{M}_{\text{in}}\mathbf{x}^{(i)}_{\mathcal{U}^\perp} = (-1 + cC_{\text{in}})\mathbf{x}^{(i)}_{\mathcal{U}^\perp},$$

and

$$\mathbf{M}_{\text{out}}\mathbf{x}^{(i)}_{\mathcal{U}^\perp} = \mathbf{0}.$$

Therefore

$$\mathbf{M}\mathbf{x}_{\mathcal{U}^\perp} = (-1 + cC_{\text{in}})\mathbf{x}_{\mathcal{U}^\perp},$$

so every vector in this $(n-2)$-dimensional subspace is an eigenvector associated with the eigenvalue

$$\lambda_0 = -1 + cC_{\text{in}}.$$

Hence this eigenvalue has multiplicity $n-2$. □

Now we can use similar arguments to the ones used for the Erdős–Rényi case ($Q = 0$) in Proposition 22 to characterize the spectrum of $\mathbf{A}$ using Theorem 21.

Proposition 29. *Let $\mathbf{A}$ be a matrix whose entries are given by Eq.* (2.22)*. Then, for large n, its spectrum is given by*

– *the bulk spectrum, which is contained in a disk centered at* $(-1 + cC_{\text{in}}, 0) = (\lambda_0, 0)$ *with radius* $\sigma_{\text{eff}}\sqrt{n}$*, where* λ_0 *is the degenerate eigenvalue of* $\mathbf{M}$ *(Proposition 28) and* σ_{eff} *is given by Eq.* (3.36)*;*

– *two isolated eigenvalue (outliers), which asymptotically converge to:*

$$\lambda_1(\mathbf{A}) = -1 + cC_{\text{in}} - c\frac{n}{2}(C_{\text{in}} + C_{\text{out}}) + o(\sqrt{n}) \xrightarrow[n\to\infty]{} \lambda_1,$$
$$\lambda_2(\mathbf{A}) = -1 + cC_{\text{in}} - c\frac{n}{2}(C_{\text{in}} - C_{\text{out}}) + o(\sqrt{n}) \xrightarrow[n\to\infty]{} \lambda_2.$$

where λ_1, λ_2 *are the outlier eigenvalues of* $\mathbf{M}$ *(Proposition 27).*

Proof. In the decomposition of Eq. (3.37), the deterministic matrix $\mathbf{M}$ can be rewritten by isolating the component proportional to the identity from the block-constant matrix $\mathbf{P}$:

$$\mathbf{A} = \mathbf{B} - (1 - cC_{\text{in}})\mathbf{I}_n + \mathbf{P},$$

where

$$\mathbf{P} = \begin{pmatrix} \mathbf{P}_{\text{in}} & \mathbf{P}_{\text{out}} \\ \mathbf{P}_{\text{out}} & \mathbf{P}_{\text{in}} \end{pmatrix},$$

with $\mathbf{P}_{\text{in}} = -cC_{\text{in}}\mathbf{J}_{n/2}$ and $\mathbf{P}_{\text{out}} = -cC_{\text{out}}\mathbf{J}_{n/2}$.

Introducing the orthonormal vectors

$$\mathbf{u}_n^{(1)} = \frac{1}{\sqrt{n}}(\mathbf{1}_{n/2}, \mathbf{1}_{n/2})^T, \qquad \mathbf{u}_n^{(2)} = \frac{1}{\sqrt{n}}(\mathbf{1}_{n/2}, -\mathbf{1}_{n/2})^T,$$

$\mathbf{P}$ admits the exact spectral decomposition:

$$\mathbf{P} = \mu_1 \mathbf{u}_n^{(1)}(\mathbf{u}_n^{(1)})^T + \mu_2 \mathbf{u}_n^{(2)}(\mathbf{u}_n^{(2)})^T,$$

with non-zero eigenvalues

$$\mu_1 = -c\frac{n}{2}(C_{\text{in}} + C_{\text{out}}), \qquad \mu_2 = -c\frac{n}{2}(C_{\text{in}} - C_{\text{out}}).$$

We define the normalized random matrix $\hat{\mathbf{B}} = \frac{1}{\sigma_{\text{eff}}}\mathbf{B}$. By construction, the entries of $\hat{\mathbf{B}}$ have zero mean and unit variance. We rescale $\mathbf{A}$ by dividing by the asymptotic bulk radius $\sigma_{\text{eff}}\sqrt{n}$:

$$\frac{\mathbf{A}}{\sigma_{\text{eff}}\sqrt{n}} = \frac{1}{\sqrt{n}}\hat{\mathbf{B}} - \frac{1 - cC_{\text{in}}}{\sigma_{\text{eff}}\sqrt{n}}\mathbf{I}_n + \mathbf{C}_n,$$

where the deterministic perturbation is $\mathbf{C}_n = \frac{1}{\sigma_{\text{eff}}\sqrt{n}}\mathbf{P}$.

The matrix $\mathbf{C}_n$ has rank $2 = O(1)$. Its non-zero eigenvalues are

$$\lambda_i(\mathbf{C}_n) = \frac{\mu_i}{\sigma_{\text{eff}}\sqrt{n}}, \qquad i = 1, 2.$$

Since μ_1 and μ_2 scale as $O(n)$, the eigenvalues $\lambda_i(\mathbf{C}_n)$ scale as $O(\sqrt{n})$.

Applying Theorem 21 to the matrix $\frac{1}{\sqrt{n}}\hat{\mathbf{B}} + \mathbf{C}_n$, its spectrum consists of a bulk contained in the unit disk and precisely two outliers located at:

$$\lambda_i\left(\frac{1}{\sqrt{n}}\hat{\mathbf{B}} + \mathbf{C}_n\right) = \frac{\mu_i}{\sigma_{\text{eff}}\sqrt{n}} + o(1), \qquad i = 1, 2.$$

The additive term $-\frac{1-cC_{\text{in}}}{\sigma_{\text{eff}}\sqrt{n}}\mathbf{I}_n$ is a multiple of the identity, which rigidly shifts the entire spectrum (Lemma 11). Multiplying by the scaling factor $\sigma_{\text{eff}}\sqrt{n}$ to return to the spectrum of the original matrix $\mathbf{A}$, the isolated eigenvalues map to:

$$\lambda_i(\mathbf{A}) = -(1 - cC_{\text{in}}) + \mu_i + o(\sqrt{n}).$$

Substituting the expressions for μ_1 and μ_2 yields the claim. □

From these considerations, the isolated eigenvalues $\lambda_1(\mathbf{A})$ and $\lambda_2(\mathbf{A})$ are asymptotically separated from the bulk spectrum. In the large-n limit, λ_1 remains strongly negative for all admissible parameter values. By contrast, λ_2 may either determine the spectral abscissa Λ or lie inside the right edge of the bulk spectrum, depending on the specific parameter regime.

These analytical predictions show excellent agreement with the numerical eigenvalue spectra presented in Figure 3.9. The predicted separation of the isolated outliers from the continuous bulk and the structural modifications induced by the modularity parameter Q are consistent with previous spectral characterizations of block-structured random matrices (see, for example, Fig. 5 of [27]).

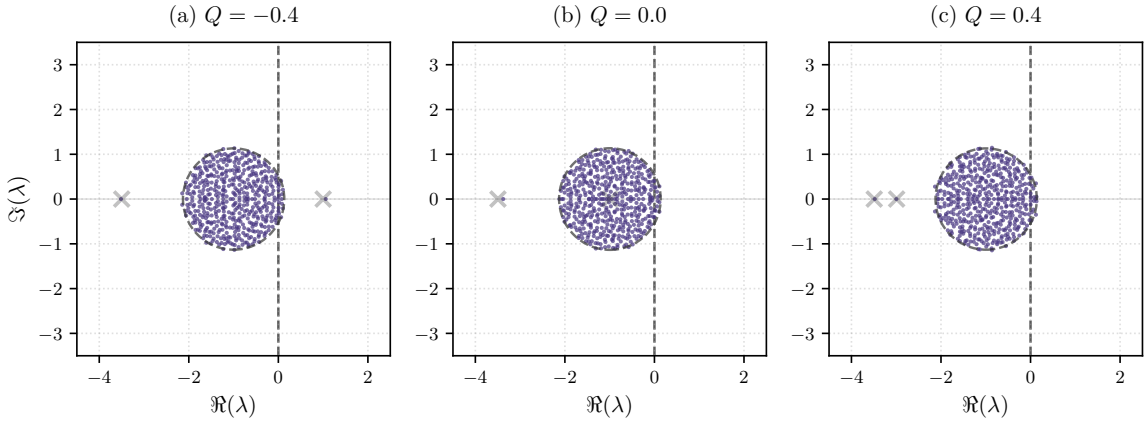

Figure 3.9.. Eigenvalue distribution in the complex plane for the modular competitive model across three distinct structural regimes: (a) antimodular configuration ($Q = -0.4$), (b) homogeneous random network ($Q = 0.0$), and (c) modular configuration ($Q = 0.4$). The remaining system parameters are fixed at size $n = 500$, global connectivity $C = 0.25$, mean interaction strength $c = -0.02$, and standard deviation $\sigma = 0.1$. The solid line marks the boundary of the continuous bulk spectrum, defined by the analytical radius $\sigma_{\text{eff}}\sqrt{n}$ and centered at $-1+cC_{\text{in}}$. The highlighted individual markers indicate the asymptotic theoretical positions of the two isolated outliers λ_1 and λ_2, obtained in Proposition 29.

In the following, we do not derive an explicit expression for the spectral abscissa Λ (Eq. (3.4)), as was done for the $Q = 0$ case. Instead, we rely on numerical simulations and interpret the results in light of the spectral characterization developed above.

3.4.3 Numerical results and discussion

Extending the approach introduced in Subsection 3.3.3, we define the *spectral shift* associated with modularity as

$$\Delta\Lambda_Q(\mathbf{A}) = \Lambda_Q(\mathbf{A}) - \Lambda_{Q=0}(\mathbf{R_A}), \tag{3.43}$$

where $\Lambda = \max_i \Re(\lambda_i)$ denotes the spectral abscissa of the corresponding matrix.

Here, $\mathbf{R_A}$ denotes the Erdős–Rényi ($Q = 0$) matrix obtained from $\mathbf{A}$ by preserving the set of off-diagonal interaction values (equivalently, the realization of the weight matrix $\mathbf{W}$) and redistributing them uniformly at random over all off-diagonal positions, while keeping the diagonal entries fixed. This operation preserves both the interaction strengths and the total number of zero and non-zero entries, while removing the block structure encoded in the adjacency matrix $\mathbf{K}$.

Therefore, the quantity $\Delta\Lambda_Q(\mathbf{A})$ measures the variation in the spectral abscissa induced solely by introducing modularity, relative to the Erdős–Rényi case ($Q = 0$), while keeping both the global connectance C and the realization of the interaction strengths fixed; consequently, the overall complexity $\gamma = \sqrt{nC}\sigma$ is identical for the two matrices. In particular,

$$\begin{aligned} \Delta\Lambda_Q(\mathbf{A}) < 0 &\implies \text{modularity has a stabilizing effect,} \\ \Delta\Lambda_Q(\mathbf{A}) > 0 &\implies \text{modularity has a destabilizing effect.} \end{aligned}$$

It is worth noting that a change in the matrix structure from $\mathbf{A}$ to $\mathbf{R_A}$ inherently alters the resulting equilibrium abundances $\mathbf{N}^*$, since the intrinsic growth rates are kept fixed to $\mathbf{r} = \mathbf{1}_n$. However, by restricting the analysis exclusively to realizations where both the modular and the randomized configurations admit a feasible interior equilibrium ($\mathbf{N}^* > \mathbf{0}$), we ensure a fair comparison, rather than an artifact of biologically unfeasible equilibrium states.

Figure 3.10 shows the average spectral shift, computed over an ensemble of 500 matrices for each parameter value, as a function of the modularity parameter Q, for both the interaction matrix $\mathbf{A}$ and the GLV stability matrix $\mathbf{S}$. Only realizations for which both the original system and the corresponding Erdős–Rényi system admit a feasible interior equilibrium (Eq. (2.11)) were included in the computation of median and percentiles. For each value of global connectance C considered, we restricted to the admissible modularity range, given by Eq. (2.20).

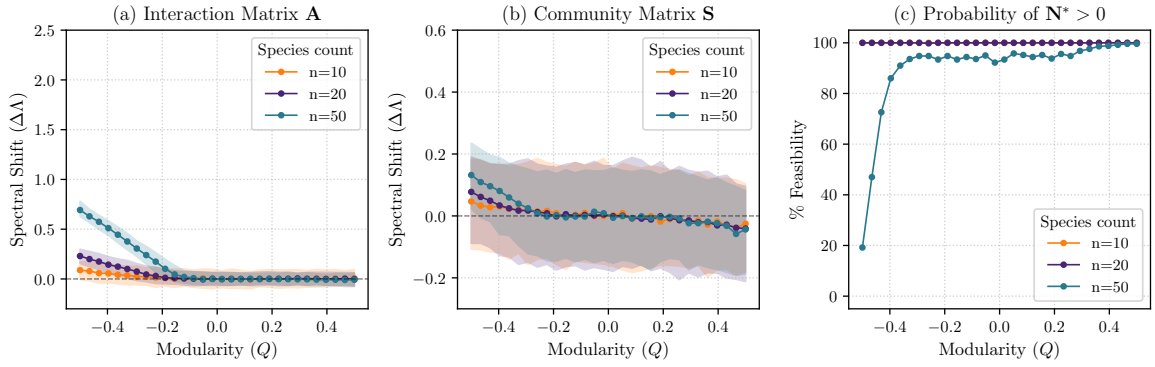

(1) Low connectance ($C = 0.2$)

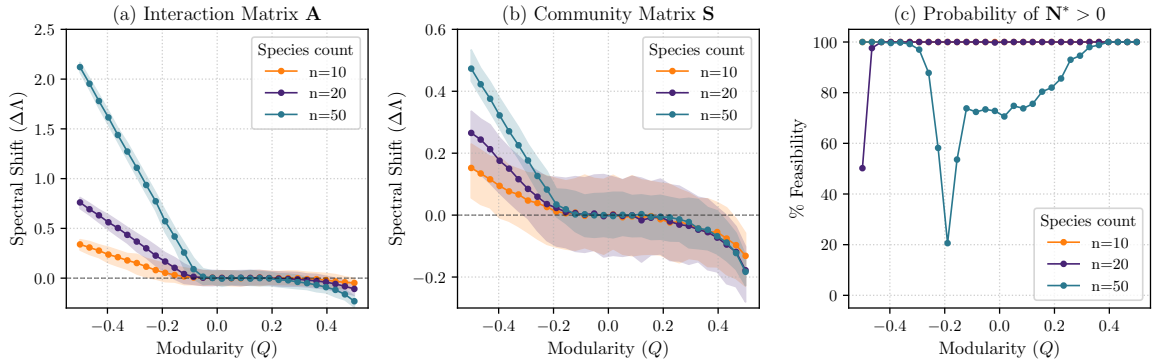

(2) Medium connectance ($C = 0.5$)

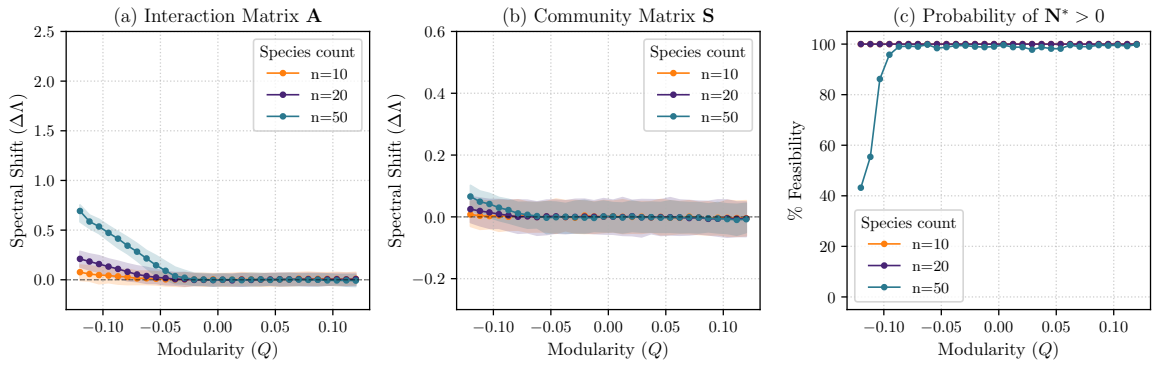

(3) High connectance ($C = 0.8$)

Figure 3.10.. Average spectral shift $\Delta\Lambda_Q$ as a function of connectance Q for the interaction matrix $\mathbf{A}$ (Eq. (2.22)) and the GLV community matrix $\mathbf{S}$. In all the panels, interaction parameters are fixed to $c = 0.1, \sigma = 0.1$. We consider different values of global connectance $C \in \{0.2, 0.5, 0.8\}$ respectively for panel (1), (2), (3). For both $\mathbf{A}$ and $\mathbf{S}$, only realizations admitting a feasible equilibrium were included. The solid lines represent the median over 500 independent realizations, while the shaded regions denote the 5th–95th percentile range. Note that in panel (3) the admissible range for Q is restricted (Eq. (2.20)).

For the interaction matrices $\mathbf{A}$, we observe that, in the competitive regime, *anti-modularity* ($Q < 0$) has a strongly destabilizing effect on the system equilibria, whereas

modularity ($Q > 0$) exerts at most a mild stabilizing effect. These results are consistent with the analysis by Grilli [27] (in particular, see Fig. 4).

Compared to previous work, we extend the analysis to the community matrices $\mathbf{S}$, for which these qualitative properties are preserved on average. However, restricting the analysis to feasible equilibria, the only robust global trend that emerges is that **anti-modularity has a destabilizing effect on feasible equilibria in competitive regime**. Under the assumptions of the present model, this result indicates that the presence of two equally sized groups competing preferentially against each other is more destabilizing than the corresponding competitive random (Erdős–Rényi) case, in which no structured factions are present.

We also notice that **the magnitude of the effect of modularity on equilibrium stability is modulated by the global connectance**. Specifically, for intermediate values of connectance, modularity exerts a stabilizing effect on feasible equilibria in the competitive regime, whereas in the other analyzed configurations the effect remains marginal.

The asymmetry between modular and anti-modular regimes can be understood from the spectral decomposition of the interaction matrix $\mathbf{A}$. In particular, it is driven by the displacement in the complex plane of the isolated eigenvalue

$$\lambda_2 = -1 + cC_{\text{in}} - c\frac{n}{2}(C_{\text{in}} - C_{\text{out}})$$

identified in Proposition 29 (see Figure 3.9).

- **Anti-modular regime ($Q < 0$).** In this case, $C_{\text{out}} > C_{\text{in}}$, so that

  $$-c\frac{n}{2}(C_{\text{in}} - C_{\text{out}}) > 0.$$

  Since this contribution scales linearly with n, the structural outlier λ_2 rapidly shifts to the right, separating from the bulk spectrum. Eventually, it crosses the imaginary axis and becomes the dominant eigenvalue, so that $\Lambda \simeq \lambda_2 > 0$. The system therefore becomes intrinsically unstable, independently of the magnitude of the random fluctuations σ.

- **Modular regime ($Q > 0$).** Here, $C_{\text{in}} > C_{\text{out}}$, causing the isolated eigenvalue λ_2 to move deep into the left half-plane. Consequently, the structural outlier no longer determines the spectral abscissa, which is instead approximately given by the rightmost edge of the bulk spectrum:

  $$\Lambda \approx -1 + cC_{\text{in}} + \sigma_{\text{eff}}\sqrt{n},$$

  where

  $$\sigma_{\text{eff}}^2 = \frac{C_{\text{in}} + C_{\text{out}}}{2}\sigma^2 + c^2\left[\frac{C_{\text{in}}(1 - C_{\text{in}}) + C_{\text{out}}(1 - C_{\text{out}})}{2}\right].$$

  Thus, in this regime, the system's stability depends on the parameters Q, C, and σ through the effective variance that controls the bulk radius.

Low modularity generally yields a higher number of feasible equilibria, although this relationship is not strictly monotonic. Furthermore, the fraction of feasible realizations decreases as the system size n increases. This behavior is consistent with the theoretical predictions discussed in Subsection 3.2.3, which state that feasibility requires $\gamma \ll 1$ for fully connected networks.

3.5 Stability and feasibility over the parameter spaces

We now generalize the study of the effect on the properties of stability and feasibility of GLV equilibria of C and Q by characterizing the relevatn parameter space for obsrvables, namely the average stability of $\mathbf{A}$, theaverage feasibility of equilibria and the average stability of $\mathbf{S}$.

In this way, we aim to characterize the relation between these three characteriztics, comparing them with the previsions presented in Subsection 3.2.3 for the fully connected case ($C = 1, Q = 0$) and Subsection 3.2.2.

3.5.1 Scan of the interaction parameter space ($C = 1, Q = 0$)

Before untangling the joint role of structural parameters, we establish a baseline by characterizing the interaction parameter space (c, σ) for a fully connected network ($C = 1, Q = 0$).

We simulate an ensemble of 50 independent interaction matrices $\mathbf{A}$ (entries given by Eq. (3.12) and Eq. (3.13)) of size $n = 50$ across a discretized grid of average competition strength $c \in [0.0, 0.35]$ and interaction heterogeneity $\sigma \in [0.0, 0.30]$.

For each matrix realization, we compute three distinct probabilistic observables:

1. **Probability of Stability of A:** Evaluated by verifying whether the Lyapunov criterion for linear stability (see Section 3.1.2) holds for the interaction matrix, i.e., if the maximum real part of its eigenvalues is strictly negative ($\max \Re(\lambda_{\mathbf{A}}) < 0$).

2. **Probability of Stability of S:** Computed as the fraction of realizations where the community matrix $\mathbf{S} = \mathbf{DA}$ evaluated at the internal equilibrium $\mathbf{N}^*$ is stable ($\max \Re(\lambda_{\mathbf{S}}) < 0$). Only feasible realization where considered.

3. **Probability of Feasibility ($\mathbf{N}^* > 0$):** Defined as the probability that the internal fixed point $\mathbf{N}^* = \mathbf{A}^{-1}\mathbf{1}_n$ possesses strictly positive abundances for all component species, assuming a uniform intrinsic growth vector (see Subsection 2.2.3).

The numerical results of this scan are summarized in Figure 3.11.

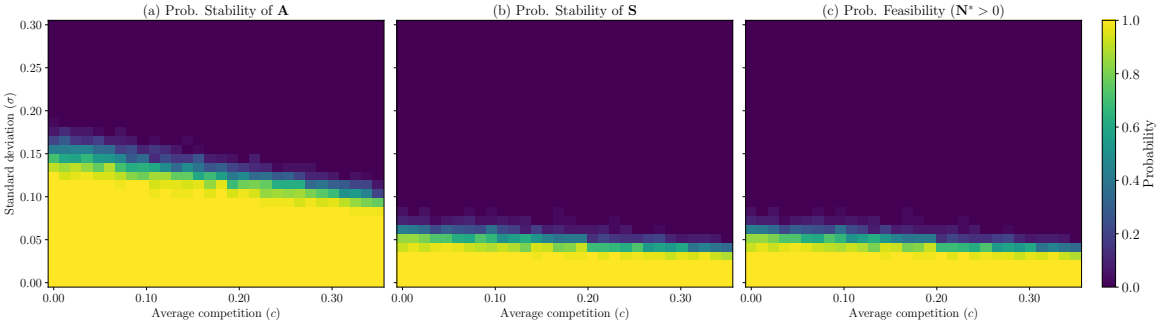

Figure 3.11.. Probabilistic landscapes of stability and feasibility across the interaction parameter space (c, σ) for a fully connected $(C = 1, Q = 0)$ competitive GLV model. Panel (a) shows the probability of structural stability of the interaction matrix **A**. Panel (b) reports the probability of dynamical stability of the community matrix **S** for feasible realizations. Panel (c) displays the probability of full feasibility ($\mathbf{N}^* > 0$). The ensemble consists of 50 matrices per grid point with system size $n = 50$. The color scale interpolates from 0.0 (dark purple, zero probability) to 1.0 (yellow, certain event).

The comparative analysis of the three panels provides several insights into the structural constraints of the competitive GLV model.

Structural Stability of A vs. Feasibility. Panel (a) shows that the structural stability of the interaction matrix **A** is primarily controlled by the heterogeneity σ, with only a weak negative dependence on c. The probability that **A** is stable remains equal to 1 up to approximately $\sigma \simeq 0.10$, beyond which it rapidly decreases to zero.

In contrast, Panel (c) shows that the feasibility boundary lies substantially lower in parameter space. The probability of obtaining a fully coexisting internal equilibrium collapses to zero already at $\sigma \simeq 0.05$. This clear separation between the two transition lines confirms the theoretical predictions discussed in Subsection 3.2.3: **in competitive systems, feasibility is a more restrictive requirement than structural stability**. Consequently, the internal equilibrium typically loses biological relevance through species extinctions well before the interaction matrix itself becomes linearly unstable.

Coupling between Feasibility and Equilibrium Stability. A direct comparison between Panels (b) and (c) reveals that the probability landscapes for the stability of the community matrix **S** and for feasibility are essentially identical. The transition from certain stability (yellow) to complete instability (purple) coincides with the feasibility boundary at $\sigma \simeq 0.05$.

The observed coincidence between Panels (b) and (c) suggests the preservation of D-stability throughout the explored parameter region (see Subsection 3.2.2). Whenever the internal equilibrium satisfies $\mathbf{N}^* > 0$, the diagonal matrix **D** is strictly positive, so the stability of **S** is constrained by the D-stability properties of the interaction matrix **A**. This behaviour is also compatible with the preservation of Volterra–Lyapunov stability, although the latter provides only a sufficient, and not a necessary, condition for D-stability (Proposition 15).

Overall, the simulations indicate that, throughout the explored parameter space,

the disappearance of stable internal equilibria is driven entirely by the loss of feasibility rather than by an intrinsic destabilization of the interaction matrix.

3.5.2 Scan of the structural parameter space (C, Q)

Having established the baseline properties in the fully connected network, we turn to analyze how the network structure, parameterized by connectance C and modularity Q, alters the stability and feasibility landscapes. To systematically decouple the effects of interaction physics from structural properties, we perform a grid scan over the (C, Q) space by selecting arepresentative point:

$$(c, \sigma) = (0.1, 0.1)$$

This parameter set is chosen because the interaction matrix $\mathbf{A}$ lies safely within the structurally stable regime in the baseline case.

It is worth noting that this point corresponds exactly to the choice of interaction parameters $(c, \sigma) = (0.1, 0.1)$ utilized in the previous numerical simulations (specifically, Subsection 3.3.4 and Subsection 3.4.3).

We therefore expand and consolidate those previous dynamical results, placing them within the random matrix theory framework to systematically investigate how structural variations modify a baseline stable interaction regime.

The probabilistic landscapes generated for the stable baseline regime are reported in Figure 3.12.

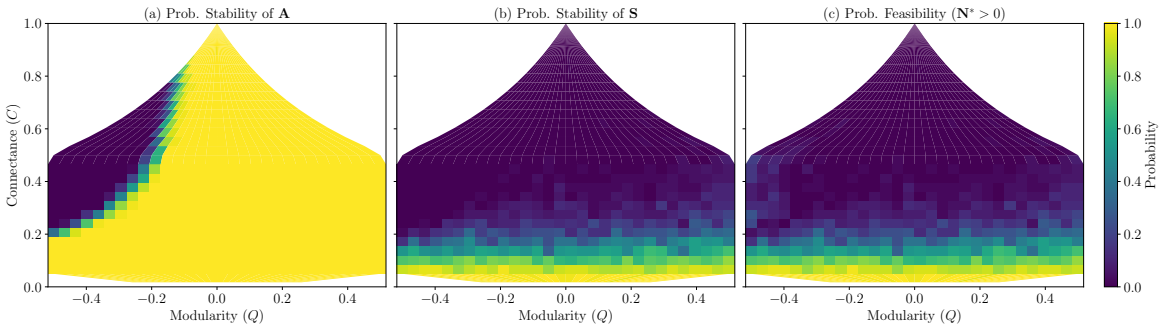

Figure 3.12.. Probabilistic landscapes of stability and feasibility across the structure parameter space (C, Q) for Point 1 ($c = 0.1, \sigma = 0.1$). Panel (a) shows the probability of structural stability of $\mathbf{A}$. Panel (b) reports the probability of dynamical stability of $\mathbf{S}$ only for feasible realizations. Panel (c) displays the probability of full feasibility ($\mathbf{N}^* > 0$). The ensemble consists of 50 matrices per grid point with system size $n = 50$.

The numerical exploration reveals a substantial divergence in how network parameters control the three properties under a stable interaction baseline:

Antimodularity destabilizes A most for intermediate connectance. Panel (a) shows that the interaction matrix $\mathbf{A}$ remains perfectly stable (yellow region) across nearly the entire structural domain, except for a specific region located at high connectance ($C \gtrsim 0.2$) and negative modularity ($Q < 0$). This transition line indicates that

antimodularity selectively destabilizes **A** as connectance varies, a result that perfectly matches the spectral analytical predictions derived for block-structured matrices in Subsection 3.4.3 (see Figure 3.10). In contrast, positive modularity ($Q > 0$) never destabilizes **A** in this regime, regardless of the connectance level.

Feasibility as a Pervasive Constraint. Panels (b) and (c) present a dramatically different landscape compared to the structural stability of **A**. The probability of obtaining a feasible internal equilibrium (Panel c) collapses to zero across almost the entire (C, Q) space, surviving exclusively at very low connectance values ($C \lesssim 0.2$). This implies that **varying the netwrok structure through modularity or connectance can recover the internal equilibrium** with respect to the fully connected case.

Moreover, the landscape of the stability of **S** (Panel b) is again perfectly identical to the feasibility landscape. The lack of feasibility immediately drives the community matrix **S** to instability, forcing the system toward competitive exclusion and boundary equilibria (see Chapter 4).

4

Dynamical evolution

In this chapter, we shift our focus from the analysis of equilibrium properties to the characterization of the full dynamics of the model. Our goal is to investigate how structural properties of the interaction network, in particular connectance C and modularity Q, influence the dynamical evolution of the system and its long-term outcome, including the equilibrium eventually reached.

4.1 Introduction to the analysis

4.1.1 Relevance of the topic

So far, our analysis has focused on the properties of equilibrium states, implicitly assuming that the ecosystem is already poised at a feasible equilibrium (see the assumptions discussed in Subsection 3.1.1).

In natural ecosystems, however, this assumption is often difficult to justify. The set of coexisting species is not an arbitrary collection but rather the outcome of an ecological assembly process acting on a much larger regional species pool. As emphasized by Allesina [48], the communities observed locally are a filtered subset of the regional pool that survive the population dynamics and are able to coexist.

More fundamentally, it has been argued that ecological systems may often operate far from equilibrium, spending ecologically relevant times in persistent nonequilibrium states rather than near a stable fixed point [49, 50].

Moreover, even if equilibrium states are accepted as a meaningful framework, the instability threshold such as the one predicted by May (Eq. (3.8)) does not necessarily represent an existential threat to the entire ecosystem. Following the loss of local stability, a community may persist through sustained chaotic fluctuations [51], or it may reorganize towards a different attractor, for instance after the extinction of one or more species or through persistent fluctuating states. Consequently, local stability is only one aspect of ecosystem persistence and should be interpreted within the broader context of ecological assembly and dynamical evolution.

The analytical characterization of the number and properties of these *attractors*, together with the prediction of transitions between different dynamical regimes, has proved to be a fertile ground for the application of methods from statistical physics,

such as the *replica* and *cavity* methods (for example, see [25, 52, 53]), using mean-field descriptions in the thermodynamic limit and often reducing to a self-consisten 1-body problem (*DMFT methods* (see for example [54]).

Although these methods often rely on restrictive assumptions—such as symmetric interactions (e.g. [52])—their main advantage lies in their independence from species-level characteristics. Instead, they provide a coarse-grained description in which the dynamical behaviour of the ecosystem is determined by a small set of effective parameters, allowing the construction of phase diagrams that identify the typical dynamical regimes of the system [10].

Extending these analytical results to more realistic interaction structures remains a significant challenge (for a perspective on future challenges, see [10]). Developing analytical frameworks capable of predicting the typical response of complex ecosystems to perturbations—whether indirect, such as environmental or climate change, or direct, such as species extinctions or invasions—is therefore a major objective. Beyond their theoretical interest, such predictions are essential for understanding biodiversity resilience and have potential applications in other complex systems, including biological, medical, and socio-economic networks (see review [55]).

4.1.2 Preliminary notions: static attractors, multistability, and chaos

To characterize the dynamical evolution of an ecological community, the state of the system at any time t can be represented as a point in an n-dimensional *phase space* (or state space), where each coordinate corresponds to the abundance of one species, $N_i(t)$ for $i = 1, \dots, n$. An ***attractor*** is a bounded subset of the phase space toward which all trajectories originating from a surrounding region, called the *basin of attraction*, converge asymptotically as $t \to \infty$.

Static attractors, or stable *fixed points*, are time-invariant configurations satisfying $dN_i/dt = 0$ for all i [48]. More precisely, they are equilibrium points that are asymptotically stable: trajectories starting sufficiently close to the equilibrium converge to it as $t \to \infty$ (see Definition 6).

For the GLV model, the characterization of equilibrium points was presented in Subsection 2.1.2. A further distinction between stable equilibria can be made according to the extent of their basin of attraction. In particular, one distinguishes between locally and globally stable equilibria.

Definition 30. *A feasible equilibrium is said to be* globally stable *if every trajectory originating from the feasible state space converges to it. Equivalently, its basin of attraction coincides with the entire feasible state space. Consequently, the system returns to the equilibrium regardless of the magnitude of any feasible perturbation.*

Recalling the definition of Volterra–Lyapunov stability (Proposition 15), the following sufficient condition for global stability of the GLV model can be stated (Proposition 3.9 in [56]):

Proposition 31. *Suppose that the GLV system admits a feasible equilibrium. If its interaction matrix* $\mathbf{A}$ *is Volterra–Lyapunov stable, then this equilibrium is globally asymptotically stable. Consequently, it is the unique attractor of the deterministic dynamics.*

When the interaction matrix $\mathbf{A}$ is Volterra–Lyapunov stable, the associated equilibrium is a *non-invasible* (or *saturated*) equilibrium [48]. At this equilibrium, a subset of k persistent species maintains positive abundances, whereas the remaining $n - k$ excluded species cannot reinvade the community because their per-capita growth rates at low density are strictly negative. Using Eq. (2.10), this condition can be expressed as

$$\mathbf{r}^{(e)} + \mathbf{A}^{(es)}\mathbf{N}^{(s)} < 0, \tag{4.1}$$

where $\mathbf{N}^{(s)}$ denotes the abundance vector of the persistent species, $\mathbf{r}^{(e)}$ the intrinsic growth-rate vector of the excluded species, and $\mathbf{A}^{(es)}$ the interaction matrix describing the effects of the persistent species (s) on the excluded ones (e). Under these conditions, the long-term state of the community is independent of the initial abundances: the same subset of k species persists, while the remaining $n-k$ species eventually become extinct.

When the mathematical conditions ensuring global stability are no longer satisfied—such as in systems characterized by strong competitive asymmetries or highly heterogeneous interaction networks (see Subsection 3.5.1)—the qualitative structure of the phase space may change, allowing multiple attractors to coexist [48, 57]. This phenomenon is known as ***multistability***.

Multistability is thus a dynamical regime in which two or more distinct attractors coexist in the phase space under the same set of structural parameters, interaction matrix, and intrinsic growth rates.

In a multistable system, each attractor is associated with its own basin of attraction. As a result, the long-term state of the community is no longer uniquely determined by the model parameters alone, but also depends on the initial species composition and abundances. In community ecology, this framework provides a mathematical description of *alternative stable states*: sufficiently large perturbations can move the system across the boundary separating two basins of attraction, causing a transition to a different long-term ecological configuration [57].

Besides static attractors, dynamical systems in a multistable regime may also exhibit *limit cycles*, namely isolated closed trajectories corresponding to periodic oscillations in species abundances. A stable limit cycle acts as an attractor: trajectories originating within its basin of attraction converge to the same periodic orbit, independently of their initial phase. Although limit cycles represent an important class of ecological dynamics, they will not be considered further in this thesis, as their identification and numerical characterization require methods beyond the scope of the present work.

Another possible long-term dynamical regime is deterministic ***chaos***. Rather than converging to a fixed point or a periodic orbit, trajectories may remain confined to a bounded region of phase space, often a chaotic attractor. Chaotic dynamics are characterized by sensitive dependence on initial conditions: trajectories starting arbitrarily close to one another diverge exponentially over time, making long-term prediction effectively impossible despite deterministic governing equations [58].

4.1.3 Methods

The temporal evolution of the GLV model was simulated by numerically integrating Eq. (2.1) using the *adaptive fourth–fifth-order Runge–Kutta (RK45) algorithm* implemented in the Python function `scipy.integrate.solve_ivp()` (see Appendix B.1 for a theoretical overview).

As shown in Subsection 2.1.1, in the GLV system species abundances may approach arbitrarily small values but remain strictly positive in continuous time. Following Bunin [25], an extinction threshold (*cutoff*) was therefore introduced to represent numerical and ecological extinction. Extinctions are implemented as terminal events of the ODE solver: when $N_i < c$, the integration is interrupted, the species is removed from the active set by setting $N_i = 0$, and the system is reintegrated from the updated state vector.

The numerical procedure adopted throughout this chapter follows the general framework proposed by [57]. First, a two-dimensional parameter space defined by the variables of interest, (x, y), was discretized into a grid, restricting the analysis to admissible parameter combinations when required (i.e. for modularity, see Eq. (2.20)).

For each point (x, y) of the parameter grid, `num_mats` = 50 independent interaction matrices, denoted by $\mathbf{A}_{(x,y)}$, were generated. For every interaction matrix, `num_ic` = 50 independent initial abundance vectors $\mathbf{N}(t_0)$ were sampled, yielding a total of `num_mats`×`num_ic` independent simulations for each parameter combination.

Each pair $(\mathbf{A}, \mathbf{N}(t_0))_{(x,y)}$ was then integrated using the adaptive RK45 solver, following Eq. (2.2). All simulations were performed using relative and absolute solver tolerances of 10^{-6} and 10^{-8}, respectively. During the integration, species with abundance below the prescribed `cutoff` = 10^{-10} were considered extinct and their abundance was permanently set to zero. The simulation was terminated either when an equilibrium $\mathbf{N}^*$ was reached or when the maximum integration time, `t_max` = 2000 time steps, was exceeded.

If convergence to an equilibrium had not been detected by this time, the simulation was terminated and a final equilibrium estimate was computed directly from the steady-state condition. Specifically, the final interaction matrix $\mathbf{A}^{(\mathrm{ss})}$ was constructed by restricting the full matrix to the subset of the k surviving species, and the corresponding equilibrium abundances $\mathbf{N}^{(s)}$ were obtained by solving

$$\mathbf{A}^{(\mathrm{ss})}\mathbf{N}^{(s)} = -\mathbf{r}^{(s)},$$

where all quantities are restricted to the surviving subcommunity. The linear system was solved using `numpy.linalg.solve()`. If the resulting solution $\mathbf{N}^{(s)}$ is feasible (i.e. all components are positive), the state is interpreted as consistent with a nearby equilibrium and is classified as an attractor.

For each simulation, the final abundance vector $\mathbf{N}^{(\mathrm{s})}(t_f)$, the final integration time t_f, and the number of surviving species $n^{(\mathrm{s})}$ were recorded.

Whenever the simulation converged to an equilibrium, the resulting equilibrium vector was compared with all previously identified equilibria associated with the same interaction matrix $\mathbf{A}_{(x,y)}$. The comparison was performed using the Python

function `numpy.allclose()`, with a prescribed absolute tolerance `atol` = 10^{-4} and zero relative tolerance (`rtol` = 0), so that two equilibria were considered identical only if all corresponding species abundances differed by less than the specified absolute threshold.

If the detected equilibrium matched a previously identified attractor, its associated observables were added to those already recorded for that attractor. Otherwise, the equilibrium was classified as a new attractor and its properties were stored separately.

After all initial conditions had been simulated for a given interaction matrix, the mean values of the quantities of interest were computed across the corresponding simulations. Finally, once all interaction matrices associated with a given parameter pair (x, y) had been analyzed, the mean values over the ensemble of interaction matrices were calculated and used in the subsequent analyses.

Convergence to equilibrium is monitored using the per-capita growth rates of the surviving species, or *fitness*:

$$\lambda_i(t) := \frac{\dot{N}_i}{N_i}(t) = r_i + \sum_{j=1}^{n} a_{ij} N_j(t), \qquad i.j \in S(t).$$

where $S(t)$ denotest the subset of survived species at time t. The system is considered to have reached a steady state when the maximum absolute deviation of λ_i across all survived species satisfies

$$\frac{\max_{i \in S(t)} |\lambda_i|}{\beta} < \epsilon,$$

where $\epsilon = 10^{-5}$ is a baseline tolerance.

The scaling factor β is defined as

$$\beta = \max\left(1, \max_{i \in S(t)} |r_i|, \max_{i \in S(t)} |(\mathbf{A}^{(\mathrm{ss})}\mathbf{N}^{(\mathrm{s})})_i|\right),$$

and introduces an adaptive normalization of the convergence criterion. In particular, when intrinsic growth rates r_i (fixed to unity in this work, see Subsection 2.2.3) or interaction-induced contributions $(\mathbf{A}^{(\mathrm{ss})}\mathbf{N}^{(\mathrm{s})})_i$ are large in magnitude, the criterion effectively becomes relative rather than absolute. The lower bound $\beta \geq 1$ ensures a minimum absolute tolerance in regimes where all dynamical terms are small.

This adaptive criterion reduces the likelihood of false convergence detections, particularly in regimes where species abundances are close to extinction and both $\dot{N}_i$ and N_i become small simultaneously.

Initial conditions (ICs) were drawn from a loguniform distribution over the interval $[10^{-4}, 1]$. This choice ensures that each order of magnitude within the range is sampled with equal probability, avoiding a bias toward either very small or very large initial abundances. In particular, this sampling strategy provides a uniform coverage in logarithmic space, which is appropriate in ecological systems where species abundances can span several orders of magnitude [59]. More generally, broad and heavy-tailed abundance distributions are a well-documented feature of

ecological communities and are often well described by lognormal-like or related distributions across taxa and ecosystems [60].

The lower bound $N_0^{\min} = 10^{-4}$ was chosen to be sufficiently above the extinction threshold ($\texttt{cutoff} = 10^{-10}$), allowing species starting from very low abundances to undergo transient dynamics under negative growth rates before being potentially classified as extinct.

The upper bound $N_0^{\max} = 1$ was selected to be consistent with the normalization used in this work (see Subsection 2.2.3), where the effective single-species carrying capacity in isolation is given by $K_i = -r_i/a_{ii} = 1$. Initial conditions larger than this value would correspond to transient regimes toward the feasible dynamical range of the system, without contributing additional ecological information.

4.2 Attractor space for interactions ($C = 1, Q = 0$)

To investigate the role of network structure in the dynamical evolution of the competitive GLV model, we first need to characterize the asymptotic behavior of the system in the random Erdős–Rényi case (see Subsection 2.3.1). In this section, we perform dynamical simulations over the interaction parameter space (c, σ) and analyze the resulting dynamical regimes. The observed regions of different asymptotic behavior are then compared with well-established analytical predictions.

4.2.1 Number of attractors: comparison with theoretical predictions

Using the methodology described in Subsection 4.1.3, we explore the interaction parameter space

$$(x, y) = (c, \sigma)$$

for the case $C = 1$, $Q = 0$. Specifically, we simulate an ensemble of GLV systems on a discretized grid of (c, σ) values, where each system is initialized with an interaction matrix $\mathbf{A}$ constructed according to Eq. (3.12) and Eq. (3.13).

The main objective is to quantify how the number of attractors to which the dynamics converge, averaged over initial conditions and interaction realizations, varies across the parameter space. In particular, we focus on distinguishing regimes characterized by global convergence to a single attractor from those exhibiting multistability, as discussed in Subsection 4.1.2.

Notably, Bunin [25] derived analytical phase boundaries between different dynamical regimes using methods from statistical physics (see Appendix A.2). These include a *unique fixed-point* (UFP) regime, corresponding to global stability; a *multiple-attractor* (MA) regime; and a regime of *unbounded growth* (UG), where the GLV dynamics are expected to break down.

In particular, the unrealistic outcome of the UG phase is due to the a positive feedback mechanism that arises when interactions are very heterogeneous, and it is due to the linear dependence of per-capita growth rate on the remaining populations (see Subsection 2.1.1, [5]). This limitation has been adressed in recent studies (i.e. [5]), but we will not address it further in this work, focusing instead on UFP and MA phases.

In Figure 4.1 we report the results of the simulations for a initial number of species $n = 50$ together with the corresponding analytical predictions derived by Bunin. The agreement between the two is good across the entire explored parameter range.

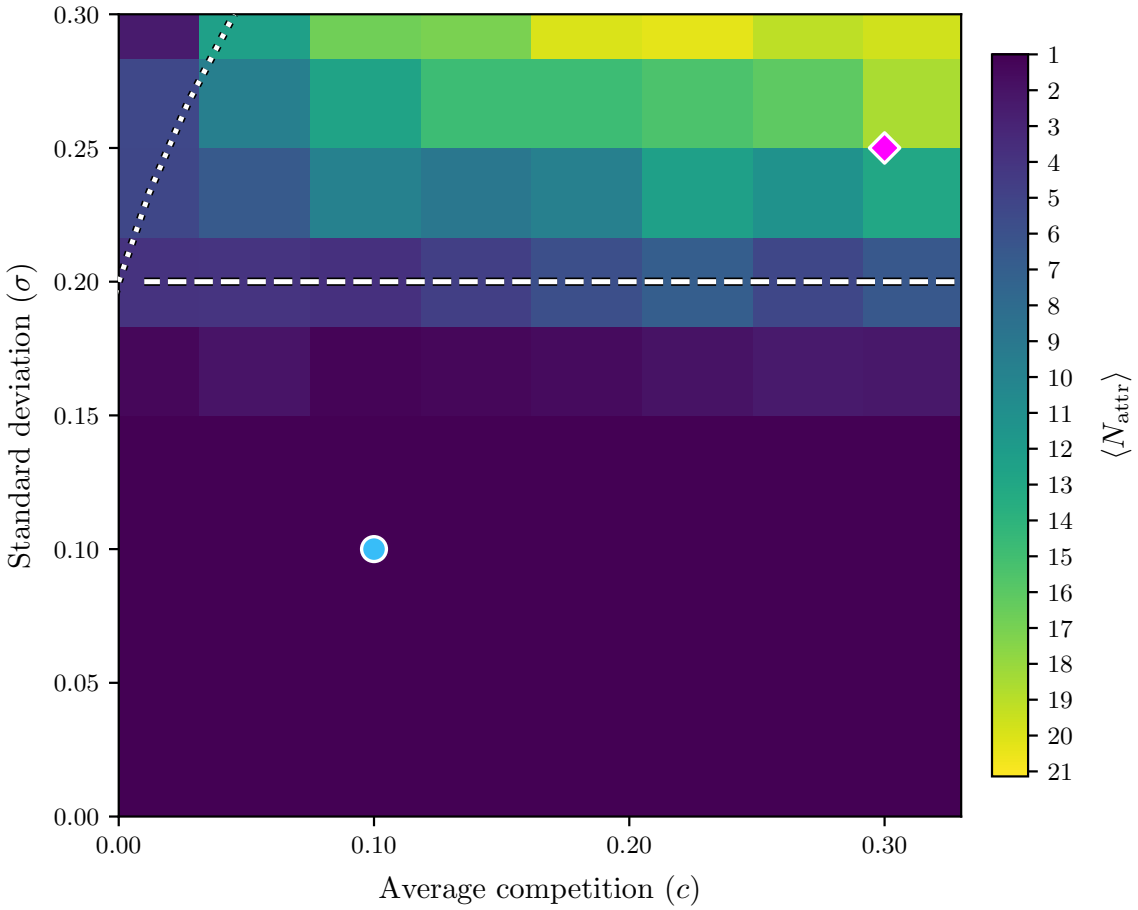

Figure 4.1.. Mean number of attractors across the interaction parameter space (c, σ) for the competitive GLV model. At each grid point, the mean was computed over an ensemble of 50 independently generated interaction matrices $\mathbf{A}$, each simulated from 50 independent initial conditions. All initial systems contain $n = 50$ species and are fully connected ($C = 1$, $Q = 0$). The numerical simulation parameters are described in Subsection 4.1.3. Dashed lines indicate the analytical boundaries between dynamical regimes predicted by Bunin [25]. The two representative points of the UFP regione and MA region (Eq. (4.2)) are marked respectively with a cyan circle and a magenta diamond.

We can therefore describe how, in a fully connected network, the average strength of competitive interactions c and their heterogeneity σ jointly control the number of attractors of the dynamics. In particular, the parameter space can be interpreted in terms of distinct dynamical regimes: **low interaction strength and low variability are associated with global convergence to a single attractor**, whereas increasing either c or σ progressively destabilizes the global attractor and leads to the emergence of multistability, characterized by multiple coexisting attractors. The analytical

prediction states that for sufficiently large values of the interaction variability, the system enters a regime of unbounded growth.

In Section 4.3 and Section 4.4, we investigate how these results are modified when the interaction network is no longer fully connected. To this end, we select two representative points in the interaction parameter space, corresponding to the unique fixed-point (UFP) and multiple-attractor (MA) regimes identified in the fully connected case. These points, indicated in Figure 4.1, are

$$(c, \sigma)_{\mathrm{UFP}} = (0.1, , 0.1), \qquad (c, \sigma)_{\mathrm{MA}} = (0.3, , 0.25), \tag{4.2}$$

for a system size of $n = 50$. In the following section, these parameter values are used as reference interaction regimes to assess the effect of varying the network topology through the parameters C and Q.

Note that, for consistency, we chose the UFP point equal to the one used in the previous numerical simulations in Chapter 3.

4.2.2 Species survival

In addition to the number of stable states, a key macro-variable characterizing the final ecological state of the system is the fraction of surviving species at steady state, that we will indicate with the symbol ϕ. Using the same simulation ensemble for $n = 50$, $C = 1$, and $Q = 0$, we evaluate the average percentage of survived species across the (c, σ) parameter space. The resulting landscape is shown in Figure 4.2.

The numerical results indicate that species survival is primarily controlled by the interaction heterogeneity σ, while displaying a weaker dependence on the average competition strength c within the explored bounds. When heterogeneity is low ($\sigma \leq 0.05$), the system systematically retains 100% of its initial pool, corresponding to a regime of total coexistence. As σ increases, the average percentage of surviving species decreases monotonically due to the onset of competitive exclusion.

It is worth noting that the fraction of surviving species begins to decline around $\sigma \approx 0.10$, well before the transition to the MA regime predicted at $\sigma = 0.20$. This implies that while for low heterogeneity ($\sigma \lesssim 0.10$) the unique fixed point corresponds to a globally stable internal equilibrium where all initial species coexist, exceeding this threshold alters the nature of the attractor. Specifically, within the intermediate region $0.10 \lesssim \sigma < 0.20$, the dynamics still converge to a unique equilibrium, but it shifts from an internal to a boundary fixed point characterized by competitive exclusion. Consequently, the initial system no longer admits a feasible internal equilibrium. This structural transition is expected to correspond approximately to the loss of Volterra–Lyapunov stability of the interaction matrix, which constitutes a sufficient condition for the existence of a unique global equilibrium (see Prop. 31).

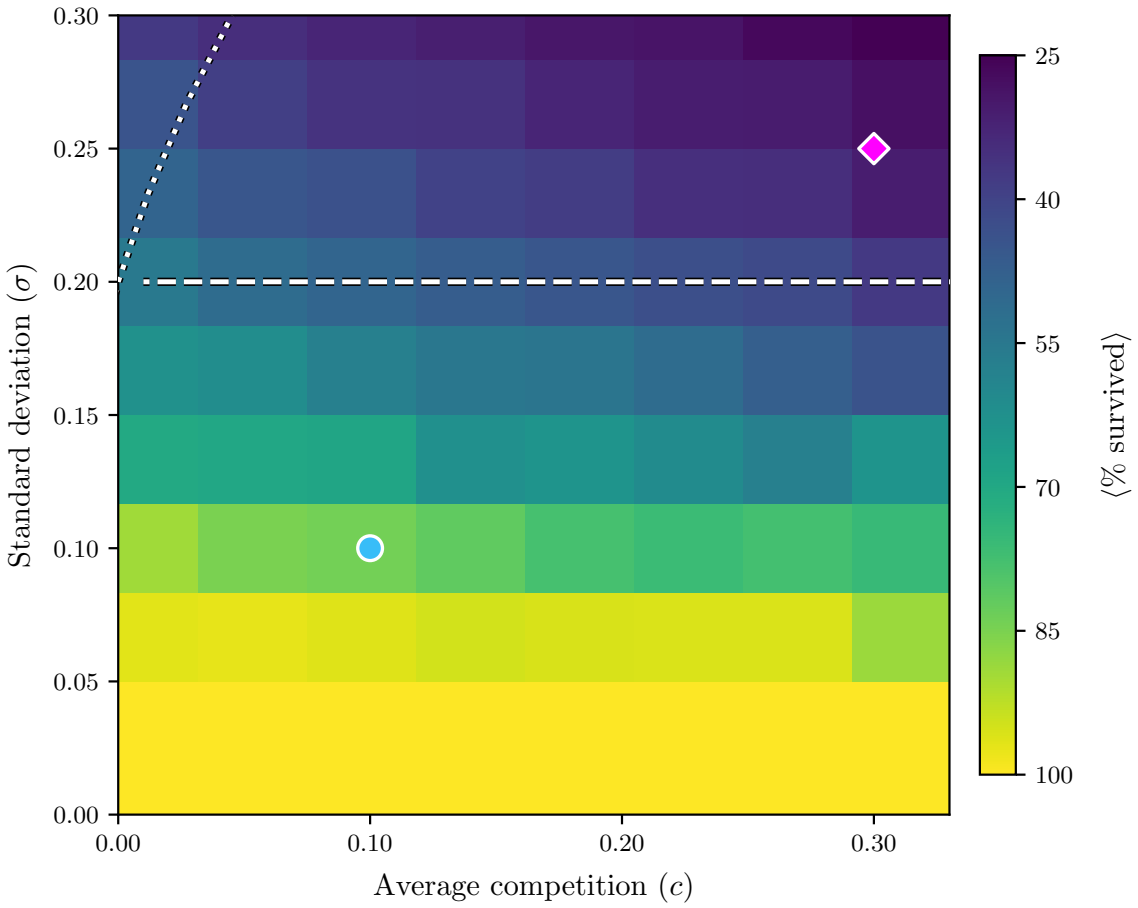

Figure 4.2.. Average percentage of survived species across the interaction parameter space (c, σ) for the competitive GLV model. The simulation parameters and ensemble size are identical to those in Figure 4.1. The color bar denotes $\phi = \langle$% survived$\rangle$, with values ranging from 100% (yellow) down to 25% (dark purple). Dashed and dotted lines indicate the transition boundaries between different survival regimes. The cyan circle and magenta diamond mark the reference UFP and MA points defined in Eq. (4.2), respectively.

The two reference points selected in Eq. (4.2) are characterized by distinct survival properties:

- The UFP point at $(c, \sigma) = (0.1, 0.1)$, indicated by the cyan circle, is located within a high-survival zone ($\approx 85\%$). This confirms that the unique fixed-point regime maintains high community robustness and low extinction rates.
- The MA point at $(c, \sigma) = (0.3, 0.25)$, indicated by the magenta diamond, lies deep within the low-survival regime ($\approx 40\%$).

This shows that the emergence of multiple attractors and complex dynamical phases is strictly coupled with significant competitive exclusion.

4.2.3 Final species abundance distribution: comparison with theoretical predictions

A comprehensive characterization of the asymptotic state GLV dynamics requires looking beyond aggregate macro-variables (such as the total number of attractors or the global survival fraction) to investigate the statistical distribution of individual species abundances. The *Species Abundance Distribution* (SAD) is a central concept in community ecology, representing the probability density function of species abundances at steady state [60].

To evaluate the empirical SAD, we integrate the competitive GLV equations starting from random initial conditions using an ensemble of 300 independent interaction matrices $\mathbf{A}$ with parameters fixed at the unique fixed-point (UFP) regime $(c, \sigma) = (0.1, 0.1)$ for an initial pool of $n = 50$ species. Once the dynamics reach a stationary state ($t = t_{\max}$), we collect the final abundances of all surviving species across all realizations to construct an empirical probability density histogram.

In the thermodynamic limit ($n \to \infty$), the self-consistent cavity method developed by Bunin [25] predicts that the continuous part of the SAD—corresponding to the persistent species—follows a **truncated Gaussian distribution** whose mean and variance are determined implicitly by the interaction statistics (c, σ) and the functional response of the system.

The comparison between our numerical simulations and the analytical framework is presented in Figure 4.3. The numerical results demonstrate good agreement with Bunin's asymptotic predictions also for relatively low n ($n = 50$). The empirical histogram tracks the continuous dark purple curve across the entire range of final abundances, validating the accuracy of the cavity method approximation even for finite initial system sizes.

Furthermore, the inset confirms the predictive power of the theory regarding competitive exclusion: the analytical survival fraction ($\phi_{\text{teor}} = 85\%$) falls squarely within the statistical error bounds of the empirical ensemble average ($\phi_{\text{exp}} = 84\%$), calculated as the mean value. This match indicates that the statistical mechanics framework accurately captures both the microscopic abundance variations and the macroscopic extinction rates that characterize the boundary equilibrium of this interaction regime.

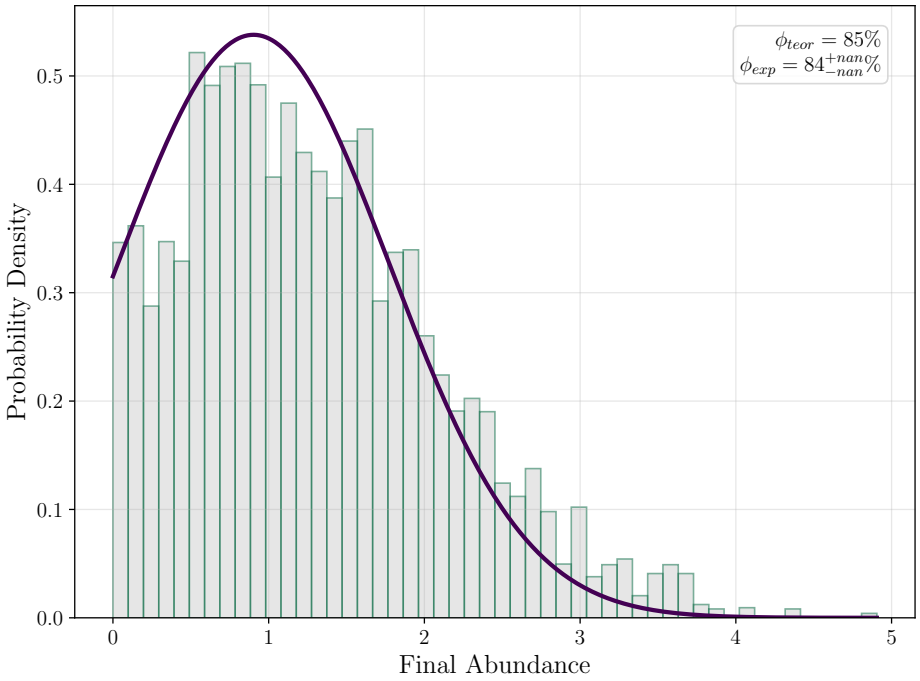

Figure 4.3.. Species Abundance Distribution (SAD) at the final steady state for the competitive GLV model in the UFP regime. The empirical histogram (green-outlined bars) represents the pooled final abundances of surviving species from 150 independent interaction matrices $\mathbf{A}$, tested over `num_ic` = 50 independent simulation runs. The solid dark purple curve shows the analytical prediction derived via the cavity method by Bunin [25]. The inset compares the theoretical survival fraction ($\phi_{\text{teor}} = 85\%$) with the empirical mean survival fraction ($\phi_{\text{exp}} = 84\%$).

To fully evaluate how the competitive GLV dynamics shape the community structure, it is instructive to compare the initial abundance distribution with the final steady-state SAD on a logarithmic scale. This comparison is reported in Figure 4.4, which contrasts the initial conditions with the asymptotic state for the already seen UFP state and also for the MA state.

For this simulations, we adopted a different sampling strategy. Specifically, we considered 50 independent interaction matrices $\mathbf{A}$, each simulated with `num_ic` = 150 initial conditions. As discussed in Appendix B.2, this choice provides a more accurate characterization of the alternative final states associated with each interaction matrix of the MA point.

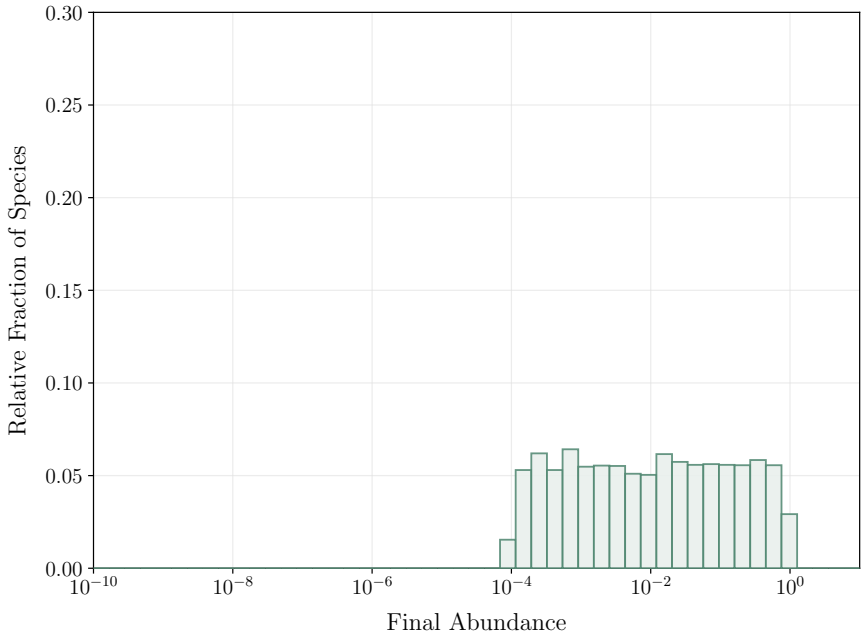

(1) Initial Abundance Distribution

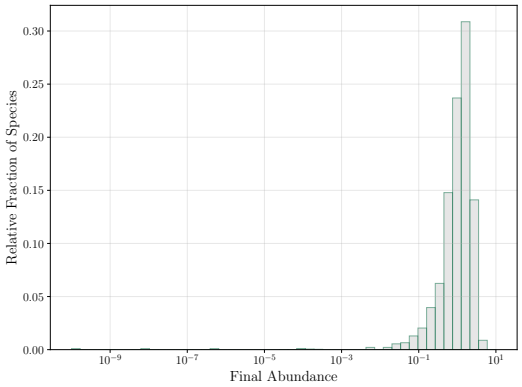

(2) Final Abundance Distribution (UFP)

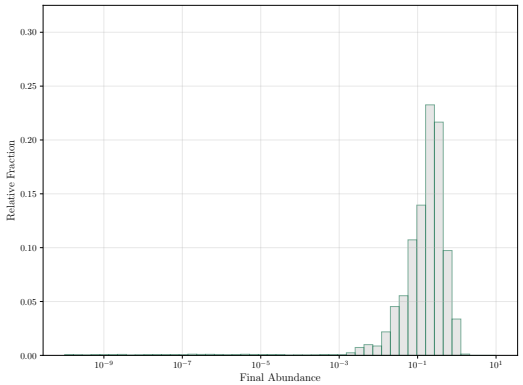

(3) Final Abundance Distribution (MA)

Figure 4.4.. Species Abundance Distribution (SAD) on a logarithmic x-axis, corresponding to the same analysis of Figure 4.3. Panel (a) shows the initial log-uniform distribution of species abundances sampled between 10^{-4} and 10^{0}. Panel (b) illustrates the final steady-state distribution under the UFP interaction regime, while panel (c) illustrates the final steady-state distribution under the MA interaction regime.

The logarithmic transformation highlights a profound dynamical restructuring of the community. Initially, the species pool is artificially constrained to a flat, log-uniform profile strictly bounded between 10^{-4} and 10^{0} (Figure 4.41). Throughout the dynamical evolution, competitive interactions systematically dismantle this uniformity, forcing the ecosystem into a highly uneven and hierarchical state (Figure 4.42, Figure 4.43).

The final SAD is characterized by a prominent peak near 10^{0}, representing a stable pool of highly abundant, dominant species. Concurrently, the system develops an elongated, heavy left tail that stretches down to the imposed cutoff value 10^{-10}.

This broad spectrum expands the dynamic range of relative abundances across different orders of magnitude, revealing the persistence of rare species, in some cases operating near the extinction threshold.

This emergent pattern strongly aligns with empirical ecological literature, where community structures are often characterized by heavy-tailed profiles with a strong presence of rare taxa [59].

We observe that the cumulative SAD at the UFP point is more peaked (maximum normalized frequency of approximately 0.31) than at the MA point (approximately 0.23). A plausible explanation is that, in the MA regime, the coexistence of multiple attractors generates a larger variety of final abundance configurations, which broadens the cumulative SAD and reduces its peak.

4.2.4 Final network structure

We analyze the structural features of the final attractors within the interaction parameter space. Figures 4.51 and 4.52 show the asymptotic values of the network modularity $\langle Q_f \rangle$ and connectance $\langle C_f \rangle$ across the (c, σ) plane for an initially fully connected community.

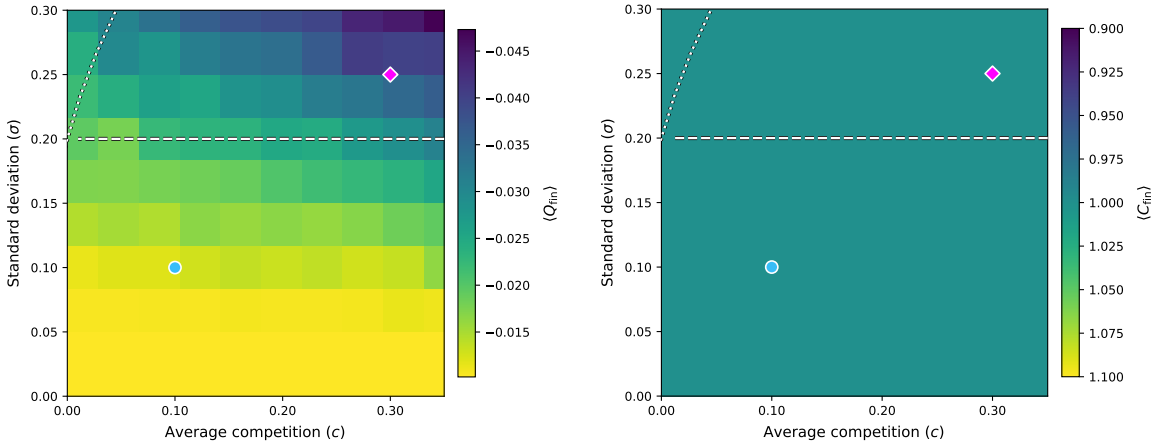

(1) Final modularity $\langle Q_f \rangle$ **(2)** Final connectance $\langle C_f \rangle$

Figure 4.5.. Mean final structural parameters over the interaction space (c, σ). For each point of the discretized grid, values are averaged over an ensemble of 50 interaction matrices $\mathbf{A}$, considering $num\_ic = 50$ initial conditions each. The white lines mark the analytical boundaries between the dynamical regimes (UFP, MA and UG) by Bunin (see Figure 4.1).

The final connectance remains strictly constant at $\langle C_f \rangle = 1.000$ across the entire parameter space. This uniform profile is a direct consequence of the fully connected framework: even when species abundances change dynamically or face selective pressures, the underlying structural matrix preserves its global path connectivity among the surviving components, preventing any link pruning.

Conversely, the final modularity metric $\langle Q_f \rangle$ displays a mild but systematic departure from zero, consistently dropping into negative values ($\langle Q_f \rangle < 0$) across all

sampled combinations of c and σ. This negative shift indicates that **the surviving interaction network tends to acquire an antimodular organization**. Moreover, the magnitude of this antimodularity increases monotonically with the interaction variance σ, reaching its largest deviation in the top-right region of the parameter space.

This systematic tendency toward antimodularity is somewhat unexpected. As discussed in Subsection 3.4.3, static equilibrium analyses indicate that antimodular interaction matrices are generally less stable than fully connected ones. The present results therefore suggest that **the network topology emerging after dynamical pruning cannot be inferred solely from the stability properties of the original interaction matrix**. Instead, the pruning process itself appears to introduce additional structural selection mechanisms.

A plausible interpretation is that increasing interaction heterogeneity (σ) promotes the survival of species configurations that reduce effective competitive overlap. Since the self-regulation terms remain fixed ($a_{ii} = -1$, see Subsection 2.2.3), this reduction can only occur through the off-diagonal interaction structure. The observed emergence of antimodularity is therefore consistent with a reorganization in which strong competitive interactions are preferentially distributed between distinct groups of surviving species rather than concentrated within them.

To gain a deeper insight into the structural reorganization of the communities, we move from analyzing mean parameter space values to examining the full probability distributions of final connectance (C_f) and modularity (Q_f). We consider the two representative points within the interaction space already discussed (one in the Unique Fixed Point regime characterized by low interaction variance, and a second in the Multiple Attractors regime driven by higher heterogeneity, Eq. (4.2)).

Figures 4.61 and 4.62 display the relative fraction of attractors as a function of their final structural metrics for the UFP and MA cases, respectively. Following the numerical analysis of Appendix B.2, we averaged the observables over 150 initial conditions for each of the 50 interaction matrices $\mathbf{A}$ considered.

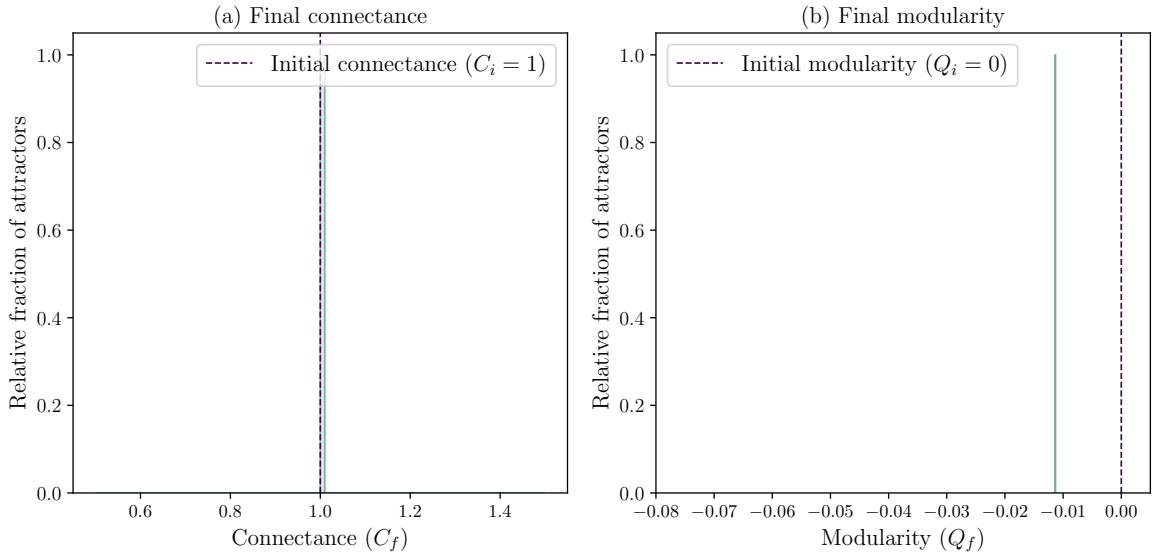

(1) Point in UFP region

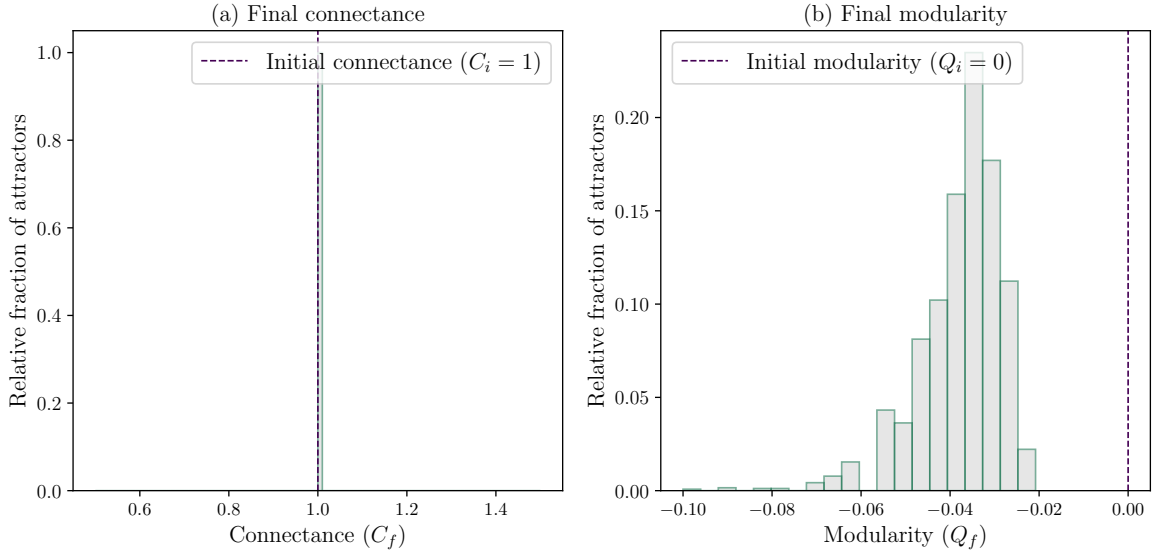

(2) Point in MA region

Figure 4.6.. Distribution of the final structural parameters over an ensemble of 50 interaction matrices **A**, each considered for `num_ic` = 150 different initial conditions. The analysis has been repeated for the UFP point (panel (a)) and for the MA point (panel (b)).

In both regimes, the final connectance distributions shown in panel (a) collapse to a deterministic peak at $C_f = 1$. This confirms that competitive dynamics preserve the complete connectivity of the interaction network, as no links are removed between surviving species.

The final modularity Q_f, however, differs markedly between the two regimes:

- **UFP regime:** The distribution collapses to a unique modularity value around $Q_f \approx -0.011$. Since each interaction matrix admits a unique stable equilibrium, the final network structure is deterministic, consistently exhibiting a weak

antimodular organization.

- **MA regime:** The distribution becomes broad, spanning approximately $Q_f \in [-0.08, -0.02]$, with a mode near -0.03. The coexistence of multiple attractors allows different initial conditions to converge to distinct sets of surviving species, producing a range of final interaction structures.

The broader distribution observed in the MA regime reflects the existence of multiple alternative stable states. While the diagonal self-regulation terms remain fixed ($a_{ii} = -1$), different subsets of surviving species induce different off-diagonal interaction patterns, leading to varying degrees of antimodularity. Consequently, unlike the UFP regime, the final modularity is not uniquely determined by the interaction matrix but depends on the attractor reached by the dynamics.

4.2.5 Attractor weight distribution in the MA phase

In this subsection, we discuss the numerical characterization of the basin of attraction volumes within the Multiple Attractor (MA) phase. To quantify the structural fragmentation of the phase space, we analyze the relative weight w of each static attractor found, defined as the fraction of random initial conditions that successfully converge to it. The numerical results are gathered by simulating an ensemble of 500 independent modular interaction matrices (`ma_params_no_ss`) without structural symmetry, sampling 200 log-uniformly distributed initial conditions per matrix configuration (see Appendix B.2).

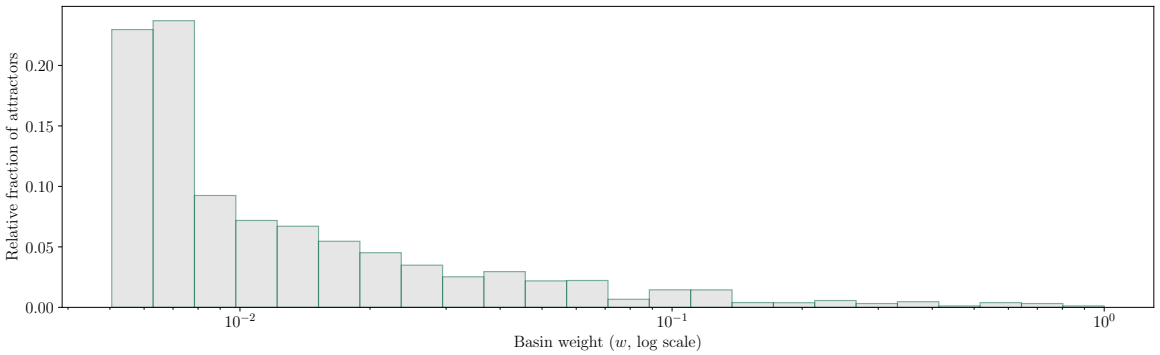

Figure 4.7.. Empirical probability distribution (relative fraction) of the attractor basin weights w in the MA phase ($c = 0.3, \sigma = 0.25$), obtained from an ensemble of 500 fully connected interaction matrices with 200 initial conditions per run. The x-axis is displayed on a logarithmic scale with log-spaced binning.

The empirical distribution of the basin weights, illustrated in Figure 4.7, exhibits a highly heterogeneous setting. The most prominent statistical feature is the sharp accumulation of attractors in the smallest weight bins close to the resolution limit ($w \sim 5 \times 10^{-3}$). The first two bins peak between 0.20 and 0.25, collectively accounting for over 40% of the total discovered attractors. This peak is followed by a rapid, monotonic decay as w increases toward 10^0. This specific profile—when evaluated under log-spaced binning—is characteristic of a **power-law distribution**. The landscape is

populated by an exceptionally large number of rare attractors commanding minuscule basins of attraction, balanced by a long and flat tail representing rare dominant attractors with macroscopic basins ($w \to 1$).

To evaluate this heavy-tailed behavior, we calculate the probability density function $P(w)$ of the unbinned, strictly positive empirical data and fit it to a power-law model. The fit is performed over the entire data domain through *Maximum Likelihood Estimation (MLE)*, which determines the values that maximize the likelihood of observing the empirical dataset under the assumed power-law model. The fit is performed over the entire data domain using the Python method `powerlaw.Fit()`.

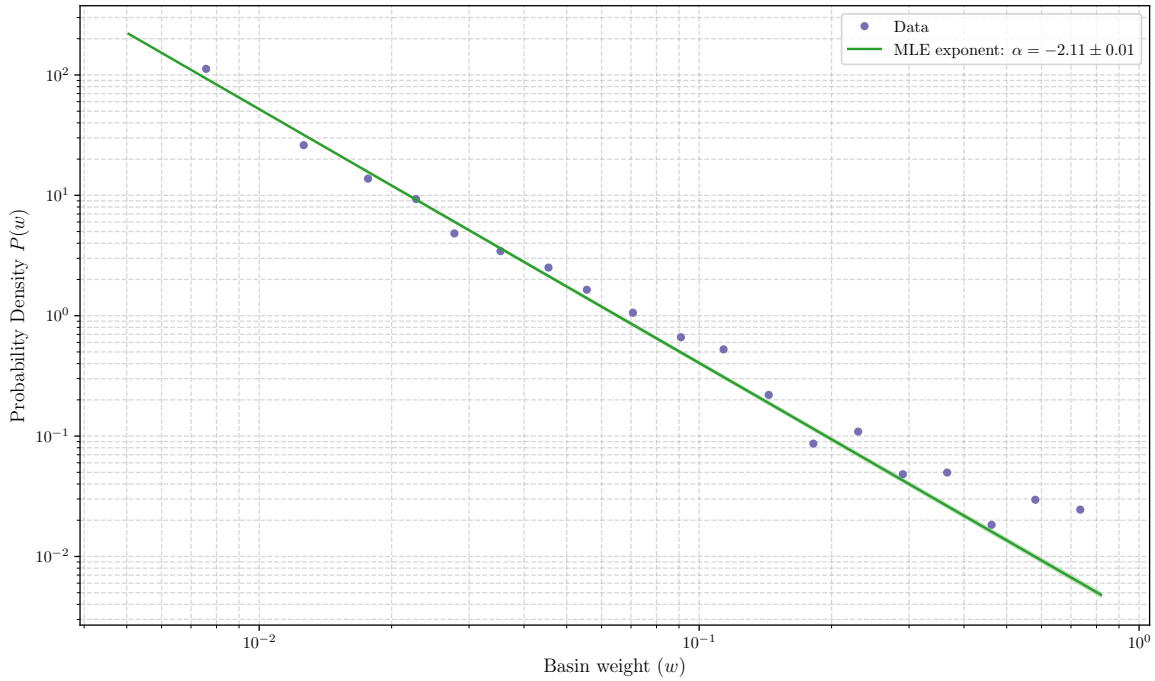

Figure 4.8.. Probability density $P(w)$ of the basin weights plotted on a log-log scale. The purple dots represent the empirical data, while the green solid line represents the Maximum Likelihood Estimation (MLE) power-law fit.

Figure 4.8 displays the probability density $P(w)$ on a log-log scale, where the visual linear decay over multiple orders of magnitude confirms the power-law nature of the distribution. The MLE fit yields a scaling exponent of $\alpha = -2.11 \pm 0.01$.

Despite the finite-size sampling limitations, the underlying trend of a heavy-tailed distribution with an exponent near -2 is consistent with analytical predictions for random Generalized Lotka-Volterra models, which demonstrate that the multistability regime generates severe phase-space fragmentation [61], although more specific analyses like this are not known to us for this particular formulation of the model.

4.3 Attractor space for structural parameters C, Q - UFP

In Section 4.2, we analyzed how the dynamical evolution of the model depends on the interaction parameters (c, σ).

In this section, we build upon those results to examine the role of the structural parameters C and Q. Specifically, we select a representative point from the unique fixed-point region identified for the fully connected case ($C = 1$, $Q = 0$):

$$(c, \sigma)_{\text{UFP}} = (0.1, 0.1).$$

We investigate how varying C and Q modifies the corresponding dynamical behavior. In particular, we assess whether changes in the network topology preserve or alter the dynamical regimes previously characterized in the fully connected system, and the characteristics of the final equilibria, such as the average number of extinctions and the species abundance distribution (SAD).

4.3.1 Number of attractors and species survival

To isolate the effect of parameters C, Q on the dynamical regimes of the model, we scan the parameter space

$$(x, y) = (Q, C)$$

for the UFP point of Eq. (4.2), corresponding to a representative of the regime of interest in the fully connected case (see Figure 4.1).

In Figure 4.9 we report the results of the simulations for $n = 50$ performed following the methodology described in Subsection 4.1.3.

We observe that **in this interaction regime, antimodularity induces a bifurcation of the unique fixed point**. Evidence for this mechanism is provided by the extinction plot, where the fraction of extinctions decreases to approximately 50% in this region of the parameter space.

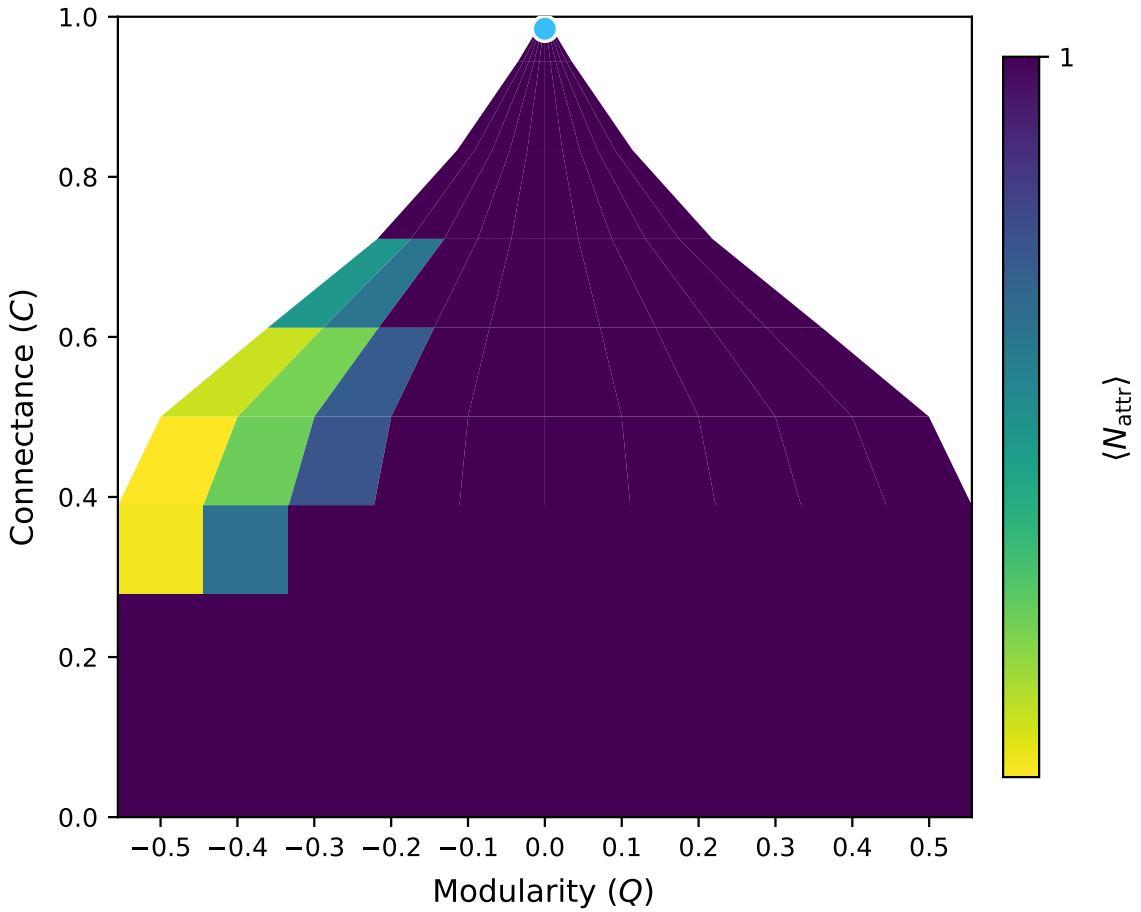

Figure 4.9.. Mean number of attractors for the UFP point across the structure parameter space (C, Q) for the competitive GLV model. At each grid point of the admitted range for Q (see Eq. (2.20)), the mean was computed over an ensemble of 50 independently generated interaction matrices $\mathbf{A}$, each simulated from 50 independent initial conditions. All initial systems contain $n = 50$ species and have fixed interaction parameter ($c = 0.1$, $\sigma = 0.1$). The numerical simulation parameters are described in Subsection 4.1.3. The cyan circle is the UFP point for the fully connected case marked also in Figure 4.1.

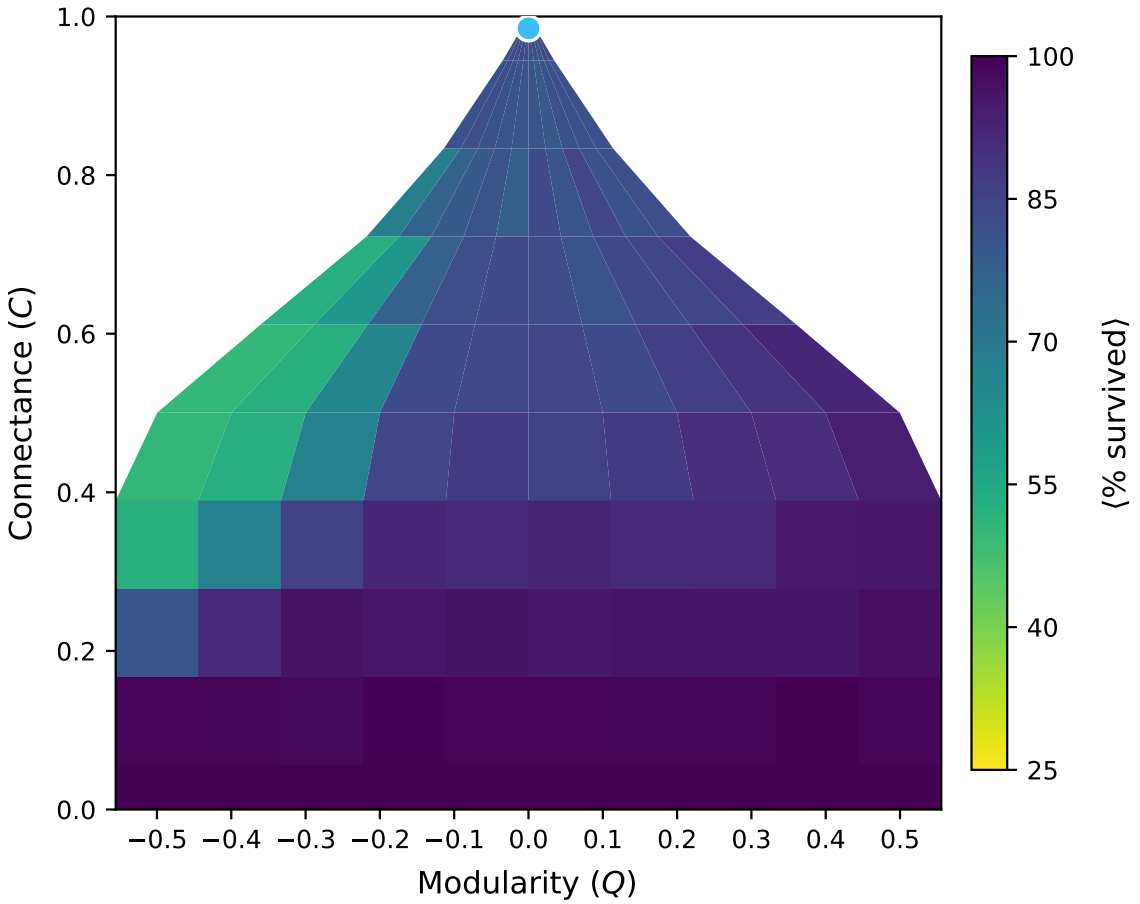

Figure 4.10.. Average percentage of survived species for the UFP point across the structure parameter space (C, Q) for the competitive GLV model. The interaction parameters are fixed at the unique fixed-point reference values $(c, \sigma) = (0.1, 0.1)$ for an initial system size of $n = 50$ species. The ensemble size and numerical simulation parameters are identical to those specified in Figure 4.1. The color bar denotes $\langle$% survived$\rangle$, with values ranging from 25% (yellow) up to 100% (dark purple). The cyan circle at the apex $(C = 1, Q = 0)$ marks the baseline fully connected configuration.

This behavior can be explained by the complete extinction of one module while the other survives. Figure 4.11 shows, for different values of the modularity parameter, the eigenvalue spectrum of the final equilibrium together with the spectra associated with the two equally sized modules, obtained from a single simulation.

- For strongly antimodular systems ($Q_i = -0.480$), competitive exclusion drives one module to extinction. Consequently, the spectrum of the global equilibrium coincides exactly with that of the surviving module, while the second module leaves no spectral signature.
- At intermediate values of Q_i, the two module spectra exhibit a non-trivial overlap.

- For modular systems ($Q_i = 0.480$), the two modules become dynamically independent, and the global equilibrium is simply the superposition of the two decoupled sub-equilibria. Notice the presence of the two outlier eigenvalues characteristic of modular matrices, as discussed in Proposition 22.

Since the two modules have identical size and interaction statistics, this result indicates that, in this interaction regime, antimodularity generates bistability: the surviving module is selected by the initial conditions, with arbitrarily small differences determining which of the two ultimately prevails.

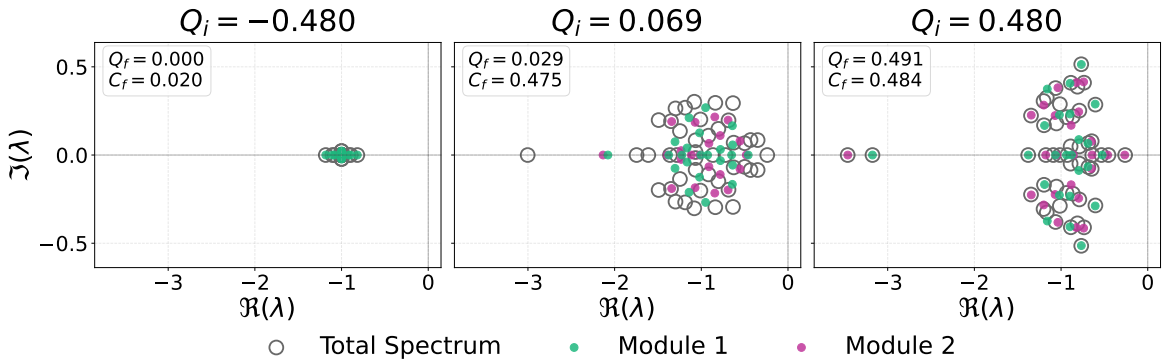

Figure 4.11.. Eigenvalue spectrum of the final interaction matrix for a single simulation realization in the UFP interaction regime $(c, \sigma) = (0.1, 0.1)$. The initial system contains $n = 50$ species structured into two equally sized modules, with an intermediate initial connectance fixed at $C_i = 0.5$. Panels from left to right show the transition from strongly antimodular ($Q_i = -0.480$), to weakly modular ($Q_i = 0.069$), and strongly modular ($Q_i = 0.480$) configurations. Empty grey circles denote the total spectrum of the global equilibrium, while filled green and magenta circles represent the spectral contributions computed independently from Module 1 and Module 2, respectively. Insets report the final modularity Q_f and connectance C_f at steady state. For $Q_i = -0.480$, competitive exclusion leads to the complete extinction of one module ($C_f \approx 0.020$, $Q_f = 0.000$), leaving the global spectrum identical to that of the single surviving module.

This interpretation is further supported by the extinction asymmetry between the two modules, shown in Fig. 4.12. The figure, obtained from the same simulation, clearly shows that one module undergoes complete extinction while the other survives in the antimodular regime.

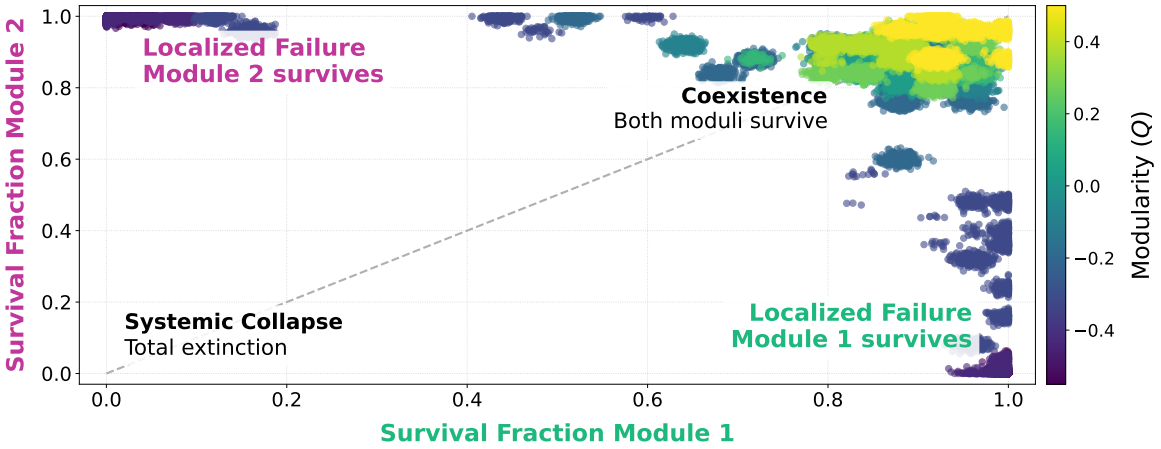

Figure 4.12.. Survival fraction of Module 1 versus Module 2 across the modularity spectrum for the UFP interaction regime. Each point represents a single simulation run from an ensemble of 50 independent interaction matrices, each evaluated across 50 initial conditions (50×50 total realizations per parameter set) for an initial pool of $n = 50$ species and intermediate initial connectance $C_i = 0.5$. The color bar denotes the initial modularity Q, ranging from strongly antimodular ($Q \approx -0.5$, dark purple) to strongly modular ($Q \approx 0.5$, yellow). The dashed diagonal line represents symmetric coexistence between modules. Antimodular configurations cluster exclusively at the top-left and bottom-right boundaries, illustrating the bistable nature of localized failure where competitive exclusion drives one module to complete extinction while the other maintains high survival.

4.3.2 Final species abundance distribution (SAD)

To understand how the topological structure of the network (defined by connectance C and modularity Q) influences the organization of the system outside the fully connected limit, we analyze the final species abundance distribution (SAD) for the UFP point ($c = 0.1, \sigma = 0.1$).

In Figure 4.13, we report the evolution of the SAD as a function of C and Q. We observe that the system maintains a persistent heterogeneous structure, characterized by a dominant peak and a long left tail describing the presence of rare species, confirming that the heavy-tailed structure of the SAD is a robust property of the competitive GLV model.

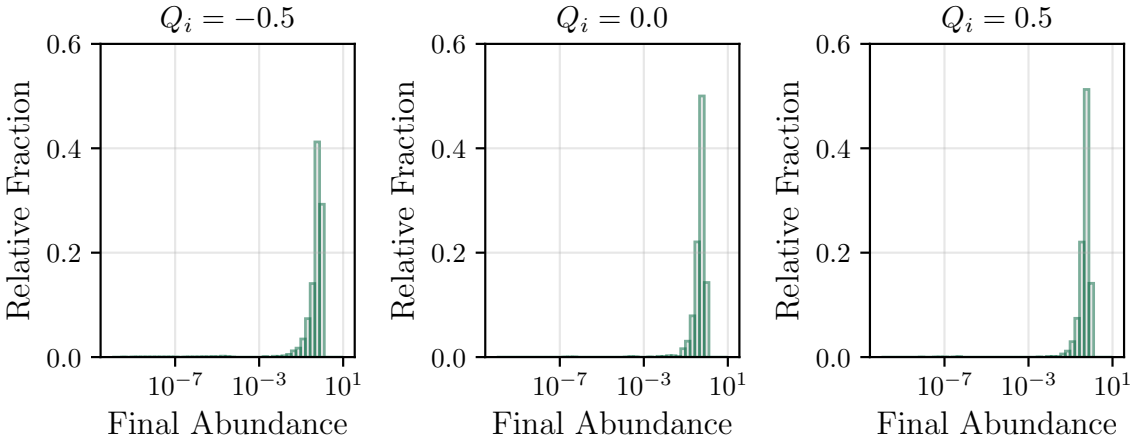

(1) Low connectance (C_i = 0.2)

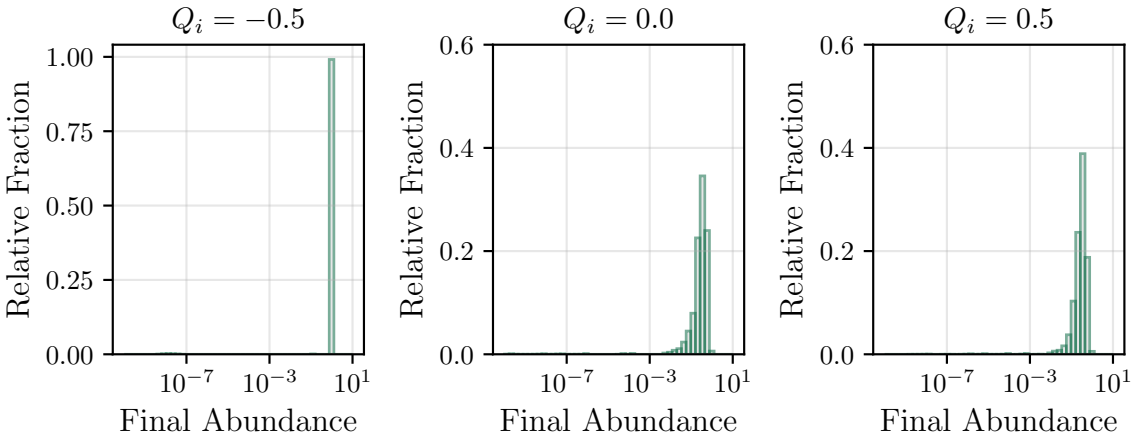

(2) Medium connectance (C_i = 0.5)

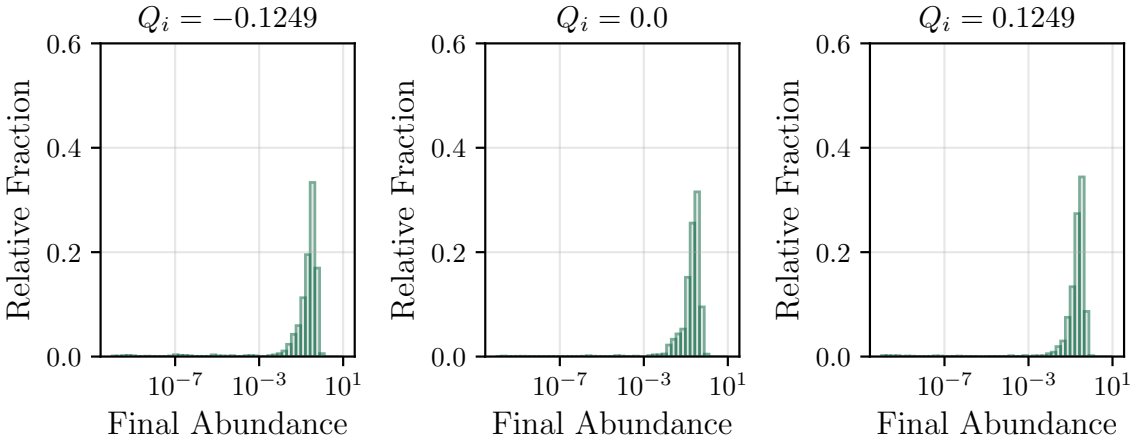

(3) High connectance (C_i = 0.8)

Figure 4.13.. Final species abundance distribution (SAD) across different values of initial connectance C and initial modularity Q_i for the UFP regime (c = 0.1, σ = 0.1). The two $Q_i \neq 0$ values are the extreme values admissible for each C_i for n = 50 (Eq. (2.20)). The distributions are plotted with a logarithmic scale on the x-axis to highlight the long left tail representing rare species.

Connectance alone seems to have an effect on the abundance distributions: **low connectance is associated with peaked SADs with respect to high connectance**, where the species are distributed more uniformly across differen orders of magnitude. This observation is further strengthened comparing these results to the SAD obtaines for the fully connected case at the same UFP point (panel (b) of Figure 4.3), where the maximimum fraction of species over the normalized histogram is around 0.3, less than the values obtained for lower values of C.

In this regime of interactions, the SADs mantain the characteristic long-tailed form of the fully connected case.

The only significant deviation is observed for $C = 0.5$ and $Q_i = -0.5$, where the distribution collapses onto a nearly singular value, consistent with the total competitive exclusion phenomenon described in Subsection 4.3.

Under the restrictive assumption of Volterra–Lyapunov stability, which guarantees the D-stability of the initial interaction matrix $\mathbf{A}$ (see Subsection 3.2.2), Allesina investigated the final SAD under different network structures and concluded that topology has no influence on this observable [48] (see Figure 1 in [48]).

Although the present analysis is based on a relatively limited sampling and should be confirmed with a larger number of realizations, our results suggest that, outside the D-stable regime, **network structure generally affects the final SAD in the UFP region**. Indeed, Figure 3.12 shows that the selected UFP point, $(c, \sigma) = (0.1, 0.1)$, is, on average, not D-stable. Therefore, our findings are not necessarily in contradiction with those of Allesina, whose conclusions were derived under the stronger assumption of D-stability.

4.3.3 Final network structure

As already done for the interaction parameter space in Subsection 4.2.4, we investigate how the final network structure—measured via final connectance $\langle C_f \rangle$ and final modularity $\langle Q_f \rangle$—is shaped by the initial topological parameters (C, Q) in the Unique Fixed Point (UFP) regime ($c = 0.1, \sigma = 0.1$). Simulations are performed using an initial pool of $n = 50$ species, averaged over 50 interaction matrices with `num_ic` = 50 initial conditions per matrix.

The resulting parameter space mapping for the final connectance is presented in Figure 4.14.

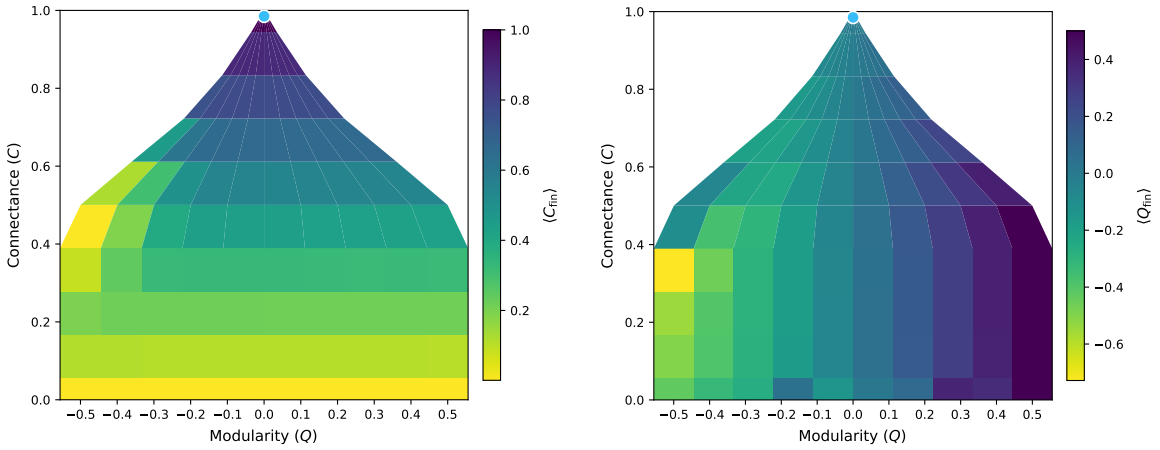

(1) Average final connectance $\langle C_f \rangle$.

(2) Average final modularity $\langle Q_f \rangle$.

Figure 4.14.. Average final structural parameters in the (Q_i, C_i) parameter space for the UFP point $c = 0.1, \sigma = 0.1$.

Across the vast majority of the (Q, C) domain, the final connectance behaves deterministically, mapping directly onto the initial connectance ($\langle C_f \rangle \approx C$). This is manifested as horizontal, uniform monochromatic bands in Figure 4.14. Because the low interaction strength and variance of the UFP phase yield high baseline species survival (Figure 4.10), the original links in the community are largely preserved during the dynamical allocation of the equilibrium.

Concurrently, Figure 4.142 shows that the average final modularity $\langle Q_{\text{fin}} \rangle$ closely mirrors the initial modularity Q. This produces a vertical banding pattern where the color gradient changes strictly along the x-axis, moving from negative, antimodular values (yellow/green) on the left to positive, modular values (dark purple) on the right. This linear alignment confirms that the stable unique fixed point dynamics do not inherently reorganize the macroscopic community partitions outside of specific localized regions

However, a prominent structural anomaly emerges in the region of intermediate connectance ($C \in [0.4, 0.6]$) coupled with strong initial antimodularity ($Q \leq -0.4$). In this zone, the final connectance drops sharply toward zero (visible as a bright yellow patch on the left flank of the triangular domain in panel (a)) and, concurrently, interal structure is lost (modularity drops to zero, as visible in panel (b) for the same parameter region).

This localized structural collapse is a direct consequence of the total competitive exclusion phenomenon. In a moderately connected, strongly antimodular competitive network, the distribution of interspecific links creates highly asymmetric competitive pressures across specific sub-groups. This asymmetry triggers systemic cascading extinctions that drastically prune the community down to a single module, as already discussed in Subsection 4.3.1. Because in the antimodular regime species intra-module interactions tend to zero $\langle C_f \rangle \to 0$, the interspecific network structure is effectively obliterated. Outside this exclusion zone, the macrostate network properties remain robust and structurally invariant under the UFP dynamical flow.

4.4 Attractor space for structural parameters C, Q - MA

We repeat the same type of analysis done in Section 4.3 for the unique fixed point in the fully connected regime, but this time for the chosen multiple attractors region (MA) representative point:

$$(c, \sigma)_{\mathrm{MA}} = (0.3, 0.25).$$

This configuration corresponds to a regime characterized by a high number of alternative stable states in the fully connected baseline case.

In particular, we discuss the deviations in the number of attractors, the average extinctions and final structure obtained by modifying the initial structural parameters C, Q for these interaction values.

4.4.1 Number of attractors and species survival

In Figure 4.15 and Figure 4.16, we report the results of the simulations performed for an initial pool of $n = 50$ species, keeping the ensemble size and numerical simulation parameters identical to those described in Subsection 4.1.3.

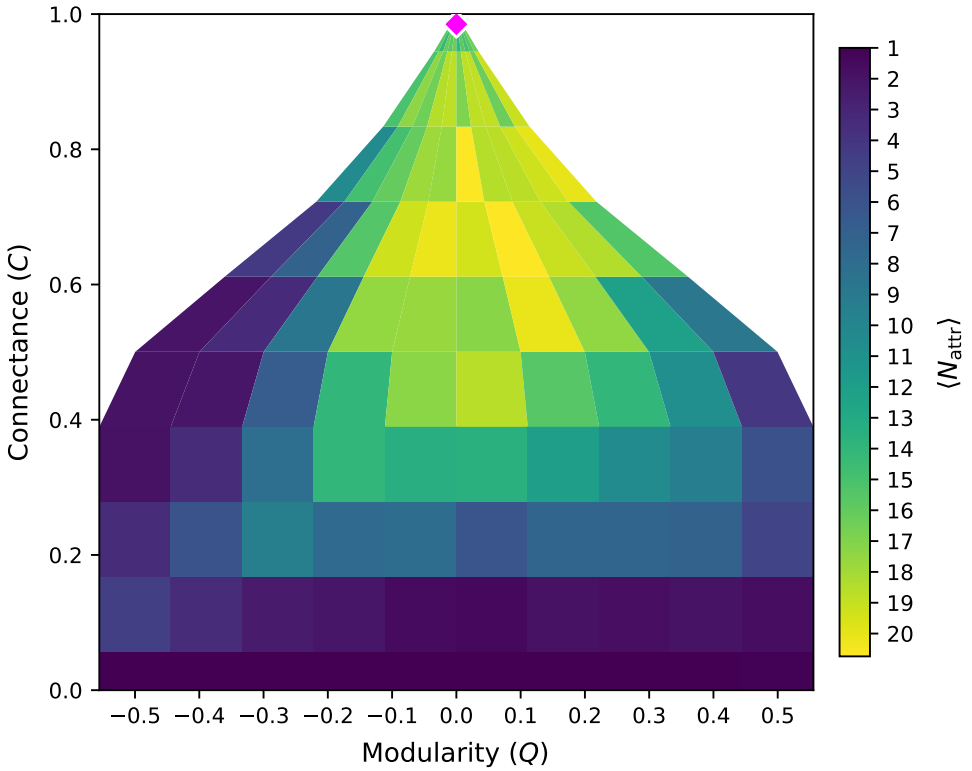

Figure 4.15.. Mean number of attractors $\langle N_{\mathrm{attr}} \rangle$ for the MA reference point across the structure parameter space (C, Q) for the competitive GLV model. The magenta diamond at the apex $(C = 1, Q = 0)$ marks the baseline fully connected configuration, where multistability peaks.

We observe that **the high multistability characteristic of the fully connected MA regime is remarkably sensitive to the structural properties of the interaction network**, as shown in Figure 4.15.

This behavior can be explained by two distinct mechanisms:

- **Connectance reduction:** Decreasing C structurally thins out the interaction matrix, weakening the complexity required to sustain multiple alternative stable states. Below $C \approx 0.2$, the system completely loses its multistable nature, converging to a unique attractor ($\langle N_{\text{attr}} \rangle = 1$) regardless of modularity.
- **Modularity and Antimodularity:** For intermediate to high connectance ($C > 0.4$), moving away from the central random axis ($Q = 0$) toward either strongly modular ($Q > 0$) or strongly antimodular ($Q < 0$) configurations sharply reduces $\langle N_{\text{attr}} \rangle$. Grouping species into defined modules breaks the global symmetry of the competitive interactions, filtering out alternative stable states and forcing the community toward a lower number of viable equilibria.

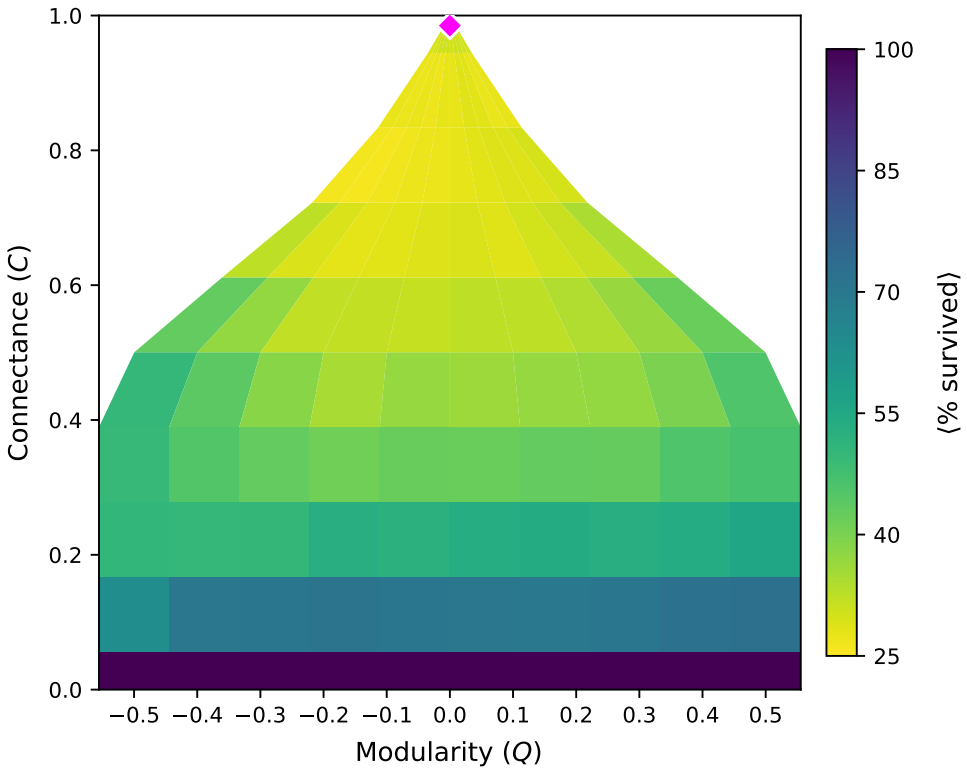

Figure 4.16.. Average percentage of survived species for the MA reference point across the structure parameter space (C, Q) for the competitive GLV model. The color bar denotes ⟨% survived⟩, ranging from 25% (yellow) up to 100% (dark purple). The magenta diamond at the apex marks the baseline fully connected configuration.

Concurrently, the **species survival plot** (Figure 4.16) **reveals a strong dependence on connectance**. The fully connected apex represents a global competitive bottleneck

where intense, unmitigated competition drives the highest fraction of extinctions, leaving only about 25% of the initial pool alive.

As connectance decreases, the dilution of competitive links effectively shields species from global exclusion, monotonically lifting the average survival rate toward 100% as $C \to 0$.

Interestingly, as shown in Figure 4.17 for $C_i = 0.5$, network structure also mitigates extinction. Rather than simply changing the total number of surviving species, modularity ($Q \neq 0$) mainly determines how extinctions are distributed across the network. Antimodular networks undergo the collapse of one module while the other remains largely preserved, whereas modular networks experience more evenly distributed extinction events but smaller than for the $Q = 0$ case.

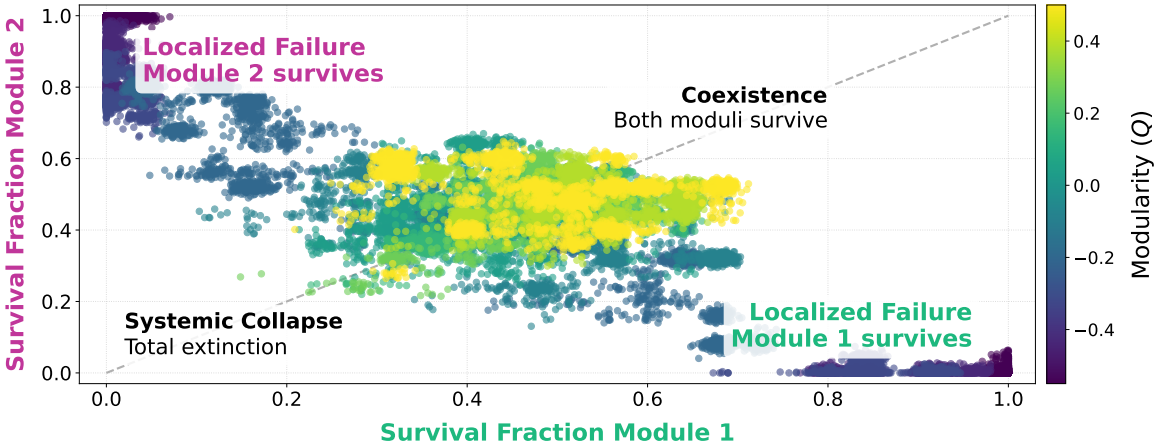

Figure 4.17.. Survival fraction of Module 1 versus Module 2 across the modularity spectrum for the MA interaction regime. Each point represents a single simulation run from an ensemble of 50 independent interaction matrices, each evaluated across 50 initial conditions (50×50 total realizations per parameter set) for an initial pool of $n = 50$ species and intermediate initial connectance $C_i = 0.5$. The color bar denotes the initial modularity Q, ranging from strongly antimodular ($Q \approx -0.5$, dark purple) to strongly modular ($Q \approx 0.5$, yellow). The dashed diagonal line represents symmetric coexistence between modules. Antimodular configurations cluster exclusively at the top-left and bottom-right boundaries, illustrating the bistable nature of localized failure where competitive exclusion drives one module to complete extinction while the other maintains high survival.

4.4.2 Final species abundance distribution

To evaluate how initial network architecture shapes community structure in the multistable regime, we analyze the final species abundance distribution (SAD) for the MA reference point ($c = 0.3, \sigma = 0.25$) across different combinations of initial connectance C_i and modularity Q_i. For each simulation, we considered 50 interaction matrices and 150 initial conditions for each interaction matrix (see Appendix B.2), The resulting distributions are displayed in Figure 4.18.

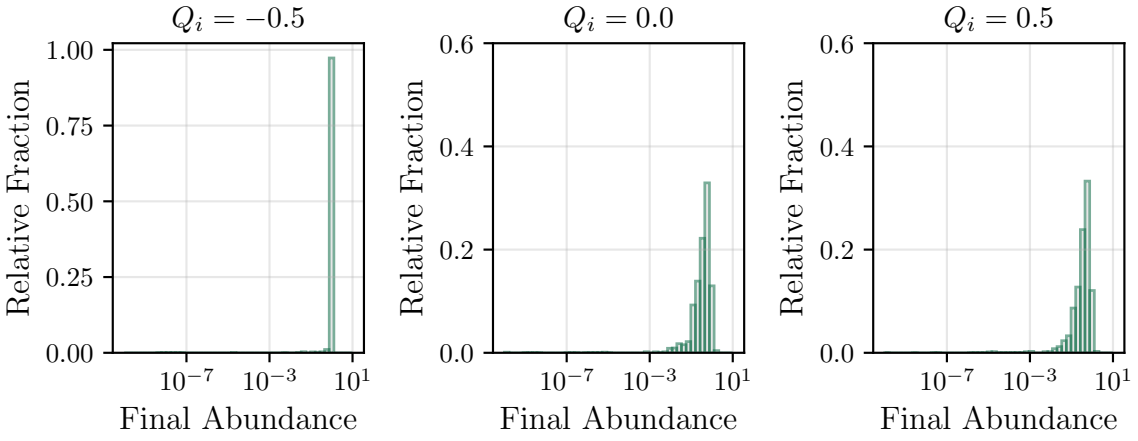

(1) Low connectance (C_i = 0.2)

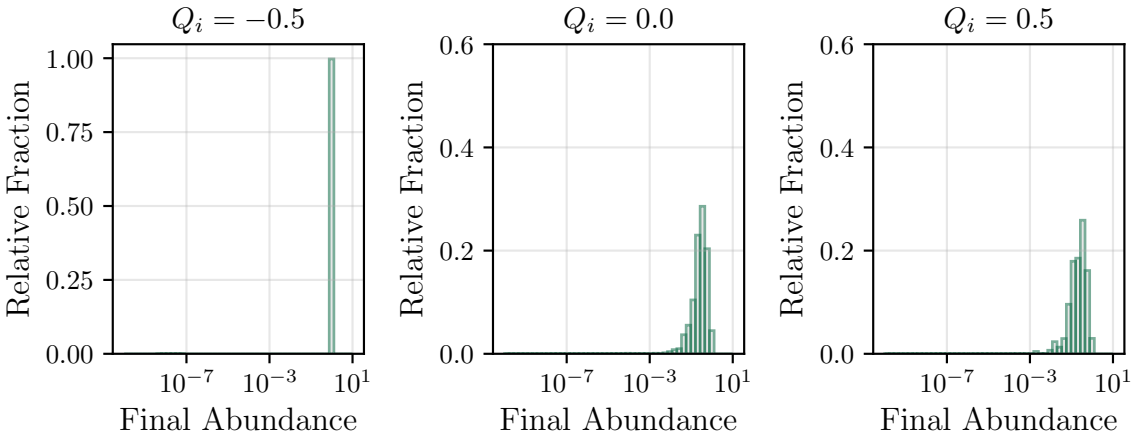

(2) Medium connectance (C_i = 0.5)

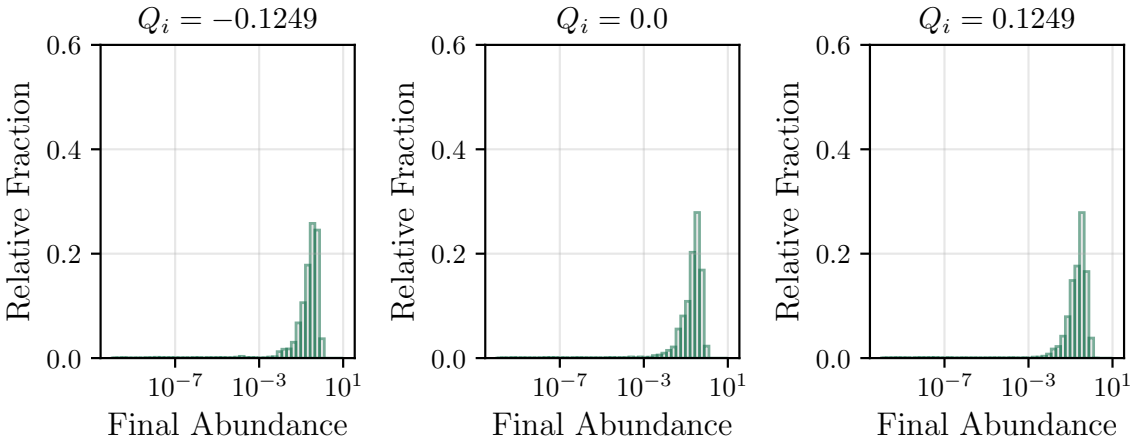

(3) High connectance (C_i = 0.8)

Figure 4.18.. Final species abundance distribution (SAD) across different values of initial connectance C_i and initial modularity Q_i for the MA regime ($c = 0.3, \sigma = 0.25$). The two $Q_i \neq 0$ values are the extreme values admissible for each C_i for $n = 50$ (Eq. (2.20)). The x-axis is plotted on a logarithmic scale to capture variations across multiple orders of magnitude.

The same trend observed for the UFP point in Subsection 4.3.2 is recovered here: the initial connectance C_i is the primary factor controlling the dispersion of the final SAD, with lower connectance leading to more peaked abundance distributions.

A notable difference is that the SAD collapses to a nearly singular distribution (i.e., only one occupied histogram bin) not only for negative Q_i and intermediate connectance, as observed in the UFP regime (Figure 4.42), but also for low connectance. This behavior is consistent with the results of Figure 4.15, which show that, in this region of the parameter space, the system loses multistability and reverts to a unique stable equilibrium.

4.4.3 Final network structure

We extend the structural analysis to the Multiple Attractors (MA) regime defined by higher competition and interaction heterogeneity ($c = 0.3, \sigma = 0.25$). Simulations are performed with an initial pool of $n = 50$ species, averaged over `num_mats` = 50 matrices. Following the validation in Appendix B.2, we utilize `num_ic` = 150 initial conditions per matrix to ensure an accurate sampling of the alternative stable states.

The average final connectance $\langle C_f \rangle$ and final modularity $\langle Q_f \rangle$ across the (Q, C) parameter space are reported in Figure 4.19.

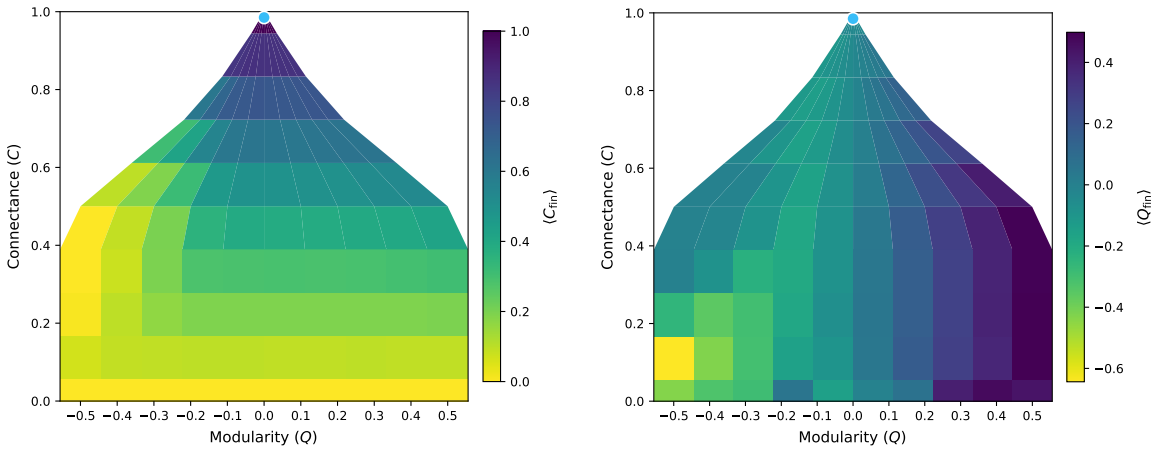

(1) Average final connectance $\langle C_{\text{fin}} \rangle$ **(2)** Average final modularity $\langle Q_{\text{fin}} \rangle$

Figure 4.19.. Average final structural parameters in the (Q_i, C_i) parameter space for the MA point $c = 0.3, \sigma = 0.25$.

The final connectance landscape (Figure 4.191) preserves the horizontal banding pattern ($\langle C_f \rangle \approx C$) in the random and modular regions ($Q \geq -0.2$). However, **the structural degradation zone observed on the antimodular region ($Q \leq -0.3$) is significantly expanded compared to the UFP regime**. Under intense mean competition ($c = 0.3$), the structural asymmetry of antimodular networks triggers widespread competitive exclusion across a broader range of intermediate connectance ($C \in [0.2, 0.5]$). The resulting species extinctions prune the interacting pairs, driving $\langle C_f \rangle$ below its nominal initial value. This is consistent with the analysis of survival

(Figure 4.16) and extinction localization (Figure 4.17) already discussed for this regime.

The final modularity landscape (Figure 4.192) exhibits a departure from the rigid vertical bands that is consequently more intense than in the UFP case.

Near the fully connected limit, the structural influence of the initial modularity Q_i is entirely erased by the global competitive coupling. All trajectories converge toward a narrow, slightly negative modularity envelope, consistent with the fully connected baseline behavior discussed in Subsection 4.2.4.

5

Conclusions

5.1 Summary of the work

This thesis set out to investigate how the two most widely used descriptors of ecological network topology, global connectance C and modularity Q, jointly shape the equilibrium properties and the dynamical evolution of competitive communities described by the generalized Lotka–Volterra (GLV) model.

Chapter 2 introduced the model and the statistical parametrization of the interaction matrix $\mathbf{A} = \mathbf{W} \circ \mathbf{K}$, in which the adjacency matrix $\mathbf{K}$ encodes C and Q through the block connection probabilities $C_{\text{in}}, C_{\text{out}}$, while the Gaussian weights encoded in $\mathbf{W}$ describe the interaction regime through the mean competition strength c and the heterogeneity σ.

Chapter 3 characterized the *static* properties of this model — local stability of $\mathbf{A}$ and of the community matrix $\mathbf{S} = \mathbf{DA}$, and feasibility of the interior equilibrium $\mathbf{N}^*$ — combining Random Matrix Theory (RMT), through the Circular Law and the theory of spectral outliers for low-rank perturbations, with Monte Carlo sampling. The effects of C and Q were first isolated separately (Sections 3.3 and 3.4) and then examined jointly over the full (C, Q) structural plane (Section 3.5).

Chapter 4 extended the analysis to the full nonlinear dynamics, integrating the GLV equations from an ensemble of random initial conditions and characterizing the resulting attractor landscape — number of attractors, species survival, species abundance distribution (SAD) and final structure — first for the fully connected case (Section 4.2), and then, reusing the same two reference interaction regimes identified in Chapter 3 (the unique-fixed-point, UFP, and multiple-attractor, MA, regimes), over the same (C, Q) structural plane explored statically (Sections 4.3 and 4.4). This design choice was deliberate: it allows the dynamical outcomes to be read directly against the static stability and feasibility landscapes obtained beforehand, rather than as an independent set of results.

The remainder of this chapter synthesizes the main findings emerging from this comparison into three central messages, followed by a discussion of the limitations of the present approach and of possible directions for future work.

Feasibility is the primary constraint on interior equilibria

The first result concerns the relative role of feasibility and of local spectral stability in determining the fate of the interior equilibrium. Our results indicate that, in the competitive regime, the spectral properties of the interaction matrix **A** alone are not sufficient to characterize the persistence of the community.

The joint scan of the interaction parameter space (c, σ) for the fully connected case (Figure 3.11) shows that the probability of feasibility collapses to zero at values of σ well below those required to destabilize **A**: feasibility is lost first, while **A** typically remains structurally stable over a much larger region. At the same time, the probability landscape of the stability of **S** is essentially indistinguishable from that of feasibility, consistent with the preservation of D-stability throughout the explored region (Section 3.5).

The same pattern recurs, and is in fact amplified, in the joint structural scan at the UFP interaction point (Figure 3.12): the stability of **A** is preserved almost everywhere in the (C, Q) plane except for a narrow region of high connectance and negative modularity, whereas feasibility survives only at low connectance ($C \lesssim 0.2$). Structural stability of **A** is therefore a comparatively weak constraint; the effective bottleneck for the existence of a biologically meaningful equilibrium is feasibility, and, whenever it holds, the stability of **S** essentially tracks it.

This is qualitatively consistent with the complexity parameter $\gamma = \sigma\sqrt{nC}$ that governs May's stability threshold (Eq. (3.8)): larger γ tends to erode both stability and feasibility together. We stress, however, that an explicit analytical feasibility threshold of this form was only derived for the fully connected case (Appendix A.1); for $C < 1$ and for $Q \neq 0$ the corresponding boundary was only characterized numerically (Section 3.5), and modularity appears to have a comparatively minor influence on it relative to connectance. A more general analytical treatment of feasibility for structured interaction matrices remains an open problem, discussed further in Section 5.3.

A direct consequence of this hierarchy is that a purely linear, equilibrium-based analysis cannot by itself predict the attractor structure emerging after feasibility is lost: it only signals *where* the interior equilibrium disappears, not *how* the system reorganizes afterward. Addressing the latter question is precisely the role of the dynamical analysis of Chapter 4, discussed next.

Antimodularity drives spectral destabilization and module-selective extinction

The spectral analysis of Section 3.4 showed that a non-zero modularity introduces two structural outliers in the spectrum of **A**, the relevant one being

$$\lambda_2(A) = -1 + cC_{\text{in}} - c\,\frac{n}{2}\,(C_{\text{in}} - C_{\text{out}})\,.$$

In the antimodular regime ($Q < 0$, $C_{\text{out}} > C_{\text{in}}$), this outlier moves rightward with n and eventually crosses the imaginary axis, destabilizing the system independently of

the interaction heterogeneity σ; positive modularity, by contrast, pushes λ_2 further into the stable half-plane and has at most a mild stabilizing effect, more visible at intermediate connectance (Section 3.4, Figure 3.10).

This asymmetry between $Q > 0$ and $Q < 0$ is not an artifact of the parametrization alone: it reappears in the joint (C, Q) scan of Section 3.5, where the instability region of $\mathbf{A}$ is confined to high connectance and negative modularity (Figure 3.12).

The dynamical analysis reveals what this destabilization actually produces. At the UFP interaction point and intermediate initial connectance, the region of the (C, Q) plane where the antimodular outlier destabilizes $\mathbf{A}$ coincides with the region where the mean number of attractors bifurcates from one to two (Figure 4.12) and the average survival fraction drops to about 50%. Tracking the two modules separately (Figure 4.11, Figure 4.12) shows that this is not a gradual transition: it corresponds to the essentially complete extinction of one module while the other survives nearly intact, with the identity of the surviving module determined by the initial condition. This shows that network structure alone, without module-specific statistical differences in interactions, can generate alternative stable states.

Positive modularity, in contrast, does not produce this bifurcation: consistently with the spectral picture, the two modules instead become dynamically decoupled, each evolving approximately as an independent subsystem (Figure 4.11).

A further, more subtle observation emerges from the MA reference point (Section 4.4, Figure 4.15): here, departing from $Q = 0$ in *either* direction reduces the number of coexisting attractors relative to the unstructured baseline. This suggests that imposing any block structure — modular or antimodular — breaks the statistical equivalence among species that characterizes the fully mixed random regime, even though modularity and antimodularity act through different mechanisms and produce qualitatively different final states (decoupled coexistence versus module-selective exclusion, see Figure 4.43).

We regard this asymmetry between the UFP and MA regimes as an interesting but still preliminary result, which would benefit from a broader exploration of the interaction parameter space before being generalized.

Overall, non-zero modularity does not necessarily protect biodiversity: its effect is better described as a redistribution of extinction risk along modules, whose outcome — mild stabilization, decoupling, or all-or-nothing module collapse — depends sensitively on both its sign and on the underlying interaction regime.

Reduced connectance promotes equilibrium feasibility, stability, and species persistence.

For the fully connected network, reducing C was found to have a broadly stabilizing effect on feasible equilibria and to increase the probability of feasibility itself (Section 3.3, Proposition (16)); this trend remained qualitatively unchanged across different ratios of c and σ, unlike the spectral shift of the bare matrix $\mathbf{A}$, which can instead be non-monotonic in C depending on the ratio σ/c (Eq. (3.33)).

When C and Q are varied jointly, however, this picture becomes more modulated by the interaction between these two parameters: intermediate connectance amplifies the influence of modularity, enhancing both the mild stabilizing effect of $Q > 0$ and the destabilizing effect of $Q < 0$ (Figure 3.10), while at low connectance the whole system becomes essentially insensitive to Q, preserving higher stability and feasibility (Figure 3.12).

The dynamical scans reproduce this dependence consistently. In both the UFP regime (Figure 4.10) and the MA regime (Figure 4.16), decreasing C monotonically increases the average survival fraction, and, in the MA case, strongly suppresses multistability below $C \approx 0.2$, restoring a unique attractor or diminishing sensitively the total number regardless of Q (Figure 4.15).

This is the dynamical counterpart of the stabilizing and feasibility-enhancing effect of sparser connectivity identified in Chapter 3: thinning the interaction network reduces both the effective variance of the competitive interactions (Eq. (3.36)) and the number of alternative stable configurations available to the system.

At the same time, connectance shapes the *internal* structure of the surviving community in a way that a survival fraction alone does not capture. The final SAD becomes more peaked and homogeneous at low C, while it mantains the characteristic long tail of rare, near-extinction species (Figures 4.42 and 4.43).

The one clear exception to this heavy-tailed pattern occurs precisely in the antimodular, module-collapse regime discussed in Subsection 4.3.1, where the SAD instead collapses onto a single dominant peak — a direct consequence of one entire module being removed from the community.

Taken together, these observations point to a trade-off rather than a single monotonic trend: sparser networks favor overall species richness, whereas denser, unstructured networks favor a more heterogeneous abundance hierarchy, at the cost of a lower total survival fraction. We consider this trade-off, rather than either effect in isolation, to be the more meaningful summary of the role of connectance in this model.

5.2 Limitations

The conclusions above should be read in light of several simplifying assumptions adopted throughout this work.

The structural model is restricted to at most two *balanced* modules ($\alpha = 1/2$); unbalanced or multi-module (hierarchical) architectures, which are common in empirical ecological networks, were not explored and may modify both the admissible range of Q and the spectral picture derived in Section 3.4.

Interactions were restricted to the competitive regime, with fixed, identical self-regulation ($a_{ii} = -1$) and uniform intrinsic growth rates ($r_i = 1$); mixed interaction types (mutualism, predation) were not considered, as well as correlations between interaction strengths (see also Subsection 2.2.3).

The topological ensembles used, directed Erdős–Rényi and two-block stochastic block models, do not capture other structural features known to matter empirically, such as degree heterogeneity or nestedness.

On the dynamical side, the analysis was restricted to static attractors: limit cycles were explicitly excluded from the scope of this thesis, and the unbounded-growth (UG) regime identified by Bunin's phase diagram was acknowledged but not further characterized.

Finally, most numerical results were obtained for moderate system sizes ($n = 50$) and finite Monte Carlo ensembles (of the order of 50–500 realizations); although the RMT predictions were shown to hold reasonably well already at these sizes, some of the finer features discussed above, in particular the asymmetry between the UFP and MA regimes noted in Section 5.1, would benefit from confirmation over larger ensembles and system sizes.

5.3 Future developments

Several directions naturally follow from the limitations above. On the analytical side, considering extensions of the cavity-method treatment used for the fully connected UFP regime (Appendix A.2) to block-structured interaction matrices would provide a genuine analytical counterpart to the numerical (C, Q) dynamical scans of Chapter 4, in the same spirit as Bunin's phase diagram for the unstructured case.

A more general derivation of the feasibility boundary for $C < 1$ and $Q \neq 0$, complementing the numerical results of Section 3.5, would also help clarify how much of the observed feasibility landscape is a finite-size effect.

On the structural side, relaxing the assumption of balanced, two-block modularity — allowing unequal module sizes, additional modules, or hierarchical structure — would test whether the module-selective bistability identified in Subsection 4.3.1 is a peculiarity of the perfectly symmetric two-module case or a more general feature of antimodular architectures. Incorporating degree heterogeneity or mixed interaction types would move the model closer to empirically observed networks.

Finally, characterizing the UG regime, extending the analysis to limit cycles and chaotic attractors, and systematically studying finite-size effects across a wider range of n would complete the picture of the attractor landscape only partially explored here. We regard these directions as natural and tractable extensions of the framework developed in this thesis, rather than as departures from it.

A

Analitical derivations

A.1 Feasibility of fully-connected competitive GLV

We present here the heuristic derivation of Proposition 16, developed by Stone [19].
Proposition. (Feasibility of fully-connected competitive GLV) *Consider the GLV model with interaction matrix* $\mathbf{A}$ *defined by Eq.* (3.12) *and Eq.* (3.13). *Then, in the limit* $n \to \infty$, *the probability that the internal equilibrium of Eq.* (2.11) *is feasible tends to one only if*

$$\gamma = \sqrt{n}\,\sigma \ll 1.$$

where γ *is the complexity defined in Eq.* (3.8).

Proof. We consider the N-dimensional competitive system at equilibrium, defined by $\mathbf{AN}^* = -\mathbf{1}$, where the interaction coefficients for a given realization are given by $a_{ij} = -(c + b_{ij})$ and $a_{ii} = -1$. From Eq. (2.10), the equilibrium equation for species i reads

$$-N_i^* - \sum_{j \neq i} (c + b_{ij}) N_j^* = -1. \tag{A.1}$$

We separe the deterministic mean interaction c from the fluctuations b_{ij}. In the homogeneous limit $b_{ij} \to 0$, the system becomes symmetric with respect to indices permutations. All species are identical, therefore they share the same equilibrium abundance $N_i^* = \kappa$. Substituting into (A.1) yields

$$\kappa\big(1 - c + nc\big) = 1, \qquad \text{hence} \qquad \kappa = \frac{1}{1 - c + nc}. \tag{A.2}$$

We now consider small fluctuations around this homogeneous solution. We rewrite (A.1) adding and subtracting cN_i^*:

$$-(1 - c)N_i^* - c \sum_{j=1}^{n} N_j^* - \sum_{j \neq i} b_{ij} N_j^* = -1.$$

We assume that fluctuations are small enough to approximate the deterministic term $\sum_{j=1}^{n} N_j^* \approx n\kappa$. Moreover, we approximate the effect of fluctuations b_{ij} on

neighboring populations N_j^* as higher order, replacing $N_j^* \approx \kappa$ inside the fluctuating term. We obtain

$$-(1-c)N_i^* - cn\kappa - \kappa \sum_{j=1} b_{ij} \approx -1.$$

Using Eq. (A.2), rearranging terms gives

$$(1-c)N_i^* \approx (1-c)\kappa - \kappa \sum_{j=1}^{n} b_{ij},$$

where we have included $j = i$ since $b_{ii} = 0$.

Dividing by $(1-c)$ and defining $\hat{b}_{ij} = b_{ij}/(1-c)$ leads to the approximate expression

$$N_i^* \approx \kappa \left(1 - \sum_{j=1}^{n} \hat{b}_{ij}\right). \tag{A.3}$$

We now analyze the random variable

$$X_i = 1 - \sum_{j=1}^{n} \hat{b}_{ij}.$$

Since $\hat{b}_{ij}$ with $i \neq j$ are i.i.d. with zero mean, the central limit theorem applied to this $n-1$ variables implies that X_i is asymptotically Gaussian for large $n \approx n-1$.

We now compute the first two moments of X_i. Since $\mathbb{E}[\hat{b}_{ij}] = 0$,

$$\mathbb{E}[X_i] = 1 - \sum_{j=1}^{n} \mathbb{E}[\hat{b}_{ij}] = 1.$$

Assuming independence of the interaction coefficients, the variance of the sum is additive. Since

$$\hat{b}_{ij} = \frac{b_{ij}}{1-c}, \qquad \mathrm{Var}(b_{ij}) = \sigma^2,$$

we obtain

$$\mathrm{Var}(\hat{b}_{ij}) = \frac{\sigma^2}{(1-c)^2},$$

and therefore

$$\mathrm{Var}(X_i) = \sum_{j=1}^{n} \mathrm{Var}(\hat{b}_{ij}) = \frac{n\sigma^2}{(1-c)^2}.$$

Defining

$$\tilde{\gamma} = \frac{\sqrt{n}\,\sigma}{1-c},$$

we conclude that

$$X_i \sim \mathcal{N}(1, \tilde{\gamma}^2)$$

in the large-n limit.

Introducing the standard normal variable

$$Z = \frac{X_i - 1}{\tilde{\gamma}},$$

the probability that species i has positive equilibrium abundance is

$$p = \mathbb{P}(X_i > 0) = \mathbb{P}\left(Z > -\frac{1}{\tilde{\gamma}}\right) = \Phi\left(\frac{1}{\tilde{\gamma}}\right),$$

where Φ denotes the cumulative distribution function of the standard normal distribution.

Assuming, to first order, that the equilibrium abundances of different species are independent, the probability that all species have positive abundance is approximated by

$$\mathbb{P}(\mathbf{N}^* > 0) \approx p^n. \tag{A.4}$$

As $n \to \infty$, the quantity p^n tends to one only if p approaches one sufficiently rapidly, which requires $\tilde{\gamma} \ll 1$. Since

$$\gamma = \frac{\sqrt{n}\,\sigma}{1 - c},$$

this condition is equivalent to

$$\gamma \ll 1,$$

completing the proof. □

A.2 Phase boundaries in the interaction parameter space

Here we report the core ideas behind the analytical derivation developed by Bunin [25] which predicts the boundaries between the different dynamical regimes obtained by evolving the competitive GLV (see Figure 4.1).

We rewrote Bunin's argument using the parametrization adopted for the model throughout this thesis. Note that the original demonstration is quite general and holds also relaxing our additional hypothesis on normalization (see Subsection 2.2.3) or introducing correlation between interactions.

The GLV dynamics for a community of n interacting species is given by:

$$\frac{dN_i}{dt} = N_i\left(r_i + \sum_{j=1}^{n} a_{ij}N_j\right)$$

Following the specific structural hypothesis of our model (Subsection 2.2.3), we set the intrinsic growth rates to $r_i = 1$ and the intraspecific competition coefficients to $a_{ii} = -1$. The dynamics then simplify to:

$$\frac{dN_i}{dt} = N_i\left(1 - N_i + \sum_{j\neq i} a_{ij}N_j\right) \tag{A.5}$$

To translate Bunin's parameterization into this notation, we model the interspecific interaction coefficients a_{ij} (for $j \neq i$) as random variables drawn from a distribution with mean $-c = -\mu_B/n$ with $\mu_B > 0$, variance $\sigma^2 = \sigma_B^2/n$, and correlation γ between reciprocal interactions. We can explicitly write this as:

$$a_{ij} = -\frac{\mu_B}{n} + \frac{\sigma_B}{\sqrt{n}} z_{ij} \tag{A.6}$$

where z_{ij} are random variables satisfying $\langle z_{ij} \rangle = 0$, $\langle z_{ij}^2 \rangle = 1$, and $\langle z_{ij} z_{ji} \rangle = \gamma$. Because we considered uncorrelated interactions, under our hypothesis it would be $\gamma = 0$.

A.2.1 Derivation of the Single-Species Effective Equation (Cavity Method)

To find the properties of the Unique Fixed Point (UFP), we compute the equilibrium abundances using the *cavity method*.

Originally developed in the statistical mechanics of disordered systems, the core idea behind this method is to derive the macroscopic properties of a complex system by analyzing the addition of a single new element to an already equilibrated environment. We consider a community of n species at equilibrium and conceptually introduce a new, $(n+1)$-th species (the "cavity" species). In the large system limit ($n \to \infty$), the introduction of this single species exerts only a microscopic perturbation on the resident community, allowing the system's reaction to be treated analytically via linear response theory. By subsequently imposing self-consistency—requiring that the newly introduced species is statistically indistinguishable from the resident ones—we can close the equations and determine the overall equilibrium abundance distribution.

In Eq. (A.5), setting the time derivative to zero for a persistent species i:

$$N_i \left(1 - N_i - \frac{\mu_B}{n} \sum_{j \neq i} N_j + \frac{\sigma_B}{\sqrt{n}} \sum_{j \neq i} z_{ij} N_j \right) = 0$$

Let $M = \frac{1}{n} \sum_j N_j$ be the mean abundance. For large n, we can approximate $\frac{1}{n} \sum_{j \neq i} N_j \approx M$. The equation becomes:

$$N_i \left(1 - \mu_B M - N_i + \frac{\sigma_B}{\sqrt{n}} \sum_{j \neq i} z_{ij} N_j \right) = 0$$

We introduce a new "cavity" species 0 into the equilibrated system. Its equilibrium condition is:

$$N_0 \left(1 - \mu_B M - N_0 + \frac{\sigma_B}{\sqrt{n}} \sum_{j} z_{0j} N_j \right) = 0 \tag{A.7}$$

The introduction of species 0 slightly perturbs the abundances of the existing species j. We express this change through linear response:

$$N_j \approx N_{j\backslash 0} + \frac{\partial N_j}{\partial \xi_j}\xi_j$$

where $N_{j\backslash 0}$ is the abundance of species j in the absence of species 0, and $\xi_j = \frac{\sigma_B}{\sqrt{n}} z_{j0} N_0$ is the effective perturbation on the growth rate of species j. Let $v_{jj} = \frac{\partial N_j}{\partial \xi_j}$ be the linear response function. Then:

$$N_j \approx N_{j\backslash 0} + v_{jj}\frac{\sigma_B}{\sqrt{n}} z_{j0} N_0$$

Substituting this back into the interaction term of Eq. A.7:

$$\frac{\sigma_B}{\sqrt{n}}\sum_j z_{0j} N_j = \frac{\sigma_B}{\sqrt{n}}\sum_j z_{0j} N_{j\backslash 0} + \frac{\sigma_B^2}{n} N_0 \sum_j z_{0j} z_{j0} v_{jj}$$

By the law of large numbers, as $n \to \infty$, the sum in the second term converges to its expected value. Since z_{0j} and z_{j0} are correlated by γ, we have $\frac{1}{n}\sum_j z_{0j} z_{j0} v_{jj} \to \gamma \langle v \rangle$, where $\langle v \rangle = \frac{1}{n}\sum_j v_{jj}$. Thus the effective equation for species 0 becomes:

$$N_0 \left(1 - \mu_B M - N_0(1 - \sigma_B^2 \gamma \langle v \rangle) + \sigma_B \zeta_0\right) = 0$$

where $\zeta_0 = \frac{1}{\sqrt{n}}\sum_j z_{0j} N_{j\backslash 0}$ is a sum of weakly correlated variables, strictly approaching a Gaussian distribution with zero mean and variance $q = \frac{1}{n}\sum_j N_j^2$.

Consequently, the abundance of the new species (and by symmetry, any species in the pool) follows a truncated Gaussian distribution:

$$N_0 = \max\left(0, \frac{1 - \mu_B M + \sigma_B \sqrt{q} Z}{1 - \sigma_B^2 \gamma \langle v \rangle}\right) \tag{A.8}$$

where $Z \sim \mathcal{N}(0, 1)$.

From this, the response function $\langle v \rangle$ is simply the average derivative of N_0 with respect to its effective growth rate. Differentiating Eq. A.8 gives $v_0 = \frac{1}{1 - \sigma_B^2 \gamma \langle v \rangle}$ if $N_0 > 0$, and 0 otherwise. Denoting the fraction of persistent species ($N_i > 0$) as ϕ, we obtain the self-consistency equation:

$$\langle v \rangle = \frac{\phi}{1 - \sigma_B^2 \gamma \langle v \rangle} \implies \langle v \rangle (1 - \sigma_B^2 \gamma \langle v \rangle) = \phi \tag{A.9}$$

Note that Eq. (A.9) is quadratic in $\langle v \rangle$ for $\gamma \neq 0$, and therefore admits two roots. Physical consistency requires selecting the branch that reduces to $\langle v \rangle = \phi$ in the uncorrelated limit $\gamma \to 0$ relevant to our model.

A.2.2 Boundary between UFP and MA Regions

The transition from the Unique Fixed Point (UFP) phase to the Multiple Attractors (MA) phase is marked by the loss of stability of the cavity solution.

The stability of the UFP is probed by introducing a small, independent random perturbation $\epsilon\eta_i$ to the intrinsic growth rate of each species and evaluating the system's linear response. The fixed point loses its stability when the variance of the resulting abundance shifts $y_i = \frac{\partial N_i}{\partial \epsilon}$ (the susceptibility of the system) diverges.

The explicit derivation of the marginal stability condition is beyond the scope of this thesis. However, by combining this condition with the self-consistency equation (A.9), one finds:

$$\sigma_{B,c} = \frac{\sqrt{2}}{1+\gamma}$$

Under our specific hypothesis of uncorrelated interspecific interactions ($\gamma = 0$), the prediction for the onset of the multiple attractors phase simplifies to:

$$\sigma_{B,c} = \sqrt{2}$$

Returning to our initial parametrization σ, the onset of multistability depends exclusively on the standard deviation of the interactions and the system size n:

$$\boxed{\sigma_c = \sqrt{\frac{2}{n}}}$$

A.2.3 Boundary of the Unbounded Growth Region

The boundary characterizing the Unbounded Growth region is reached when interspecific competition is too weak to constrain the intrinsic population growth, causing the mean species abundance M to diverge ($M \to \infty$).

The explicit derivation of this divergence from the cavity method equations is beyond the scope of this thesis. However, by analyzing the self-consistency equations, one can determine the exact point at which the restoring competitive forces are overpowered.

In Bunin's transformed variables, the divergence corresponds analytically to the condition:

$$\sigma_B h + \mu_B = 0 \tag{A.10}$$

where $h = \Delta\sqrt{q}$ is an effective field parameter. The quantities Δ and q are auxiliary variables determined by the roots of functions defined as truncated Gaussian integrals:

$$w_k(\Delta) = \int_{-\Delta}^{\infty} \frac{1}{\sqrt{2\pi}} e^{-z^2/2} (z+\Delta)^k dz$$

In the numerical simulations, these integrals are evaluated explicitly using the standard normal probability density function $\varphi(x)$ and cumulative distribution

function $\Phi(x)$ (implemented via `scipy.stats.norm.pdf` and `norm.cdf` in Python). The expressions for the relevant moments are:

$$w_0(\Delta) = \Phi(\Delta)$$
$$w_1(\Delta) = \varphi(\Delta) + \Delta\Phi(\Delta)$$
$$w_2(\Delta) = w_0(\Delta) + \Delta w_1(\Delta)$$

Δ is defined as the root for the following equation, obtained as a first-order approximation for $n \gg 1$:

$$\sqrt{w_2(\Delta)} = \frac{1}{\sigma_B}.$$

To represent this curve in Figure 4.1, we solved this equation numerically using the root-finding algorithm `scipy.optimize.root_scalar`.

Once Δ is determined, we compute the variance parameter

$$q := \frac{w_2(\Delta)}{w_1(\Delta)^2}$$

and evaluate $h = \Delta\sqrt{q}$.

To translate this boundary back into our initial parametrization (c, σ) for a system of size n, we substitute the scaling relations $\mu_B = cn$ and $\sigma_B = \sigma\sqrt{n}$ into the transition condition of Eq.(A.10):

$$\sigma\sqrt{n}h + cn = 0$$

Solving for the mean interspecific interaction c, we obtain the critical threshold that delineates the Unbounded Growth regime:

$$\boxed{c_c = -\frac{\sigma h}{\sqrt{n}}}$$

This equation defines the exact curve in the (c, σ) parameter space beyond which the deterministic Lotka-Volterra saturation assumptions break down, leading to unbounded dynamics, as represented in Figure 4.1.

B

Numerical methods

B.1 The Runge-Kutta Method

We introduce here the integration method used to discretized and numerically resolve the GLV equations used in the simulations presented in Chapter 4.

Runge-Kutta (RK) methods generalize Euler's classic approach by introducing multiple estimates of the vector field's slope within a single time step h, aiming to achieve a higher order of convergence.

B.1.1 The Classical Runge-Kutta Method (RK4)

The classical fourth-order method (RK4) provides a good balance between accuracy and computational cost. It advances the solution from time t_n to $t_{n+1} = t_n + h$ by computing a weighted average of four increments:

$$\mathbf{x}_{n+1} = \mathbf{x}_n + \frac{h}{6}(\mathbf{k}_1 + 2\mathbf{k}_2 + 2\mathbf{k}_3 + \mathbf{k}_4) + O(h^5),$$

where the coefficients $\mathbf{k}_i$ are defined as:

- $\mathbf{k}_1 = \mathbf{f}(t_n, \mathbf{x}_n)$ is the slope at the beginning of the interval, evaluated at $\mathbf{x}_n$ (Euler's method);
- $\mathbf{k}_2 = \mathbf{f}\left(t_n + \frac{h}{2}, \mathbf{x}_n + h\frac{\mathbf{k}_1}{2}\right)$ is the slope at the midpoint of the interval, estimated using $\mathbf{k}_1$;
- $\mathbf{k}_3 = \mathbf{f}\left(t_n + \frac{h}{2}, \mathbf{x}_n + h\frac{\mathbf{k}_2}{2}\right)$ is again the slope at the midpoint, but now estimated using $\mathbf{k}_2$;
- $\mathbf{k}_4 = \mathbf{f}(t_n + h, \mathbf{x}_n + h\mathbf{k}_3)$ is the slope at the end of the interval, estimated using $\mathbf{k}_3$.

Note that greater weight is assigned to the slopes evaluated at the center of the integration interval.

From Eq. (B.1.1), the ***local truncation error***—that is, the error introduced at each integration step, assuming the starting point $\mathbf{x}_n$ has zero uncertainty—is of order $O(h^5)$. Specifically, expanding the $\mathbf{k}_i$ terms up to the fourth order using the multivariate Taylor expansion,

$$\mathbf{f}(t_n + \Delta t, \mathbf{x}_n + \Delta \mathbf{x}) \approx \mathbf{f}(t_n, \mathbf{x}_n) + \partial_t \mathbf{f} \Delta t + \partial_{\mathbf{x}} \mathbf{f} \Delta \mathbf{x} + \dots,$$

and substituting these expansions into Eq. (B.1.1), it can be shown that all terms combine perfectly to match the fourth-order Taylor expansion of the exact solution:

$$\mathbf{x}_{n+1} = \mathbf{x}_n + \sum_{i=1}^{4} \frac{h^i}{i!} \frac{d^i \mathbf{x}}{dt^i}(t_n) + O(h^5).$$

The ***global error*** over the integration interval $[t_0, T]$ can be estimated by noting that the required number of integration steps N is inversely proportional to the step size:

$$N = \frac{T - t_0}{h}.$$

Consequently,

$$NO(h^5) = \frac{T - t_0}{h} O(h^5).$$

Assuming the considered system does not exponentially amplify perturbations in $\mathbf{x}$, the global error accumulates to:

$$NO(h^5) = O(h^4).$$

In linear systems of the form

$$\dot{\mathbf{x}} = \mathbf{A}\mathbf{x}, \qquad \mathbf{x}(t) = e^{\mathbf{A}t}\mathbf{x}_0,$$

such as the GLV system linearized around an equilibrium, the perturbation evolves as

$$\|\delta \mathbf{x}(t)\| \sim \|\delta \mathbf{x}_0\| e^{\Lambda t},$$

where Λ is the largest real part of the eigenvalues of $\mathbf{A}$ (the spectral abscissa). This result is at base of Lyapunov method for linear stability 7. Therefore:

- if the spectrum of $\mathbf{A}$ has a negative real part, perturbations decay over time and the numerical error is not amplified. In this case, the global order $O(h^4)$ effectively represents the quality of the approximation over finite time intervals;
- if the spectrum of $\mathbf{A}$ has a positive real part, the local numerical error, despite being $O(h^5)$ at each step, is amplified exponentially. As a result, the numerical trajectory fails to remain a reliable approximation of the exact trajectory over long times.

In the context of this project, the numerical integration method is employed strictly to infer statistical properties of GLV systems through ensemble analysis, rather than to accurately track exact individual trajectories.

B.1.2 Adaptive Runge-Kutta Methods (RK45)

In ecological simulations, multi-scale dynamics characterized by disparate timescales—such as rapid population collapses alternating with prolonged quasi-stationary phases—render a fixed time step h highly inefficient. Because the local truncation error is bound to the higher-order derivatives of the vector field $\dot{\mathbf{x}} = \mathbf{f}(t, \mathbf{x})$, a constant step size is either computationally wasteful during slowly evolving dynamics or numerically unstable during sharp transients where $\|\mathbf{f}\|$ or its derivatives vary rapidly.

To optimize both accuracy and computational efficiency, the `solve_ivp()` routine utilized in our simulations implements the Dormand-Prince method (commonly referred to as RK45). This algorithm belongs to the class of *embedded* Runge-Kutta schemes: by sharing the evaluation of intermediate stages, it simultaneously computes two separate approximations of the solution, of order 4 and 5, respectively. Denoting these estimates as $\mathbf{x}_{n+1}^{(4)}$ and $\mathbf{x}_{n+1}^{(5)}$, the local truncation error at step n is approximated directly by their difference:

$$\epsilon_n = \left\| \mathbf{x}_{n+1}^{(5)} - \mathbf{x}_{n+1}^{(4)} \right\|.$$

The step size h is dynamically adapted by comparing ϵ_n against a local tolerance threshold determined by the absolute tolerance (`atol`) and relative tolerance (`rtol`) parameters. If ϵ_n exceeds this threshold, the current step is rejected and recomputed using a reduced step size h. Conversely, if the error is well below the tolerance, h is increased for the subsequent integration step, maximizing performance without compromising accuracy.

B.2 Selection of sampling size for the Multiple Attractors regime

In the Unique Fixed Point (UFP) regime, the system converges globally to a single equilibrium, making the characterization of the attractor landscape independent of the number of initial conditions (`num_ic`) tested per matrix realization. Conversely, in the Multiple Attractors (MA) regime, a single interaction matrix can sustain a high number of alternative stable states, requiring an explicit optimization of the initial condition sample size to properly chart the phase space.

To determine the optimal value for `num_ic`, we performed a saturation analysis on the baseline fully connected configuration ($n = 50, C = 1, Q = 0$) for the MA representative point considered in the thesis ($\sigma = 0.25, c = 0.3$). We evaluated two metrics as a function of `num_ic`:

1. The total number of unique discovered attractors (blue solid line).
2. The smallest discovered basin weight, $b_{\min}$ (red dashed line), which represents the relative fraction of initial conditions leading to the rarest detected attractor.

The other parameters used for the dynamical simulations are the same of Subsection 4.1.3.

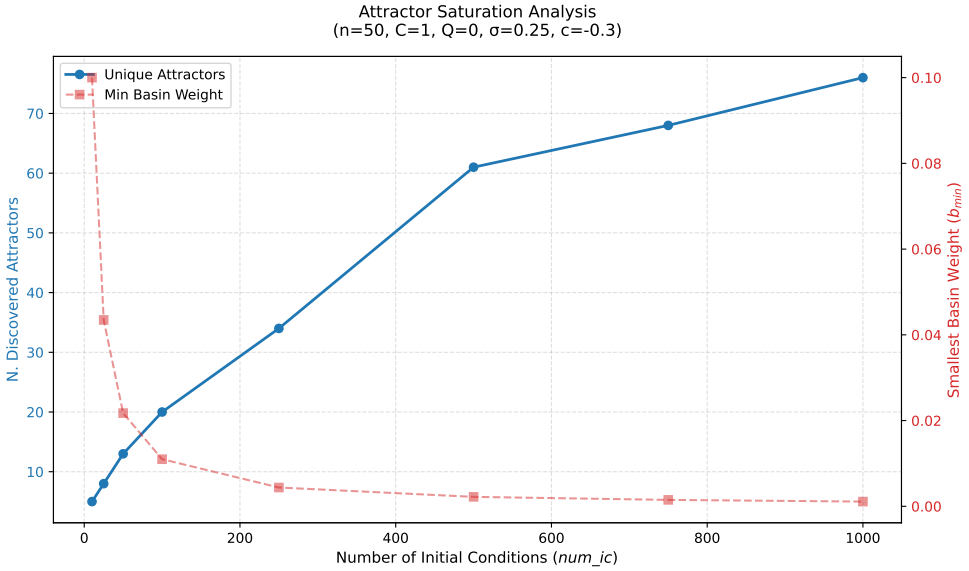

Figure B.1.. Attractor saturation analysis in the multiple attractors (MA) regime for a community with $n = 50$, $C = 1$, $Q = 0$, $\sigma = 0.25$, and $c = 0.3$. The plot displays the number of unique discovered attractors (blue solid line, left axis) and the size of the smallest identified basin of attraction ($b_{\min}$, red dashed line, right axis) as a function of the number of initial conditions (`num_ic`).

Choosing `num_ic` = 50 as done for the UFP point analysis is insufficient for the MA phase. As shown by the scaling behavior in Figure B.1, at `num_ic` = 50 the number of unique attractors has not yet approached saturation, and the minimum basin weight remains relatively high ($b_{\min} \approx 0.025$). This indicates that a sample size of 50 fails to resolve a substantial portion of the stable equilibria, undersampling the true diversity of the attractor landscape.

The choice of `num_ic` = 150 represents a well-defined trade-off between computational cost and statistical completeness. This value sits almost at the elbow of the $b_{\min}$ curve, after which the minimum basin weight flattens out asymptotically toward zero.

Beyond `num_ic` $\approx$ 200, the return on investment for numerical sampling drops drastically. Increasing the sample size further yields diminishing returns: it primarily uncovers highly rare, peripheral attractors with negligible basin sizes ($b_{\min} < 0.01$) while increasing the computational overhead linearly. Therefore, `num_ic` = 150 ensures that an acceptable fraction of the macroscopically relevant attractors defining the community properties are captured without incurring prohibitive numerical costs.

Bibliography

[1] Pietro Landi, Henintsoa O. Minoarivelo, Åke Brännström, Cang Hui, and Ulf Dieckmann. "Complexity and stability of ecological networks: a review of the theory". In: *Population Ecology* 60.4 (2018), pp. 319–345. DOI: 10.1007/s10144-018-0628-3.

[2] Alfred J. Lotka. *Elements of Physical Biology*. Baltimore, MD: Williams & Wilkins, 1925.

[3] Vito Volterra. "Fluctuations in the Abundance of a Species considered Mathematically". In: *Nature* 118 (1926), pp. 558–560.

[4] Giorgos D. Kokkoris, Vincent A. A. Jansen, Michel Loreau, and Andreas Y. Troumbis. "Variability in interaction strength and implications for biodiversity". In: *Journal of Animal Ecology* 71.2 (2002), pp. 362–371. DOI: 10.1046/j.1365-2656.2002.00604.x.

[5] Marco Zenari, Francesco Ferraro, Sandro Azaele, Amos Maritan, and Samir Suweis. "Generalized Lotka–Volterra Systems with Quenched Random Interactions and Saturating Nonlinear Response". In: *Physical Review E* 113 (2026), p. 024206. DOI: 10.1103/PhysRevE.113.024206.

[6] Robert M. May. "Will a Large Complex System be Stable?" In: *Nature* 238 (1972), pp. 413–414. DOI: 10.1038/238413a0.

[7] Eugene P. Wigner. "On the distribution of the roots of certain symmetric matrices". In: *Annals of Mathematics* 67 (1958), pp. 325–327.

[8] Eugene P. Wigner. "Random Matrices in Physics". In: *SIAM Review* 9.1 (1967), pp. 1–23. DOI: 10.1137/1009001.

[9] Can Chen, Xu-Wen Wang, and Yang-Yu Liu. "Stability of Ecological Systems: A Theoretical Review". In: *Physics Reports* (2024). DOI: 10.1016/j.physrep.2024.08.001.

[10] Ada Altieri and Silvia De Monte. "Unveiling complexity: Statistical physics approaches to ecological communities". In: *Europhysics Letters (EPL)* 150.5 (2025). DOI: 10.1209/0295-5075/addae2.

[11] Alex James, Michael J. Plank, Axel G. Rossberg, Jonathan Beecham, Mark Emmerson, and Jonathan W. Pitchford. "Constructing random matrices to represent real ecosystems". In: *The American Naturalist* 185.5 (2015), pp. 680–692. DOI: 10.1086/680496.

[12] Terence Tao and Van Vu. "Random matrices: Universality of local eigenvalue statistics up to the edge". In: *Communications in Mathematical Physics* 298.2 (2010), pp. 549–572. DOI: 10.1007/s00220-010-1044-5.

[13] Terence Tao, Van Vu, and Manjunath Krishnapur. "Random Matrices: Universality of ESDs and the Circular Law". In: *Annals of Probability* 38.5 (2010), pp. 2023–2065. DOI: 10.1214/10-AOP534.

[14] Joseph W. Baron, T. Jewell, Chris Ryder, and T. Galla. "Breakdown of Random-Matrix Universality in Persistent Lotka-Volterra Communities". In: *Physical Review Letters* 130 (2023), p. 137401. DOI: 10.1103/physrevlett.130.137401.

[15] Ibrahim Akjouj, Matthieu Barbier, Maxime Clenet, Walid Hachem, Mylène Maïda, François Massol, Jamal Najim, and Viet Chi Tran. "Complex systems in ecology: a guided tour with large Lotka–Volterra models and random matrices". In: *Proceedings of the Royal Society A* 480.2287 (2024), p. 20230284. DOI: 10.1098/rspa.2023.0284.

[16] Michael E. Gilpin and Ted J. Case. "Multiple domains of attraction in competition communities". In: *Nature* 261 (1976), pp. 40–42. DOI: 10.1038/261040a0.

[17] Alan Roberts. "The stability of a feasible random ecosystem". In: *Nature* 251 (1974), pp. 607–608. DOI: 10.1038/251607a0.

[18] Vincent A. A. Jansen and Giorgos D. Kokkoris. "Complexity and stability revisited". In: *Ecology Letters* 6.6 (2003), pp. 498–502. DOI: 10.1046/j.1461-0248.2003.00464.x.

[19] Lewi Stone. "The feasibility and stability of complex ecosystems". In: *Nature Communications* 9.1 (2018), pp. 1–12. DOI: 10.1038/s41467-018-05154-0.

[20] Lewi Stone and Alan Roberts. "Conditions for a Species to Gain Advantage from the Presence of Competitors". In: *Ecology* 72.6 (1991), pp. 1964–1972. DOI: 10.2307/1941551.

[21] Si Tang, Samraat Pawar, and Stefano Allesina. "Correlation between interaction strengths drives stability in large ecological networks". In: *Ecology Letters* 17.9 (2014), pp. 1104–1114. DOI: 10.1111/ele.12312.

[22] Robert Warren II. "Reduced Intraspecific Competition in Introduced Plant Populations Suggests a Role for Self-Limitation in Invasion Success". In: *Plant Ecology* 227 (2026), p. 48. DOI: 10.1007/s11258-026-01623-4.

[23] Peter B. Adler, Danielle Smull, Karen H. Beard, Ryan T. Choi, Tucker Furniss, Andrew Kulmatiski, Joan M. Meiners, Andrew T. Tredennick, Kari E. Veblen, and Liza S. Comita. "Competition and Coexistence in Plant Communities: Intraspecific Competition Is Stronger Than Interspecific Competition". In: *Ecology Letters* 21.9 (2018), pp. 1319–1329. DOI: 10.1111/ele.13098.

[24] A. McNabb. "Comparison Theorems for Differential Equations". In: *Journal of Mathematical Analysis and Applications* 119.1 (Oct. 1986), pp. 130–142. DOI: 10.1016/0022-247X(86)90163-0.

[25] Guy Bunin. "Ecological communities with Lotka–Volterra dynamics". In: *Physical Review E* 95.4 (2017), p. 042414. DOI: 10.1103/PhysRevE.95.042414.

[26] Mark E. J. Newman and Michelle Girvan. "Finding and evaluating community structure in networks". In: *Physical Review E* 69.2 (2004), p. 026113. DOI: 10.1103/PhysRevE.69.026113.

[27] Jacopo Grilli, Tim Rogers, and Stefano Allesina. "Modularity and stability in ecological communities". In: *Nature Communications* 7 (2016), p. 12031. DOI: 10.1038/ncomms12031.

[28] Robert M. May. *Stability and Complexity in Model Ecosystems*. Vol. 1. Princeton Landmarks in Biology. Princeton University Press, 1974. DOI: 10.2307/j.ctvs32rq4.

[29] Mark Novak, Justin D. Yeakel, Andrew E. Noble, and Daniel F. Doak. "Characterizing Species Interactions to Understand Press Perturbations: What Is the Community Matrix?" In: *Annual Review of Ecology, Evolution, and Systematics* 47 (2016), pp. 409–432. DOI: 10.1146/annurev-ecolsys-032416-010215.

[30] Terence Tao. *Topics in Random Matrix Theory*. Vol. 132. Graduate Studies in Mathematics. American Mathematical Society, 2012.

[31] Anirban Basak and Mark Rudelson. "The Circular Law for Sparse Non-Hermitian Matrices". In: *Annals of Probability* 47.6 (2019), pp. 4111–4162. DOI: 10.1214/18-AOP1324.

[32] J. Fox and Jill McGrady-Steed. "Stability and complexity in microcosm communities". In: *Journal of Animal Ecology* 71.5 (Sept. 2002), pp. 748–756. DOI: 10.1046/j.1365-2656.2002.00640.x.

[33] Yogev Yonatan, Guy Amit, Jonathan Friedman, and Avi Bashan. "Complexity-stability relationship in empirical microbial ecosystems". In: *bioRxiv* (Aug. 2021). DOI: 10.1101/2021.07.29.454345.

[34] Jiliang Hu, Daniel R. Amor, Matthieu Barbier, Guy Bunin, and Jeff Gore. "Emergent phases of ecological diversity and dynamics mapped in microcosms". In: *Science* 378.6615 (2022), pp. 85–89. DOI: 10.1126/science.abm7841.

[35] Stefano Allesina and Si Tang. "Stability criteria for complex ecosystems". In: *Nature* 483.7388 (2012), pp. 205–208. DOI: 10.1038/nature10832.

[36] Akihiko Mougi and Michio Kondoh. "Diversity of Interaction Types and Ecological Community Stability". In: *Science* 337.6092 (July 2012), pp. 349–351. DOI: 10.1126/science.1220529.

[37] Samir Suweis, Jacopo Grilli, and Amos Maritan. "Disentangling the Effect of Hybrid Interactions and of the Constant Effort Hypothesis on Ecological Community Stability". In: *Oikos* 123.5 (2014), pp. 525–532. DOI: 10.1111/j.1600-0706.2013.00822.x.

[38] Theo Gibbs, Jacopo Grilli, Tim Rogers, and Stefano Allesina. "Effect of population abundances on the stability of large random ecosystems". In: *Physical Review E* 98.2 (Aug. 2018), p. 022410. DOI: 10.1103/PhysRevE.98.022410.

[39] Ian A. Hatton, Onofrio Mazzarisi, Ada Altieri, and Matteo Smerlak. "Diversity begets stability: Sublinear growth and competitive coexistence across ecosystems". In: *Science* 383.6688 (2024). DOI: 10.1126/science.adg8488.

[40] Simone Cenci, Chuliang Song, and Serguei Saavedra. "Rethinking the importance of the structure of ecological networks under an environment-dependent framework". In: *Ecology and Evolution* 8.14 (2018), pp. 6852–6859. DOI: 10.1002/ece3.4252.

[41] Johannes Nauta and Manlio De Domenico. "Topological conditions drive stability in meta-ecosystems". In: *Physical Review Research* 6.4 (2024), p. 043055. DOI: 10.1103/PhysRevResearch.6.043055.

[42] Prajwal Padmanabha, Giorgio Nicoletti, Davide Bernardi, Samir Suweis, Sandro Azaele, Andrea Rinaldo, and Amos Maritan. "Landscape and environmental heterogeneity support coexistence in competitive metacommunities". In: *Proceedings of the National Academy of Sciences* 121.44 (2024), e2410932121. DOI: 10.1073/pnas.2410932121.

[43] Davide Bernardi, Alice Doimo, Giorgio Nicoletti, Prajwal Padmanabha, Andrea Rinaldo, Samir Suweis, Sandro Azaele, and Amos Maritan. "Habitat heterogeneity and dispersal network structure as drivers of metacommunity dynamics". In: *arXiv preprint arXiv:2602.06640* (2026). arXiv: 2602.06640 [q-bio.PE].

[44] Dmitrii O. Logofet. "Stronger-than-Lyapunov notions of matrix stability, or how "flowers" help solve problems in mathematical ecology". In: *Linear Algebra and its Applications* 398 (2005), pp. 75–100. DOI: https://doi.org/10.1016/j.laa.2003.04.001.

[45] Sean O'Rourke and David Renfrew. "Low Rank Perturbations of Large Elliptic Random Matrices". In: *Electronic Journal of Probability* 19.43 (2014), pp. 1–65. DOI: 10.1214/EJP.v19-2797.

[46] Lewi Stone. "The Google matrix controls the stability of structured ecological and biological networks". In: *Nature Communications* 7 (2016), p. 12890. DOI: 10.1038/ncomms12890.

[47] Andries E. Brouwer and Willem H. Haemers. *Spectra of Graphs*. Springer, 2012. DOI: 10.1007/978-1-4614-1939-6.

[48] Carlos A. Serván, José A. Capitán, Jacopo Grilli, Kent E. Morrison, and Stefano Allesina. "Coexistence of Many Species in Random Ecosystems". In: *Nature Ecology & Evolution* 2.8 (2018), pp. 1237–1242. DOI: 10.1038/s41559-018-0603-6.

[49] Alan Hastings, Karen C. Abbott, Kim Cuddington, Tessa Francis, Gabriel Gellner, Ying-Cheng Lai, Andrew Morozov, Sergei Petrovskii, Katherine Scranton, and Mary Lou Zeeman. "Transient phenomena in ecology". In: *Science* 361.6406 (2018), eaat6412. DOI: 10.1126/science.aat6412.

[50] Thierry Mora and William Bialek. "Are biological systems poised at criticality?" In: *Journal of Statistical Physics* 144.2 (2011), pp. 268–302. DOI: 10.1007/s10955-011-0229-4.

[51] Felix Roy, Matthieu Barbier, Giulio Biroli, and Guy Bunin. "Complex interactions can create persistent fluctuations in high-diversity ecosystems". In: *PLOS Computational Biology* 16.5 (2020), e1007827. DOI: 10.1371/journal.pcbi.1007827.

[52] Giulio Biroli, Guy Bunin, and Chiara Cammarota. "Marginally stable equilibria in critical ecosystems". In: *New Journal of Physics* 20.8 (2018), p. 083051. DOI: 10.1088/1367-2630/aada58.

[53] Ada Altieri, Felix Roy, Chiara Cammarota, and Giulio Biroli. "Properties of Equilibria and Glassy Phases of the Random Lotka–Volterra Model with Demographic Noise". In: *Physical Review Letters* 126 (2021), p. 258301. DOI: 10.1103/PhysRevLett.126.258301.

[54] Félix Roy, Giulio Biroli, Guy Bunin, and Chiara Cammarota. "Numerical Implementation of Dynamical Mean Field Theory for Disordered Systems: Application to the Lotka–Volterra Model of Ecosystems". In: *Journal of Physics A: Mathematical and Theoretical* 52.48 (2019), p. 484001. DOI: 10.1088/1751-8121/ab3d00.

[55] Oriol Artime, Marco Grassia, Manlio De Domenico, James P. Gleeson, Hernán A. Makse, Giuseppe Mangioni, Matjaž Perc, and Filippo Radicchi. "Robustness and Resilience of Complex Networks". In: *Nature Reviews Physics* 6 (2024), pp. 114–131. DOI: 10.1038/s42254-023-00678-2.

[56] M. C. Bortolan, P. Kalita, J. A. Langa, and R. O. Moura. "A Theoretical and Computational Study of Heteroclinic Cycles in Lotka–Volterra Systems". In: *Journal of Mathematical Biology* 90 (2025), p. 28. DOI: 10.1007/s00285-025-02185-0.

[57] Guim Aguadé-Gorgorió, Jean-François Arnoldi, Matthieu Barbier, and Sonia Kéfi. "A taxonomy of multiple stable states in complex ecological communities". In: *Ecology Letters* (2024). DOI: 10.1111/ele.14413.

[58] Heinz Georg Schuster and Wolfram Just. *Deterministic Chaos: An Introduction*. 4th ed. Weinheim: Wiley-VCH, 2005. ISBN: 9783527404155. DOI: 10.1002/3527604804.

[59] Meha Jain, Dan F. B. Flynn, Case M. Prager, Georgia M. Hart, Caroline M. DeVan, Farshid S. Ahrestani, Matthew I. Palmer, Daniel E. Bunker, Johannes M. H. Knops, Claire F. Jouseau, and Shahid Naeem. "The importance of rare species: a trait-based assessment of rare species contributions to functional diversity and possible ecosystem function in tall-grass prairies". In: *Ecology and Evolution* 4.1 (2013), pp. 104–112. DOI: 10.1002/ece3.915.

[60] Brian J. McGill et al. "Species abundance distributions: moving beyond single prediction theories to integration within an ecological framework". In: *Ecology Letters* 10.10 (2007), pp. 995–1015. DOI: 10.1111/j.1461-0248.2007.01094.x.

[61] Valentina Ros, Felix Roy, Giulio Biroli, Guy Bunin, and Ari M. Turner. "Generalized Lotka–Volterra Equations with Random, Nonreciprocal Interactions: The Typical Number of Equilibria". In: *Physical Review Letters* 130.25 (2023), p. 257401. DOI: 10.1103/PhysRevLett.130.257401.

Ringraziamenti

Questo lavoro di tesi ha per me un significato molto importante, non solo dal punto di vista del mio percorso accademico, ma anche sul piano umano ed emotivo: rappresenta la conclusione di tre anni che sento mi abbiano davvero arricchita, sia come studentessa sia come persona.
Guardandomi indietro, provo un profondo senso di gratitudine, perché ho avuto la fortuna di essere circondata da persone che mi hanno, ognuna a suo modo, sostenuta e fatta crescere.

Ringrazio in primo luogo i professori che hanno alimentato la mia curiosità per la fisica, in particolare per la fisica dei sistemi complessi, e che, riponendo fiducia in me, mi hanno permesso di cogliere opportunità preziose: sebbene io sia solo all'inizio di quello che spero sarà un lungo percorso di apprendimento, non avrei potuto desiderarne uno più stimolante.
Ringrazio il mio relatore, il prof. Bazzani, per l'interesse genuino dimostrato nel mio lavoro. Senza i momenti di discussione spontanea e le critiche costruttive avrei approfondito molto meno, e di certo avrei imparato molto meno.

Grazie ai vecchi amici di Astronomia per aver supportato la mia scelta di seguire dei nuovi interessi e per avermi salutata con calore ad ogni successivo incontro, quasi come se non me ne fossi mai andata.
Grazie a tutti i nuovi compagni di Fisica per avermi accolta a braccia aperte, quasi come se fossi sempre stata qui.

Grazie a chi ha trascorso con me pranzi sul prato e serate di *Lupus* (forse finalmente ho imparato le regole!), a chi mi ha regalato conversazioni stimolanti e a chi ha condiviso con me sogni e preoccupazioni, permettendomi di fare altrettanto. Grazie a chi ha assecondato i miei slanci di entusiasmo e a chi ha cercato di moderarli. Anche se non vi chiamo per nome, sapete che avete tutti un posto speciale nel mio cuore.

Grazie agli amici di sempre: è bello vedere ognuno di noi cercare la propria strada, potendo contare sulla presenza degli altri.

Grazie a chi è stato una casa anche lontano dalla mia città e grazie, in particolare, alle persone speciali che si sono prese cura di me: a te che hai saputo custodire la mia quotidianità, cucinando con amore per me quando ero troppo impegnata, e a te che in questi anni mi hai aiutata a immaginare il futuro che desidero, prendendomi per mano.

Grazie alla mia famiglia per avermi sempre incoraggiata in questo percorso, anche quando le mie spiegazioni su cosa voglio fare da grande non risultano così chiare. Vi vorrò per sempre bene.

Grazie a chiunque si sia interessato a leggere, almeno in parte, questo lavoro: spero che abbiate imparato anche solo una piccola cosa nuova.